

UNIVERSITY OF CALGARY

Asphaltene Precipitation from Bitumen/Multicomponent Solvent Mixtures

by

Javier Alberto Rivero Sanchez

A THESIS

SUBMITTED TO THE FACULTY OF GRADUATE STUDIES
IN PARTIAL FULFILMENT OF THE REQUIREMENTS FOR THE
DEGREE OF MASTER OF SCIENCE

GRADUATE PROGRAM IN CHEMICAL ENGINEERING

CALGARY, ALBERTA

MARCH, 2021

© Javier Alberto Rivero Sanchez 2021

Abstract

Bitumen is sometimes diluted with multicomponent solvents in oilfield processes and it is useful to predict if and how much asphaltenes may precipitate from these mixtures. The Modified Regular Solution (MRS) approach was adapted for these applications. For this purpose, the onset and yield of asphaltene precipitation from heavy oil diluted with multicomponent solvents were determined at temperatures from 21 to 180°C and pressures up to 10 MPa. The solvents considered include: 1) mixtures of *n*-pentane, *n*-heptane, cyclohexane, and toluene; 2) petroleum solvents such as condensates, diesel, and kerosene. The asphaltene yields at ambient conditions and high pressures were measured gravimetrically in a bench top apparatus and in a blind cell apparatus, respectively. The onset of asphaltene precipitation was extrapolated from asphaltene yield data at ambient conditions and determined optically at higher pressures with titrations performed in a high-pressure microscope.

Temperature dependent binary interaction parameters (BIP) were introduced to a previously developed MRS approach to model asphaltene precipitation from heavy oil diluted with blended pure solvents. BIP for the cyclohexane/asphaltene and toluene/asphaltene pseudo-component pairs were sufficient to match all of the data collected with binary solvent blends. All other BIP were set to zero. The model with the BIP obtained from the binary solvent blends predicted the asphaltene onsets and yields from heavy oil with ternary solvent blends, generally to within the error of the measurements.

A methodology to characterize petroleum solvents based on their GC assays to predict their molecular weight, density, and solubility parameters was developed. The methodology was tested against their measured densities at standard conditions and the solubility parameters determined by fitting the MRS model to yield data collected for bitumen diluted with these solvents. The asphaltene yields modeled using the proposed correlations as input to the MRS model matched the experimental data for all but one of the petroleum solvents and their blends with *n*-heptane with an overall average absolute deviation and bias of 1.1 wt% and -0.8 wt%, respectively. The MRS model did not match the asphaltene yield from the naphtha.

Acknowledgements

Firstly, I wish to express my deepest gratitude to my supervisor, Dr. Harvey Yarranton, whose continuous support and guidance during my studies helped me become a better engineer. His suggestions and words of encouragement pushed me to always give my best effort. I cannot thank him enough for giving me the chance to be part of his work team.

I would also like to acknowledge the outstanding support from my PVT Lab Manager, Florian Schoeggl. I will always be thankful for his patience during my training, the many pieces of advice he gave me along the way, and for teaching me the importance of asking "why?". I would like to express my gratitude to Elaine Baydak for her support and guidance in the laboratory. I would also like to extend my gratitude to my friend and former postdoc, Dr. Francisco Ramos-Pallares, for many fruitful discussions over coffee and his guidance with the MRS model.

I am grateful to the sponsors of the Natural Science and Engineering Research Council of Canada (NSERC) Industrial Research Chair in Heavy Oil Properties and Processing, including NSERC, Canadian Natural Resources Limited (CNRL), CNOOC Nexen, Ecopetrol, Petrobras, Schlumberger, Suncor Energy, Virtual Materials Group, Alberta Innovates, and ConocoPhillips for funding this research project.

I would also like to thank my friends, especially Franklin, Nicson, and Daniela, who made the long days at school a lot more fun. Finally, the key ingredient to succeed was the love and support from my family and my girlfriend. They helped me build the confidence to keep going every day and constantly encouraged me to be the best version of myself.

Dedication

This thesis is dedicated to my family and my girlfriend, who are the driving force in my life.

Table of Contents

Abstract.....	ii
Acknowledgements.....	iii
Dedication.....	iv
Table of Contents.....	v
List of Tables.....	viii
List of Figures.....	xi
List of Symbols, Abbreviations, and Nomenclature.....	xiv
CHAPTER 1: INTRODUCTION.....	1
1.1 Objectives.....	3
1.2 Thesis Structure.....	4
CHAPTER 2: LITERATURE REVIEW.....	6
2.1 Oil Chemistry.....	6
2.2 Asphaltenes.....	9
2.2.1 Composition.....	9
2.2.2 Molecular Structure.....	9
2.2.3 Molecular Weight.....	11
2.2.4 Density.....	11
2.2.5 Solubility Parameters.....	12
2.2.6 Asphaltene Self-Association.....	13
2.3 Asphaltene Precipitation.....	14
2.3.1 Phase Behavior of Mixtures of Heavy Oil and <i>n</i> -Alkanes.....	14
2.3.2 Asphaltene Precipitation from Mixtures of Heavy Oil and Solvents.....	16
2.4 Asphaltene Precipitation Models.....	25
2.4.1 Cubic Equation of State.....	26
2.4.2 Cubic Plus Association Equation of State.....	28
2.4.3 Perturbed-Chain Statistical Associating Fluid Theory.....	29

2.4.4 Regular Solution Theory	31
CHAPTER 3: EXPERIMENTAL METHODS	34
3.1 Materials	34
3.2 Asphaltene Yield and Onset Measurement at Ambient Conditions	36
3.3 Asphaltene Onset Measurement above Atmospheric Pressure.....	39
3.4 Asphaltene Yield Measurement above Atmospheric Pressure	42
CHAPTER 4: MODIFIED REGULAR SOLUTION MODEL.....	46
4.1 Modified Regular Solution Model.....	46
4.2 Fluid Characterization.....	48
4.3 MRS Model Implementation	51
CHAPTER 5: BLENDED PURE SOLVENTS RESULTS AND DISCUSSION	53
5.1 Bitumen with Single Component Solvent.....	53
5.2 Bitumen with Binary Solvent Blends	55
5.3 Testing the Predictive Capability of the Model with Binary Interaction Parameters	61
5.4 Bitumen with Solvent Blends at Elevated Temperatures and Pressures.....	64
CHAPTER 6: PETROLEUM SOLVENTS RESULTS AND DISCUSSION	68
6.1 Petroleum Solvent Characterization Based on Gas Chromatography	68
6.1.1 Generation of Pseudo-Components	69
6.1.2 Pseudo-Component Properties at Standard Conditions	71
6.1.3 Pseudo-Component Properties at non-Standard Conditions.....	79
6.1.4 Model Implementation.....	80
6.2 Asphaltene Precipitation Data.....	80
6.3 Asphaltene Precipitation Modeling Results.....	86
6.3.1 Initial Testing.....	86
6.3.2 Updated Characterization.....	87
CHAPTER 7: CONCLUSIONS AND RECOMMENDATIONS	93

7.1 Conclusions.....	93
7.1.1 Experimental Methods.....	93
7.1.2 Experimental Results.....	94
7.1.3 Modeling.....	95
7.2 Recommendations.....	95
References.....	97
Appendix A: SARA and GC Assays.....	115
Appendix B: Pump Displacement Method for Saturation Pressure Measurements.....	118
Appendix C: Solvent Properties.....	121
Appendix D: Yield Data.....	124

List of Tables

Table 2.1 UNITAR crude oil definition. Specific gravity (SG) and API gravity at 15.6°C (Jamaluddin <i>et al.</i> , 2018).	6
Table 3.1 Selected properties and SARA assays of the WC-B-A3 and WC-B-B5 bitumens; data for the WC-B-B5 bitumen is from Perez Claro <i>et al.</i> (2019). “C5-asphaltenes” are the <i>n</i> -pentane insoluble asphaltenes.	36
Table 4.1 Molecular weights and solubility parameters at 25°C and 0.1 MPa for selected solvents. Solubility parameters taken from Barton’s handbook (Barton, 1991).	48
Table 4.2 Values of temperature dependence parameter <i>k</i> in Eq. 4.10 for SAR fractions, C5-asphaltene pseudo-components, and solvents used in this thesis.	49
Table 4.3 Density (ρ°), molecular weight (<i>MW</i>) and solubility parameter (δ°) at 25°C and 0.1 MPa for saturates, aromatics, and resins fractions for MRS model (Ramos-Pallares and Yarranton, 2020).	51
Table 4.4 Parameters for the saturate and aromatic density correlation (Eq. 4.16).	51
Table 5.1 Fitted and modeled asphaltene precipitation onsets from WC-B-A3 bitumen diluted with <i>n</i> -alkanes and blends of <i>n</i> -alkanes at 21°C and 0.1 MPa. The overall average absolute deviation and bias in the modeled onsets were 1.1 wt% and 0.7 wt%, respectively.	55
Table 5.2 Deviations of the modeled asphaltene yields for WC-B-A3 bitumen diluted with <i>n</i> -alkanes and blends of <i>n</i> -alkanes at 21°C and 0.1 MPa. The overall average absolute deviation and bias in the modeled yields were 1.0 wt% and 0.5 wt%, respectively.	55
Table 5.3 Fitted binary interaction parameters for asphaltene/toluene and asphaltene/cyclohexane pairs at 21°C and 0.1 MPa.	58
Table 5.4 Fitted and modeled asphaltene onsets from WC-B-A3 bitumen diluted with binary blends of solvents from different chemical families at 21°C and 0.1 MPa. The overall average absolute deviation and bias in the modeled onsets were 2.0 wt% and -1.9 wt%, respectively.	60
Table 5.5 Deviations of the modeled asphaltene yields for WC-B-A3 bitumen diluted with binary blends of solvents from different chemical families at 21°C and 0.1 MPa. The overall average absolute deviation and bias in the modeled yields were 0.5 wt% and -0.1 wt%, respectively.	60
Table 5.6 Fitted and predicted asphaltene onsets from WC-B-A3 bitumen diluted with ternary blends of solvents from different chemical families at 21°C and 0.1 MPa. The overall average absolute deviation and bias in the modeled onsets were 1.7 wt% and -1.7 wt%, respectively.	62
Table 5.7 Deviations of the predicted asphaltene yields for WC-B-A3 bitumen diluted with ternary blends of solvents from different chemical families at 21°C and 0.1 MPa. The overall	

average absolute deviation and bias in the modeled yields were 0.6 wt% and 0.1 wt%, respectively.	62
Table 5.8 Fitted and modeled asphaltene precipitation onsets from WC-B-B5 bitumen diluted with <i>n</i> -alkanes and blends of <i>n</i> -alkanes at 21°C and 0.1 MPa. The overall average absolute deviation and bias in the predicted onsets were 1.8 wt% and -1.8 wt%, respectively.....	64
Table 5.9 Deviations of the modeled asphaltene yields for WC-B-B5 bitumen diluted with <i>n</i> -alkanes and blends of <i>n</i> -alkanes at 21°C and 0.1 MPa. The overall average absolute deviation and bias in the predicted yields were 0.6 wt% and 0.0 wt%, respectively.	64
Table 5.10 Deviations of the modeled onsets and yields for WC-B-A3 bitumen diluted with binary blends of solvents from different chemical families at temperatures of 21 and 180°C and pressure of 10 MPa. The overall average absolute deviation and bias in the yields after adjustment were 1.1 wt% and 0.3 wt%, respectively.	66
Table 5.11 Fitted binary interaction parameters for asphaltene/toluene and asphaltene/cyclohexane pairs at 180°C and 10 MPa.	66
Table 5.12 Measured and modeled asphaltene precipitation onsets from WC-B-A3 bitumen diluted with binary blends of solvents from different chemical families at temperatures of 21 and 180°C and pressure of 10 MPa. The overall average absolute deviation and bias in the onsets after adjustment were 0.7 wt% and 0.7 wt%, respectively.	67
Table 6.1 Measured and lumped GC assay of Condensate 1.....	70
Table 6.2 Fitted constants for the effective liquid density fluid-specific parameters for SCN pseudo-components with carbon numbers higher than seven.....	75
Table 6.3 Asphaltene yields from WC-B-A3 bitumen diluted with Condensate 1 and Condensate 2 at 21°C and 0.1 MPa. The precipitate was washed with <i>n</i> -pentane unless otherwise noted. The solvent in parenthesis indicates the solvent used to wash the precipitate.....	82
Table 6.4 Asphaltene yields from WC-B-A3 bitumen diluted with Diesel 1 and binary blends of Diesel 1 and <i>n</i> -heptane at 21°C and 0.1 MPa. The precipitate from bitumen diluted with Diesel 1 and the solvent blends was washed with <i>n</i> -pentane and the same solvent blend, respectively, unless otherwise noted. The solvent in parenthesis indicates the solvent used to wash the precipitate.	83
Table 6.5 Asphaltene yields from WC-B-A3 bitumen diluted with Diesel 3 and binary blends of Diesel 3 and <i>n</i> -heptane at 21°C and 0.1 MPa. The precipitate from bitumen diluted with Diesel 3 and the solvent blends was washed with <i>n</i> -pentane and the same solvent blend, respectively.	84
Table 6.6 Asphaltene yields from WC-B-A3 bitumen diluted with Kerosene 1 and binary blends of Kerosene 1 and <i>n</i> -heptane at 21°C and 0.1 MPa. The precipitate from bitumen diluted with Kerosene 1 and the solvent blends was washed with <i>n</i> -pentane and the same solvent blend, respectively.	85

Table 6.7 Asphaltene yields from WC-B-A3 bitumen diluted with Naphtha 1 at 21°C and 0.1 MPa. The solvent in parenthesis indicates the solvent used to wash the precipitate..... 86

Table 6.8 Predicted molecular weight, density, and solubility parameter of petroleum solvents at temperatures of 21 and 25°C and pressure of 0.1 MPa. 88

Table 6.9 Fitted and modeled asphaltene onsets from WC-B-A3 bitumen diluted with petroleum solvents and binary blends of petroleum solvents and *n*-heptane at 21°C and 0.1 MPa. The overall average absolute deviation and bias in the modeled onsets after adjustment were 0.3 wt% and 0.2 wt%, respectively. Naphtha 1 and the solvents with no measured yield are not included in the overall deviation calculation. 91

Table 6.10 Deviations of the modeled asphaltene yields from WC-B-A3 bitumen diluted with petroleum solvents and binary blends of petroleum solvents and *n*-heptane at 21°C and 0.1 MPa. The overall average absolute deviation and bias in the modeled yields were 1.1 wt% and -0.8 wt%, respectively. The petroleum solvents with no measured yield are not included in the overall deviation calculations..... 92

List of Figures

- Figure 2.1 Relationship between carbon number, boiling point, and structure of chemical compounds in crude oil. Figure adapted from Altgelt and Boduszynski (1993). 7
- Figure 2.2 Hypothetical asphaltene structures: a) Continental with molecular weight of 756 g/mol; b) Archipelago with molecular weight of 754 g/mol. Figure adapted from Schulze *et al.* (2015). 10
- Figure 2.3 Comparison of the phase behavior of mixtures of bitumen diluted with propane, *n*-butane, and *n*-pentane at 90°C. Propane data from Mancilla-Polanco *et al.* (2019), *n*-butane data from Perez Claro *et al.* (2019), and *n*-pentane data from Johnston *et al.* (2017b). Figure adapted from Perez Claro *et al.* (2019). 16
- Figure 2.4 Effect of temperature on C5-asphaltene onsets and yields from a Western Canadian bitumen diluted with *n*-pentane: a) onset; b) yield. Figure adapted from Johnston *et al.* (2017b). 18
- Figure 2.5 Effect of pressure on C5-asphaltene yield from Western Canadian bitumen diluted with *n*-pentane at 180°C. Figure from Johnston *et al.* (2017b). 19
- Figure 2.6 Effect of solvent type and composition on asphaltene precipitation yields from Athabasca bitumen diluted with different *n*-alkanes at 23°C and 0.1 MPa. Data from Akbarzadeh *et al.* (2005), figure adapted from Perez Claro (2019). 21
- Figure 3.1 Schematic of a typical asphaltene solubility curve for an *n*-alkane diluted bitumen. . 34
- Figure 3.2 Asphaltene yield from WC-B-A3 bitumen diluted with condensate 1 at 21°C and 0.1 MPa using two different solvents to wash the precipitate: a) condensate; b) *n*-pentane. . 38
- Figure 3.3 Determination of the onset of asphaltene precipitation from measured asphaltene yield curve for WC-B-A3 bitumen diluted with *n*-pentane at 21°C and 0.1 MPa. Note that the first data point appears to have a non-zero yield but is in fact below the onset of precipitation. It has a non-zero yield because some precipitation occurs in the mixing process due to localized areas of high solvent concentration. 39
- Figure 3.4 Schematic of the High-Pressure Microscope (HPM) system. Figure from Johnston *et al.* (2017b). 40
- Figure 3.5 HPM micrographs from WC-B-A3 bitumen diluted with a binary blend of 85 wt% *n*-pentane and 15 wt% toluene at 21°C and 10 MPa: a) 60.0 wt% solvent; b) 61.9 wt% solvent. The onset was reported as 60.9 ±1.5 wt% solvent. 42
- Figure 3.6 Schematic of the blind cell apparatus. Figure from Johnston *et al.* (2017b). 43
- Figure 3.7 Sample collection methodology to measure light phase compositions and C5-Aphaltene yields in the blind cell apparatus. 44
- Figure 5.1 Measured and modeled asphaltene yields from WC-B-A3 bitumen diluted with *n*-pentane, *n*-hexane, and *n*-heptane at 21°C and 0.1 MPa. Solid lines are the model with

default solubility parameters; dashed line is the model with an updated <i>n</i> -hexane solubility parameter.....	54
Figure 5.2 Measured and modeled asphaltene yields from WC-B-A3 bitumen diluted with binary blends of <i>n</i> -alkanes at 21°C and 0.1 MPa: a) <i>n</i> -pentane (C5) and <i>n</i> -heptane (C7); b) <i>n</i> -pentane (C5) and <i>n</i> -hexane (C6). The “50:50 X:Y” in the legend indicates a mixture of 50 wt% X and 50 wt% Y. Solid and dashed lines are the model results for a single component solvent and blended solvent, respectively.....	56
Figure 5.3 Measured and modeled asphaltene yields from WC-B-A3 bitumen diluted with binary blends of <i>n</i> -pentane and toluene at 21°C and 0.1 MPa; original version of model ($\lambda_{jk} = 0$). Solid and dashed lines are the model results for a single component solvent and blended solvent, respectively.....	57
Figure 5.4 Measured and modeled asphaltene yields from WC-B-A3 bitumen diluted with binary blends of solvents from different chemical families at 21°C and 0.1 MPa: a) <i>n</i> -pentane and toluene; b) <i>n</i> -heptane and toluene; c) <i>n</i> -pentane and cyclohexane; d) <i>n</i> -heptane and cyclohexane. Solid and dashed lines are the model results for a single component solvent and blended solvent, respectively.	59
Figure 5.5 Measured and predicted asphaltene yields from WC-B-A3 bitumen diluted with ternary blends of solvents from different chemical families at 21°C and 0.1 MPa: a) mixtures of <i>n</i> -pentane, toluene, and cyclohexane; b) mixtures of <i>n</i> -heptane, toluene, and cyclohexane. The model results for the ternary blends are predictions using the binary interaction parameters determined from the binary blends.....	61
Figure 5.6 Measured and modeled asphaltene yields from WC-B-B5 bitumen diluted with: a) <i>n</i> -pentane, <i>n</i> -heptane, and a binary blend of <i>n</i> -pentane and <i>n</i> -heptane at 21°C and 0.1 MPa; b) a binary blend of <i>n</i> -pentane and toluene and a binary blend of <i>n</i> -pentane and cyclohexane. The model results for the blends are predictions using the binary interaction parameters determined from the binary blends of WC-B-A3 bitumen.....	63
Figure 5.7 Measured and predicted asphaltene onsets and yields from WC-B-A3 bitumen diluted with binary blends of solvents at 21°C and pressures of 0.1 and 10 MPa: a) blend of 85:15 C5:Tol; b) blend of 75:25 C5:CH. The solid symbols are measured onsets (HPM) and the open symbols are measured yields (blind cell apparatus).....	65
Figure 5.8 Measured, predicted, and adjusted asphaltene onsets and yields from WC-B-A3 bitumen diluted with binary blends of solvents at temperatures of 21 and 180°C and pressure of 10 MPa: a) blend of 85:15 C5:Tol; b) blend of 75:25 C5:CH. The dashed lines are the predicted yields with the original BIPs and the solid line is the modeled yield with the adjusted BIPs from Table 5.11. The solid symbols are measured onsets (HPM) and the open symbols are measured yields (blind cell apparatus).....	67
Figure 6.1 Molecular weights of selected hydrocarbons from different chemical families. The solid line is a best fit of the molecular weights of paraffins with carbon numbers higher than five, provided as visual aid. The dashed line is the proposed correlation (Eq. 6.4) to calculate the molecular weights of SCN pseudo-components with carbon numbers higher than five when $A_F = 1$	73

Figure 6.2 Effective liquid densities at standard conditions of selected hydrocarbons from different chemical families. The solid line represents the density of selected *n*-alkanes with carbon numbers higher than five calculated with Eq. 6.1. The dashed line is the proposed correlation (Eq. 6.5) to calculate the density of SCN pseudo-components with carbon numbers higher than five when $A_F = 1$ 75

Figure 6.3 Fluid-specific parameters for the effective liquid density of *n*-alkanes. The closed symbols are the parameters for methane to *n*-heptane from Saryazdi *et al.* (2013). The open symbols are the fitted parameters for *n*-octane to *n*-hexadecane tuned in this thesis. The solid lines are the proposed correlations (Eq. 6.6 to 6.9) to calculate the fluid-specific parameters for the effective liquid density of *n*-alkanes with carbon numbers higher than seven. 76

Figure 6.4 Normal boiling points of selected hydrocarbons from different chemical families. Solid line is the empirical correlation (Eq. 6.13) to calculate the normal boiling points of *n*-alkanes with carbon numbers higher than five. 78

Figure 6.5 Solubility parameters at standard conditions of selected hydrocarbons from different chemical families. The solid line represents the solubility parameters of selected *n*-alkanes with carbon numbers higher than five at standard conditions calculated with Eq. 6.12. The dashed lines are the proposed correlations (Eq. 6.10 and 6.11) to calculate the solubility parameters of SCN pseudo-components with carbon numbers higher than five when $A_F = 1$ 78

Figure 6.6 Schematic of the fluid characterization methodology..... 80

Figure 6.7 Asphaltene yields from WC-B-A3 bitumen diluted with petroleum solvents and binary blends of petroleum solvents and *n*-heptane at 21°C and 0.1 MPa. The precipitate from bitumen diluted with petroleum solvents and solvent blends was washed with *n*-pentane and the same solvent blend, respectively, unless otherwise noted. The solvent in parenthesis indicates the solvent used to wash the precipitate. 81

Figure 6.8 Measured and modeled asphaltene yields from WC-B-A3 bitumen diluted at 21°C and 0.1 MPa: a) Condensate 1 and Condensate 2; b) binary blends of *n*-heptane and Diesel 1. The solid lines are the model results for the single or multicomponent component solvent and the dashed lines are the blended solvents..... 87

Figure 6.9 Measured and modeled asphaltene yields from WC-B-A3 bitumen diluted with Naphtha 1 at 21°C and 0.1 MPa. The open symbols indicate that the precipitate was washed with naphtha and the closed symbols that it was washed with *n*-pentane. 89

Figure 6.10 Measured and modeled asphaltene yields from WC-B-A3 bitumen diluted with petroleum solvents and binary blends of petroleum solvents and *n*-heptane at 21°C and 0.1 MPa: a) Condensate 1 and Condensate 2; b) binary blends of *n*-heptane and Diesel 1; c) binary blends of *n*-heptane and Diesel 3; d) binary blends of *n*-heptane and Kerosene 1. The solid lines are the model results for the single or multicomponent component solvent and the dashed lines are the blended solvents..... 90

List of Symbols, Abbreviations, and Nomenclature

Symbols

a	Attractive parameter in EoS
$a_{o,i}, b_{o,i}, c_{o,i}$	Fluid-specific parameters of saturates and aromatics
a_0	Parameter for pure non-associating components in CPA EoS
a_1, a_2	Fluid-specific parameters for effective density
$a_{1,i}, b_{1,i}$	Fluid-specific parameters of saturates and aromatics
A_i, B_i, C_i	Fitted constants for the effective liquid density fluid-specific parameters for SCN pseudo-components with carbon numbers higher than seven
A_F	Aromaticity factor
A^{assoc}	Helmholtz free energy contribution from association
A^{disp}	Helmholtz free energy contribution from dispersion forces
A^{hc}	Helmholtz free energy contribution from hard-chains
A^{res}	Residual Helmholtz free energy
b	Co-volume parameter in EoS, parameter for pure non-associating components in CPA EoS
b_1, b_2	Fluid-specific parameters for effective density
c	Cohesive energy density, volume translation parameter
c_1	Parameter for pure non-associating components in CPA EoS
C	Adjustable constant in empirical fitting equation
D	Adjustable constant in empirical fitting equation
D_{ij}	Function of solubility parameter in activity coefficient equation
E%	Maximum percentage of solvent blend evaporated in the oven
f_i^0	Standard fugacity
g	Radial distribution function
H/F	Mass ratio of heavy phase to feed components
k	Temperature dependence of the solubility parameter
K_i	Partition coefficient

m_i	Component specific constant of C5-asphaltenes and resins, segment number of pure non-associating components in PC-SAFT EoS
MW	Molecular weight
MW_{avg}	Average molecular weight of the C5-asphaltene aggregate
MW_{max}	Maximum molecular weight of the C5-asphaltene aggregate
MW_{mon}	Molecular weight of the monomer in the C5-asphaltene aggregate
P	Absolute Pressure
R	Universal gas constant
T	Absolute temperature
T_b	Normal boiling point
v	Molar volume
w	Mass fraction
$W_{A,i}$	Cumulative mass fraction of C5-asphaltenes
x	Mole fraction
X_{A_i}	Fraction of unbonded sites in CPA EoS
Y	Yield
Z_{RA}	Rackett compressibility factor

Superscripts

o	Standard condition
α	Phase
H	Heavy (asphaltene-rich) phase
L	Light (solvent-rich) phase
F	Feed component

Subscripts

A	Asphaltenes
A_i	Sites of type A on molecules of component i
adj	Any SCN pseudo-component with a carbon number higher than five
c	Critical condition
i	Component i

iCX	Iso-paraffin component with carbon number of X
j	Component j
k	Component k
max	Maximum
min	Minimum
$onset$	Solvent content at the onset of precipitation
r	Reduced property
R	Resins
ref	Reference n -alkane with same carbon number as the SCN pseudo-component
S	Solvent
ToP	Standard temperature and actual pressure

Greek Symbols

$\alpha(T)$	Energy parameter in CPA EoS
$\alpha(T_r, \omega)$	Dimensionless function of the reduced temperature in PR EoS
β	Shape factor in Gamma distribution
$\beta^{A_i B_j}$	Association volume in CPA EoS
γ	Activity coefficient
Γ	Gamma function
δ	Solubility Parameter
$\Delta^{A_i B_j}$	Association strength between sites A and B in CPA EoS
Δu_{vap}	Energy of complete vaporization
$\epsilon^{A_i B_j}$	Association energy in CPA EoS
ϵ/k	Segment energy of pure non-associating components in PC-SAFT EoS
$\epsilon^{A_i B_i}/k$	Association strength in PC-SAFT EoS
$\kappa^{A_i B_i}$	Association volume in PC-SAFT EoS
λ_{jk}	Binary interaction parameters between components j and k
ρ	Density
σ	Segment diameter of pure non-associating components in PC-SAFT EoS

ϕ	Volume fraction
ω	Acentric factor

Abbreviations

AAD	Average Absolute Deviation
API	American Petroleum Institute
BIP	Binary Interaction Parameters
BPR	Back Pressure Regulator
C5	<i>n</i> -Pentane
C6	<i>n</i> -Hexane
C7	<i>n</i> -Heptane
CEoS	Cubic Equation of State
CH	Cyclohexane
CPA	Cubic Plus Association
D1	Diesel 1
D3	Diesel 3
EoS	Equation of State
GC	Gas Chromatography
H/C	Hydrogen-to-Carbon
Heptol	<i>n</i> -Heptane and Toluene
HPM	High-Pressure Microscope
IRMPD	Infrared Multiphoton Dissociation
KER	Kerosene 1
L	Liquid
L ² MS	Two-Step Laser Mass Spectrometry
LDI-MS	Laser Desorption Ionization Mass Spectroscopy
LDI-TOF	Laser Desorption Ionization Time-of-Flight
LL	Liquid-Liquid
MAD	Maximum Absolute Deviation
MRS	Modified Regular Solution
N/C	Nitrogen-to-Carbon

NMR	Nuclear Magnetic Resonance
PC-SAFT	Perturbed-Chain Statistical Associating Fluid Theory
PR	Peng-Robinson
PVT	Pressure Volume Temperature
SAFT	Statistical Associating Fluid Theory
SAGD	Steam Assisted Gravity Drainage
SANS	Small-Angle Neutron Scattering
SAR	Saturates, Aromatics, and Resins
SARA	Saturates, Aromatics, Resins, and Asphaltenes
SAXS	Small-Angle X-Ray Scattering
SCN	Single Carbon Number
SMFS	Single-Molecule Force Spectroscopy
SRK	Soave-Redlich-Kwong
TI	Toluene Insolubles
TOF	Time-of-Flight
Tol	Toluene
TRFD	Time-Resolved Fluorescence Depolarization
UV-Vis	Ultraviolet-Visible
VL	Vapor-Liquid
VLL	Vapor-Liquid-Liquid
VLLL	Vapor-Liquid-Liquid-Liquid
VPO	Vapor Pressure Osmometry
WL	Water-Liquid
WLL	Water-Liquid-Liquid
WVLL	Water-Vapor-Liquid-Liquid
XRD	X-ray diffraction

CHAPTER 1: INTRODUCTION

Asphaltenes are the heaviest, most polar fraction, and least soluble fraction of a crude oil, and they can precipitate from crude oils upon a change in pressure, temperature, or composition. Asphaltene precipitation in the reservoir can occur when a solvent is injected. For example, in solvent-assisted and solvent-based heavy oil recovery schemes, hydrocarbon solvents are injected into the reservoir to reduce the viscosity of heavy oil and aid its mobilization towards the production well. Asphaltene precipitation deep in the reservoir allows a more valuable, partially deasphalted oil to be produced. However, asphaltene precipitation may also plug the pores of the formation near the wellbore and reduce the oil production rate (Bayestehparvin *et al.*, 2019; Haghghat and Maini, 2010).

Asphaltene precipitation can also be an issue in the production of conventional oils. The depressurization of the oil during production and/or solvent injection can induce asphaltene precipitation. The precipitated asphaltenes may deposit and form a solid layer on the surface of the wellbore tubing. Asphaltene deposition gradually reduces the diameter of the pipeline decreasing the oil production rates sometimes to the point where production completely stops (Ghloum *et al.*, 2010; Hammami *et al.*, 2000; Joshi *et al.*, 2001; Juyal *et al.*, 2013).

Flow assurance issues related with asphaltenes also occur in surface facilities. For example, heavy oils are diluted with diluents to facilitate its transportation through pipelines to refineries for processing. The diluents of choice typically include gas condensates, light crude oils, or refinery distillation products such as kerosene, diesel, or naphtha. Diluents are multicomponent solvents that contain a wide range of hydrocarbons, some of which may be poor solvents to asphaltenes (Alomair and Almusallam, 2013; Qi *et al.*, 2018). Asphaltene precipitation in pipelines may lead to asphaltene deposition and pipeline blockage (Martínez-Palou *et al.*, 2011).

Blending different crude oils for refining is a common practice in the petroleum industry and asphaltene precipitation can occur if the blended fluids are incompatible. Asphaltene precipitation accelerates the fouling of heat exchangers (Stark and Asomaning, 2003; Wang *et al.*, 2015). Fouling of heat transfer equipment considerably increases the cost of refining operations because

additional fuel is required to make up for the reduced heat transfer efficiency, increased pumping power is needed to overcome pressure drops, and production may be reduced for maintenance (Macchietto *et al.*, 2011; Watkinson, 2007). Asphaltenes are also known to cause issues in hydrotreating processes, where they are associated with the poisoning of catalysts (Bartholomew, 2001; Durand *et al.*, 2010; Usui *et al.*, 2004).

Asphaltenes are deliberately precipitated in applications such as solvent deasphalting and paraffinic froth treatment. In solvent deasphalting processes, heavy oil feedstocks are mixed with a light hydrocarbon or mixture of hydrocarbons to remove the carbon-rich components, resins, and asphaltenes from the oil. The resulting deasphalted oil is an upgraded oil that may be used as a lube base oil or refined to be converted into fuels or chemical raw materials. Propane and mixtures of propane and *n*-butane are common choices of solvent for deasphalting (Speight, 2010). Paraffinic froth treatment is a process used to separate bitumen from the bitumen froth, which is a mixture of bitumen, water, and mineral solids formed in the mining of oil sands. In paraffinic froth treatment, light *n*-alkanes or mixtures of *n*-alkanes are injected into the bitumen froth at dilution ratios above the onset of precipitation. The aggregates of precipitated asphaltenes, solids, and water droplets are left to settle, producing a partially upgraded bitumen with minimal content of water and solids (Rao and Liu, 2013; Wu and Xu, 2019; Xu, 2018; Zawala *et al.*, 2012).

Models are required to predict the onset and yield of asphaltene precipitation. The onset is defined as the temperature, pressure, and composition at which asphaltene precipitation occurs. The yield is defined as the mass of precipitated asphaltenes divided by the mass of crude oil in the feed. Predicting the onset is essential for flow assurance. Predicting both the onset and the yield are required for the design and operation of solvent-based and solvent-assisted processes.

There are several models that can be used to predict asphaltene precipitation including cubic equations of state (Fahim *et al.*, 2001; Johnston *et al.*, 2017a; Tavakkoli *et al.*, 2010), the cubic plus association equation of state (Arya *et al.*, 2017; Li and Firoozabadi, 2010; Shirani *et al.*, 2012; Zhang *et al.*, 2019), the PC-SAFT equation of state (Gonzalez *et al.*, 2005; Panuganti *et al.*, 2012; Ting *et al.*, 2003; Zúñiga-Hinojosa *et al.*, 2014), and regular solution theory (Akbarzadeh *et al.*, 2005; Alboudwarej *et al.*, 2003). The equation of state models represent vapor-liquid equilibrium

accurately and can also model liquid-liquid and vapor-liquid-liquid equilibrium. However, they require a relatively complex fluid characterization, a computationally demanding equilibrium flash procedure, and tuning for each solvent. The Modified Regular Solution (MRS) model is based on activity coefficients and is only applicable to liquid-liquid equilibrium. The flash procedure is straightforward because the equilibrium values are explicit unlike equations of state where the equilibrium values require the solution of roots and derivatives. While the regular solution model must be tuned for each oil, the tuning is minimal, and the model can predict the effect of some hydrocarbon solvents without tuning. Hence, the regular solution approach is well suited for applications involving mixtures of heavy oil and solvents.

This thesis focuses on heavy oil applications. One gap in the existing asphaltene precipitation models is multicomponent solvents. Data are available for asphaltene precipitation from heavy oils and pure *n*-alkanes (Akbarzadeh *et al.*, 2005; Alboudwarej *et al.*, 2003; Buenrostro-Gonzalez *et al.*, 2004; Calles *et al.*, 2008; Fuhr *et al.*, 1991; Hu and Guo, 2001; James and Mehrotra, 1988; Johnston *et al.*, 2017b; Mancilla-Polanco *et al.*, 2019; Peramanu *et al.*, 1999a; Perez Claro *et al.*, 2019; Sattari *et al.*, 2016) but few data are available for multicomponent solvents. Similarly, phase behavior models have been tested on heavy oil diluted with an *n*-alkane but not with multicomponent solvents.

1.1 Objectives

The overall goal of this thesis is to collect and model asphaltene precipitation data for heavy oils and multicomponent solvents, both pure solvents and petroleum solvents. The MRS model is to be adapted for these mixtures. The specific objectives of this thesis are as follows:

1. Measure asphaltene precipitation onsets and yields from bitumen diluted with the following multicomponent solvents:
 - a. binary and ternary blends of pure hydrocarbons from different chemical families including *n*-alkanes, toluene, and cyclohexane at three conditions (21°C and 0.1 MPa; 21°C and 10 MPa; 180°C and 10 MPa).
 - b. petroleum solvents including oilfield condensates and refinery distillation products at ambient conditions.

The onsets are extrapolated from asphaltene yield data at ambient conditions and determined from titrations performed in a high-pressure microscope (HPM) apparatus at 10 MPa. The yields are measured in a bench top apparatus at ambient conditions and in a blind cell apparatus at higher pressures and temperatures.

2. Test and adapt a previously developed MRS model to predict asphaltene precipitation onsets and yields from bitumen diluted with multicomponent solvents.
 - a. Introduce a binary interaction parameter distribution between the solvent/asphaltene pairs to the model to match experimental onset and yield data.
 - b. Test and adapt a characterization procedure for the required properties for asphaltene precipitation modeling applicable to petroleum solvents such as condensates.
 - c. Test and adapt property correlations used in the MRS model to predict asphaltene precipitation onset and yield data from bitumen diluted with multicomponent solvents at elevated temperature and pressure.

1.2 Thesis Structure

This thesis is organized into seven chapters and the remaining chapters are outlined below.

Chapter 2 briefly describes the chemistry of crude oil and the properties of the SAR (saturates, aromatics, and resins) fractions. The distribution of properties of asphaltenes and the effect of different variables on asphaltene precipitation are reviewed. The main approaches for asphaltene precipitation modeling are presented.

Chapter 3 lists the materials and selected properties of the bitumen samples used in this thesis. The experimental procedures used to measure the condition at which asphaltenes start precipitating (onset) and the amount of precipitation relative to feed bitumen (yield) are provided.

Chapter 4 presents the Modified Regular Solution model used to predict asphaltene precipitation in this thesis. The main assumptions of the model, the fluid characterization, and the correlations to determine the properties of the different pseudo-components are provided.

Chapter 5 presents the experimental data and modeling results from two Western Canadian bitumens diluted with single component solvents and blended solvents. A new correlation to calculate binary interaction parameters (BIP) is proposed. The predictive ability of the MRS model with BIP for different bitumens and at high temperature and pressure is assessed.

Chapter 6 presents the experimental data and modeling results from a Western Canadian bitumen diluted with petroleum solvents and binary blends of *n*-heptane and petroleum solvents. A new fluid characterization methodology for the required properties for asphaltene precipitation modeling applicable to petroleum solvents is developed. The model performance is assessed against experimental data and modifications to match the onset and yields are proposed.

Chapter 7 summarizes the main contributions of this thesis and provides recommendations for future projects.

CHAPTER 2: LITERATURE REVIEW

This chapter begins with a brief description of the chemistry of crude oil and the properties of the saturates, aromatics, resins, and asphaltenes (SARA) fractions of heavy oils. Then a detailed review of the distribution of properties of the asphaltene fraction is provided. The effect of temperature, pressure, solvent type, and composition on asphaltene precipitation are discussed. Finally, the main approaches to model asphaltene precipitation are summarized.

2.1 Oil Chemistry

Petroleum fluids are naturally occurring mixtures of hydrocarbons in the liquid, gaseous, or solid state. They contain traces of metallic constituents along with small amounts of sulfur, oxygen, and nitrogen compounds (Speight, 2014). Crude oils are liquid petroleum (Cronquist, 2000) and can be classified according to their dead oil viscosity at reservoir temperature, specific gravity, and API gravity, as shown in Table 2.1 (Gray, 1994; Jamaluddin *et al.*, 2018). The term “dead oil” refers to produced crude oils that no longer contain dissolved gases. Crude oils in petroleum reservoirs still contain dissolved gas and are known as live oils (Joseph *et al.*, 2002; Malone *et al.*, 2020).

Table 2.1 UNITAR crude oil definition. Specific gravity (SG) and API gravity at 15.6°C (Jamaluddin *et al.*, 2018).

Classification	Viscosity mPa·s	Specific Gravity	API Gravity
Light/Medium Oil	$<10^2$	<0.93	$>20^\circ$
Heavy Oil	10^2 - 10^5	0.93-1.00	10- 20°
Bitumen	$>10^5$	>1.00	$<10^\circ$

The hydrocarbon components of crude oil can be classified into three main chemical families: paraffins, naphthenes, and aromatics. Each family includes a large variety of chemical species spanning a wide range of molecular weights and elemental compositions. The complexity, aromaticity, polarity, heteroatom content, and metal content of these species increases as their molecular weights (carbon numbers) increase, as shown in Figure 2.1 (Shaw *et al.*, 2017; Speight,

1999). The boiling points of each chemical family also increase with molecular weight as the result of increasing van der Waals attractive intermolecular forces. Additional intermolecular forces such as hydrogen bonding or other polar interactions contribute to the distribution of boiling points (Boduszynski, 1987; Ovalles, 2019).

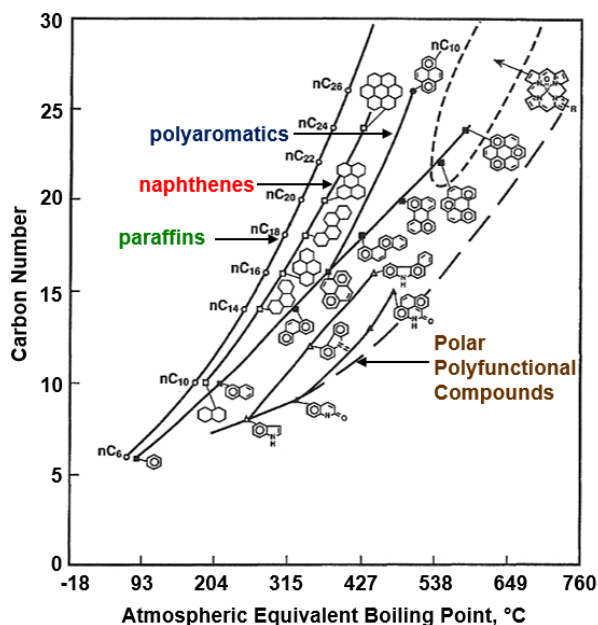


Figure 2.1 Relationship between carbon number, boiling point, and structure of chemical compounds in crude oil. Figure adapted from Altgelt and Boduszynski (1993).

The large diversity of components in crude oil, particularly that of the heavier fractions, makes it practically impossible to characterize it into individual components (Boduszynski, 2015; Ramirez-Corredores, 2017). Consequently, the objective of the characterization is to represent the complexity of components within the crude oil with a computationally manageable number of pseudo-components sufficient for reliable process modeling. The level of detail required on the compositional characterization is typically restricted by the application and the type of crude oil (Bissada *et al.*, 2016; Fan and Buckley, 2002; Sisco *et al.*, 2018).

Dead heavy oils, the subject of this thesis, are commonly characterized into saturates, aromatics, resins, and asphaltenes (SARA) fractions for asphaltene precipitation modeling (Akbarzadeh *et al.*, 2005; Hemmati-Sarapardeh *et al.*, 2013; Punnapala and Vargas, 2013). In the SARA analysis,

asphaltenes are separated by their solubility and the other fractions by liquid chromatography (Punase and Hascakir, 2017). There are several variations of the methodology and the results from each methodology may not be equivalent (Bissada *et al.*, 2016; Hsu and Robinson, 2019; Rahimi and Gentzis, 2006). Nonetheless, the properties of SAR (saturates, aromatics and resins) fractions such as density, molecular weight and solubility parameters from different crude oils are similar (Yarranton *et al.*, 2018) and are summarized below.

Saturates consist of saturated hydrocarbons; that is, hydrocarbons with no double bonds. Their molecular structure can be normal, branched, or cyclic (Hollebone, 2015). The average molar mass of saturates ranges from 361 to 524 g/mol (Akbarzadeh *et al.*, 2004; Akmaz *et al.*, 2011; Hao *et al.*, 2017) and their density ranges between 853 and 900 kg/m³ (Akbarzadeh *et al.*, 2004; Peramanu *et al.*, 1999b). The average saturate solubility parameter at standard conditions was determined to be 16.5 MPa^{0.5} (Ramos-Pallares and Yarranton, 2020).

Aromatics are hydrocarbons of at least one aromatic nucleus that may be linked with naphthenic and paraffinic compounds (Sjöblom *et al.*, 2005). Aromatics also include small proportions of nitrogen, oxygen, or sulfur heteroatoms. The average molar mass of aromatics ranges from 450 to 550 g/mol (Akbarzadeh *et al.*, 2004; Castro and Vazquez, 2009) and their density ranges from 960 to 1003 kg/m³ (Akbarzadeh *et al.*, 2004; Peramanu *et al.*, 1999b). The aromatic solubility parameter has been reported to range from 19.2 to 19.4 MPa^{0.5} (Ramos-Pallares and Yarranton, 2020; Rogel, 1997).

Resins are similar to aromatics but are larger, more aromatic, and have a higher heteroatom content (Sjöblom *et al.*, 2007). The composition of this fraction depends on the precipitant and temperature used in the SARA fractionation (Andersen and Speight, 2001). The molecular weight of resins ranges from 859 to 1240 g/mol (Akbarzadeh *et al.*, 2004; Akmaz *et al.*, 2011; Marufuzzaman and Henni, 2015) and their density ranges from 1007 to 1066 kg/m³ (Akbarzadeh *et al.*, 2004; Peramanu *et al.*, 1999b). Reported solubility parameters of resins range from 19.6 to 21.1 MPa^{0.5} (Akbarzadeh *et al.*, 2004; Rogel, 1997).

Asphaltenes are defined as a solubility class fraction of crude oil, soluble in aromatic solvents such as toluene but insoluble in *n*-alkanes such as *n*-pentane or *n*-heptane (Akbarzadeh *et al.*, 2005). They are the heaviest, most aromatic, and most polar fraction of bitumen and heavy oils (Speight, 2004). The properties of the asphaltene fraction are described in detail in the following section.

2.2 Asphaltenes

2.2.1 Composition

Asphaltenes are a polydisperse fraction that includes thousands of species with diverse molecular structures (Javanbakht *et al.*, 2018; McKenna *et al.*, 2019). They consist of polycyclic aromatic hydrocarbon ring structures that also include cyclics, alkane chains, various trace metals, and heteroatoms such as sulfur, nitrogen, and oxygen (Akbarzadeh *et al.*, 2007; Langevin and Argillier, 2016). The most abundant trace metals within the asphaltenes fraction are vanadium and nickel. They are usually but not exclusively present in the form of chelated porphyrin complexes (Gawrys *et al.*, 2006a; Kharrat, 2009). The composition of the asphaltenes changes from one oil source to another (Gharbi *et al.*, 2017) and depending on the solvent used for precipitation. For example, C7-asphaltenes have a higher degree of aromaticity and usually higher proportions of heteroatoms than C5-asphaltenes (Speight, 1999). Heteroatom contents are typically in the order of a few weight percent while atomic hydrogen-to-carbon (H/C) ratios are between 1 and 1.2 (McKenna *et al.*, 2013; Spiecker *et al.*, 2003).

2.2.2 Molecular Structure

Two different concepts have been considered for the typical molecular structure of asphaltenes: the continental or island structure and the archipelago structure. According to the continental model (Figure 2.2a), a representative asphaltene molecule consists of a single polyaromatic core made of roughly 7 rings with pendant aliphatic chains (Mullins *et al.*, 2012; Sabbah *et al.*, 2010). Fluorescence depolarization measurements were among the first to suggest that asphaltenes consisted of a single aromatic core (Groenzin and Mullins, 1999, 2000). Sabbah *et al.* (2011) compared the fragmentation behavior of model compounds with both molecular structures to that of asphaltene samples through two-step laser mass spectrometry (L²MS). Single aromatic core compounds showed little or no fragmentation, while archipelago model compounds fragmented. They concluded that the continental structure was dominant because asphaltenes and single-

aromatic core compounds exhibited similar fragmentation behaviors. Molecular imaging by atomic force microscopy also suggested that a structure with a central aromatic core and peripheral alkanes was dominant in petroleum asphaltenes (Schuler *et al.*, 2015).

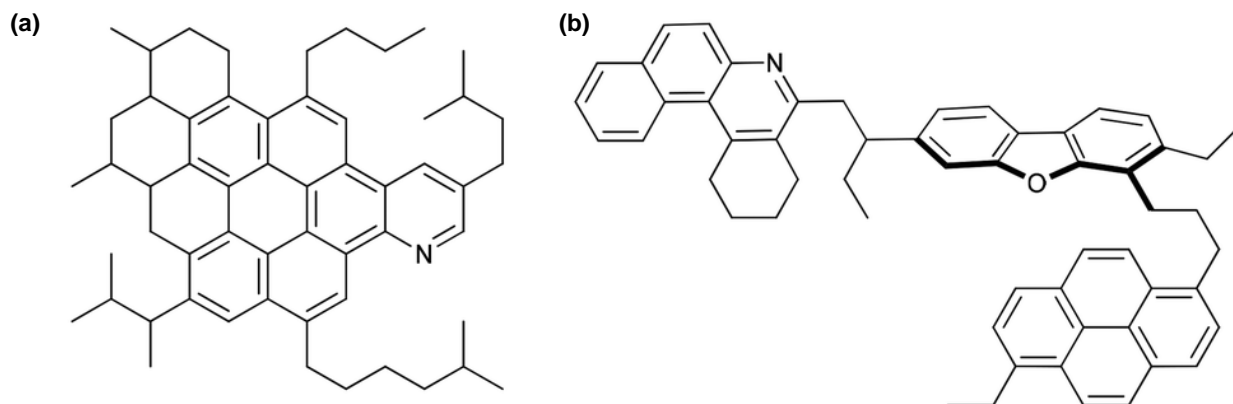


Figure 2.2 Hypothetical asphaltene structures: a) Continental with molecular weight of 756 g/mol; b) Archipelago with molecular weight of 754 g/mol. Figure adapted from Schulze *et al.* (2015).

Alternatively, the archipelago model (Figure 2.2b) proposes that asphaltenes consist of smaller aromatic cores linked by aliphatic chains (Schulze *et al.*, 2015; Sheremata *et al.*, 2004). This model has been supported by calculations of significant solvent entrainment inside asphaltene aggregates. Entrainment is more consistent with loose fractal aggregates of archipelago structures as opposed to stacked continental structures (Gawrys *et al.*, 2006b). The products from cracking and pyrolysis of asphaltenes are consistent with an architecture of bridged aromatic groups substituted by aliphatic groups (Gray, 2003). Karimi *et al.* (2011) demonstrated the significant existence of bridges linking clusters of ring groups in asphaltenes by thin film pyrolysis. Other studies indicate that both structures are present in asphaltenes and that their relative amounts influence properties such as aggregation (Da Silva Oliveira *et al.*, 2014; Durand *et al.*, 2010). The coexistence of archipelago and continental asphaltenes was recently demonstrated by infrared multiphoton dissociation (IRMPD) (Chacón-Patiño *et al.*, 2017). This work and others from the Rodger's group has demonstrated that continental structures are more easily detected than archipelago structures and that in fact archipelago structures dominate in many crude oils (Chacón-Patiño *et al.*, 2018a, 2018b; McKenna *et al.*, 2019).

2.2.3 Molecular Weight

Asphaltenes have the widest distribution of molecular weights among the fractions of crude oil due to their nanoaggregation (self-association) and solubility behavior (Gray, 2015). Asphaltene self-association is discussed later and this section focuses on monomer molecular weights. The molecular weight of asphaltenes has been measured using various techniques. Molecular diffusion measurements suggest that the average non-associated molecular weight of asphaltene ranges from 700 to 800 g/mol. These results are consistent with laser desorption ionization mass spectroscopy (LDI-MS) measurements that indicate a range between 600 and 800 g/mol (Hortal *et al.*, 2007). Note that LDI-MS results are sensitive to operating parameters and inadequate selection may lead to erroneous molecular weights. In contrast, L²MS avoids aggregation and detects asphaltenes as monomers. The average molecular weights measured with L²MS are in the range of 600 to 700 g/mol (Pomerantz *et al.*, 2015; Wu *et al.*, 2014). Time-resolved fluorescence depolarization (TRFD) data indicate an average molecular weight of approximately 750 g/mol with a range from 500 to 1000 g/mol (Mullins and Groenzin, 2007).

2.2.4 Density

Rogel and Carbognani (2003) measured the densities of asphaltenes extracted from different sources in pycnometers using *n*-heptane as the displacing fluid. The reported densities ranged between 1160 and 1280 kg/m³. The asphaltenes obtained from deposits and unstable crude oils were denser than the asphaltenes from stable crude oils. Different studies have indirectly calculated asphaltene densities from the densities of mixtures of asphaltenes in toluene. Barrera *et al.* (2013) assumed that asphaltenes formed regular solutions with toluene and calculated their density from the specific volumes of solutions of asphaltenes in toluene. They reported experimental densities of asphaltenes from four crude oils in the range of 1078 to 1209 kg/m³.

Following the same approach of Barrera *et al.* (2013), Prakoso *et al.* (2016) estimated the density of asphaltenes from 11 different crude oils in solutions of toluene. The experimental densities were in the range of 1050 to 1280 kg/m³, except for one sample with a density of 950 kg/m³. Ghouloum *et al.* (2010) determined asphaltene densities ranging from 1208 to 1310 kg/m³. Hashmi and Firoozabadi (2012) reported densities of asphaltenes in the range of 1100 to 1200 kg/m³. Simulation approaches have also been used to estimate the density of asphaltenes. Diallo *et al.*

(2000) determined the density of model asphaltene isomers from isothermal and isobaric molecular dynamics simulations followed by energy minimization. They reported densities in the range of 1030 to 1180 kg/m³.

2.2.5 Solubility Parameters

The solubility parameters of asphaltenes have been indirectly determined by different experimental and modeling approaches as discussed below. The magnitude of the solubility parameter changes depending on their source and, due to the complexity of the asphaltene fraction, their solubility parameter is not a single value but rather a distribution of values (Aguiar *et al.*, 2014; Painter *et al.*, 2015). Lian *et al.* (1994) reported solubility parameters of C5-asphaltenes (*n*-pentane extracted) from asphalt in the range of 17.6 to 21.3 MPa^{0.5}. These parameters were estimated from miscibility measurements in various solvents. Aguiar *et al.* (2014) determined the solubility parameters of C5-asphaltenes and C7-asphaltenes (*n*-heptane extracted) from two crude oils ranging between 17.5 and 23.8 MPa^{0.5} from heats of solubilization measured with microcalorimetry. The C5-asphaltenes had a lower limit in the distribution of solubility parameters than the C7-asphaltenes. The solubility parameters calculated with microcalorimetry were in good agreement with the parameters determined for the same samples from ultraviolet-visible (UV-Vis) spectroscopy measurements.

Chandio *et al.* (2015) calculated the solubility parameters of asphaltenes from two Malaysia crude oils, two Middle East crude oils, and an Australia crude oil using automated flocculation onset titration measurements. They reported average values from 19.42 to 20.75 MPa^{0.5} for asphaltenes from six different oils. Rogel *et al.* (2016) correlated the solubility parameter of C7-asphaltenes from a Kuwaiti crude oil to their average elution time in a packed column. The average solubility parameters of petroleum asphaltene were between 19.8 to 20.3 MPa^{0.5} but the distribution of values for each asphaltene fraction ranged from approximately 18 to 25 MPa^{0.5}. Powers *et al.* (2016) back-calculated solubility parameters from asphaltene yields using a Modified Regular Solution (MRS) model. The fitted solubility parameter distributions for C7-asphaltenes from native oils ranged between 19.95 and 21.50 MPa^{0.5}.

2.2.6 Asphaltene Self-Association

Asphaltenes are known to self-associate and form nanoaggregates in crude oil and in solvents with sizes in the range of 2 to 20 nm (Gray and Yarranton, 2019). The extent of aggregation of asphaltenes is directly proportional to their concentration and inversely proportional to the temperature, solvent “power”, and resins content (Derakhshesh *et al.*, 2013; Yarranton, 2005). Asphaltenes can form nanoaggregates at concentrations below 0.2 kg/m³ (Durand *et al.*, 2010). Barrera *et al.* (2013) fractionated C7-asphaltenes into solubility cuts and measured their molecular weights in solutions of toluene using vapor pressure osmometry (VPO). They observed that the molecular weight monotonically increased with the concentration of asphaltenes in solution. Their molecular weight measurements were in the range of 1000 and 30000 g/mol, indicating that nanoaggregates consist of about 1 to 30 asphaltene monomers. Acevedo *et al.* (2005) determined the molecular weight distributions of seven asphaltene samples using laser desorption ionization-time-of-flight (LDI-TOF) mass spectrometry. They reported molecular weights ranging between 100 and 10000 g/mol. These measurements were validated and found in good agreement with those from VPO. Time-of-flight (TOF) mass spectrometry measurements indicate nanoaggregate molecular weights ranging between 6000 and approximately 22000 g/mol (McKenna *et al.*, 2013). Small-angle neutron scattering (SANS) and small-angle X-ray scattering (SAXS) data indicate an average nanoaggregate molecular weight of 16000 g/mol (Eyssautier *et al.*, 2011).

The mechanisms that cause asphaltenes self-association can be explained with different concepts depending on their molecular structure. If asphaltenes have a continental structure, then they are likely to form colloidal stacks through π - π bonds (Schulze *et al.*, 2015). The colloidal nature of asphaltenes has been supported by various experimental techniques including X-ray diffraction (XRD), SANS, and SAXS measurements (Eyssautier *et al.*, 2011; Tanaka *et al.*, 2004; Yen *et al.*, 1961). From this point of view, asphaltenes are suspended in the oil as colloids stabilized by resins instead of being dissolved, and their precipitation is triggered when there is a loss of the stabilizing effect of resins (Forte and Taylor, 2015).

However, if asphaltenes have an archipelago structure, they are more likely to form supramolecular assemblies through π - π stacking, hydrogen bonding, and acid-base and van der Waals interactions (Gray *et al.*, 2011). In this case, asphaltenes could self-associate analogously to either linear

polymerization or micellization (Hosseini-Dastgerdi *et al.*, 2015). Yarranton *et al.* (2000) studied asphaltenes self-association using interfacial tension measurements and found no evidence of micelle formation. The linear polymerization model was shown to provide a qualitative fit to the molecular weight of asphaltenes and asphaltene subfractions (Agrawala and Yarranton, 2001; Powers *et al.*, 2016). Gray *et al.* (2011) demonstrated that the supramolecular assembly concept provided a better explanation of numerous experimental observations that models based on aromatic stacking fail to predict. Long *et al.* (2007) studied the stretching behavior of single asphaltene aggregates using single-molecule force spectroscopy (SMFS). They showed that asphaltene aggregates under the pulling of an external force behaved as long-chain polymers. If the polymer approach is correct, then aggregates can be treated as macromolecules and their precipitation as the result of a phase transition (Duran *et al.*, 2019; Yarranton, 2005).

2.3 Asphaltene Precipitation

Asphaltene precipitation is considered to be a thermodynamic liquid-liquid phase separation (Sirota, 2005). It is most commonly observed in the depressurization of live oils and solvent addition to heavy oils. This review focuses on the latter and in particular on poor solvents for asphaltenes (*n*-alkanes). Mixtures of heavy oil and solvents may exhibit multiple phases in equilibrium, including vapor-liquid (VL), liquid-liquid (LL), vapor-liquid-liquid (VLL) and vapor-liquid-liquid-liquid (VLLL) (Azinfar *et al.*, 2018; Badamchi-Zadeh *et al.*, 2009a; Badamchi-Zadeh *et al.*, 2009b; Eastick *et al.*, 1992; Johnston *et al.*, 2017a; Mehrotra and Svrcek, 1988; Nourozieh *et al.*, 2015; Peramanu *et al.*, 1999a; Yazdani and Maini, 2010). The type and number of phases in equilibrium will be determined by the temperature, pressure, and composition of the mixture. In some cases, the second liquid phase is an asphaltene-rich phase and this form of LL phase behavior is often described as asphaltene precipitation because at low temperatures the asphaltene-rich phase appears as glassy particles.

2.3.1 Phase Behavior of Mixtures of Heavy Oil and *n*-Alkanes

Badamchi-Zadeh *et al.* (2009a) studied the phase behavior of mixtures of Athabasca bitumen with propane at temperatures ranging from 10 to 50°C. They observed L and VL regions for feed solvent contents below about 20 wt%. The formation of a LL region at propane contents above 20 wt% was indirectly determined based on density, viscosity, and saturation pressure measurements. Dini

et al. (2016) constructed pressure-composition phase diagrams of propane diluted Peace River bitumen at temperatures between 40 and 120°C. They experimentally observed L, LL, and VL phase equilibria. Also, they predicted VL/VLL boundaries from a limited number of measurements. Mancilla-Polanco *et al.* (2019) mapped the phase behavior of a Western Canadian bitumen diluted with propane at temperatures in the range of 20 to 180°C and pressures up to 10 MPa. They identified both VL and LL regions in the range of conditions studied. The liquid phases were a light propane-rich phase and a heavy bitumen-rich phase that contained asphaltenes, maltenes, and propane. The L/LL boundary shifted to higher propane contents as pressure increased but was insensitive to temperature.

Yazdani and Maini (2010) reported phase behavior data for mixtures of Frog Lake heavy oil diluted with butane at room temperature and different saturation pressures, including solubilities, densities and viscosities. Gao *et al.* (2017) mapped the phase behavior for mixtures of Athabasca bitumen, water, and *n*-butane at temperatures up to 160°C and pressures of up to 10 MPa. They observed up to four phase equilibria including, L, LL, VLL, WL, WLL and WVLL regions. The liquid phases were water, bitumen-rich and *n*-butane-rich phases. Perez Claro *et al.* (2019) studied the phase behaviour of mixtures of bitumen and *n*-butane at temperatures in the range from 20 to 230°C and pressures from 2 to 10 MPa. They observed L, LL and VL regions. The liquid phases were a light *n*-butane-rich phase and a heavy bitumen-rich phase. The L/LL boundary was found to be slightly sensitive to pressure but insensitive to temperature. The heavy liquid phase separated at about 40 wt% *n*-butane content at all experimental conditions.

Zou *et al.* (2007) reported the phase behaviour of mixtures of Athabasca vacuum Bottoms with *n*-pentane at temperatures up to 340°C and pressures of up to 17 MPa. They observed multiphase equilibria of up to four regions (VLLL). Johnston *et al.* (2017b) mapped the phase behavior of mixtures of a Western Canadian bitumen with *n*-pentane at temperatures in the range of 21 to 280°C and pressures of up to 14 MPa. They reported both VL and LL regions, where the liquid phases were a solvent-rich phase and an asphaltene-rich phase. The L/LL boundary was found relatively insensitive to both the temperature and pressure. Figure 2.3 shows a comparison of the pressure-composition phase diagram of propane, *n*-butane, and *n*-pentane diluted bitumen at 90°C. It can be seen that the L/LL boundary shifts to higher solvent contents as the carbon number of the

solvent increases. Also, the saturation pressures (L/VL and LL/VL boundaries) decrease with increasing carbon number as the solvents become less volatile (Perez Claro *et al.*, 2019).

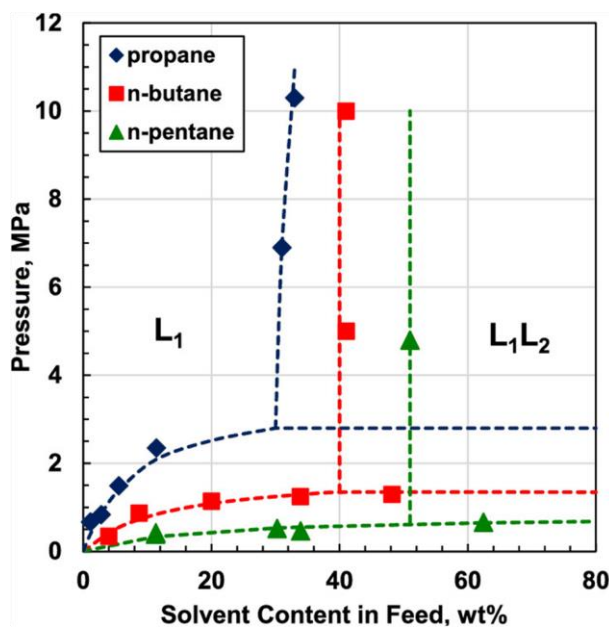


Figure 2.3 Comparison of the phase behavior of mixtures of bitumen diluted with propane, *n*-butane, and *n*-pentane at 90°C. Propane data from Mancilla-Polanco *et al.* (2019), *n*-butane data from Perez Claro *et al.* (2019), and *n*-pentane data from Johnston *et al.* (2017b). Figure adapted from Perez Claro *et al.* (2019).

2.3.2 Asphaltene Precipitation from Mixtures of Heavy Oil and Solvents

The extent of asphaltene precipitation is typically quantified in terms of asphaltene yields; that is, the amount of precipitated asphaltenes relative to feed oil. The feed solvent content at which asphaltenes start precipitating is known as the onset of asphaltene precipitation and delimits the L/LL boundary of the LL region. The lower boundary of the LL region is defined by the saturation pressure of the mixture. A brief discussion of the effect of different variables on the solubility of asphaltenes within the LL region is presented below.

Effect of Temperature

Different trends have been reported in the literature regarding the effect of temperature on asphaltene precipitation. Most investigations have reported an increase in the solubility of asphaltenes (less precipitation, higher onset) with temperature including the following studies:

- Boscan and Kuwait crude oils diluted with *n*-heptane at temperatures from -2 to 80°C (Andersen, 1994).
- Chinese crude oil at temperatures from 20 to 65°C using various *n*-alkanes (Hu and Guo, 2001).
- Cold Lake vacuum residue and an Athabasca atmospheric tower bottom with a blend of two multicomponent solvents (an aliphatic diluent and heavy vacuum gas oil) at temperatures from 60 to 300°C (Hong and Watkinson, 2004).
- a South American crude oil residue with *n*-pentane, *n*-hexane, and *n*-heptane at temperatures from 25 to 98°C (Calles *et al.*, 2008).
- an Athabasca bitumen with *n*-alkanes and an aromatic diluent at temperatures from 22 to 90°C (Bjørøy *et al.*, 2012).
- Alberta bitumens diluted with *n*-pentane, *n*-hexane, and *n*-heptane at temperatures between 25 and 80°C and pressures up to 2.76 MPa (Sattari *et al.*, 2016).

In contrast, some studies have reported a decreased solubility of asphaltenes with temperature. Mitchell and Speight (1973) measured asphaltene precipitation from an Athabasca bitumen diluted with different solvents. They reported increased asphaltene precipitation at high temperatures of up to 70°C, indicating that asphaltenes became less soluble. Fuhr *et al.* (1991) measured the amount and onset of asphaltene precipitation from a North Sea waxy crude oil diluted with different *n*-alkanes at temperatures ranging from 33 to 100°C. They observed an increase in asphaltene yields and a slight decrease in the precipitation onsets with temperature. However, the observed differences in the onsets were within the experimental error of the measurements.

Other authors have reported a minimum or maximum in the solubility of asphaltenes versus temperature. Andersen and Birdi (1990) measured asphaltene precipitation from a Kuwait flash residue at temperatures in the range of 4 to 98°C using *n*-alkanes from *n*-pentane to *n*-octane. Their results showed a minimum in the asphaltene solubility at approximately 25°C. That is, the amount of asphaltene precipitation increased to a maximum at 25°C and then gradually decreased at temperatures over 25°C. This trend was more pronounced in solvents with lower carbon numbers. Johnston *et al.* (2017b) measured asphaltene precipitation yields from a Western Canadian bitumen diluted with *n*-pentane at temperatures from 21 to 250°C and pressures of up to

13.8 MPa. Figure 2.4 shows the reported maximum in asphaltene solubility at approximately 140°C. In other words, at temperatures below 140°C, the asphaltene yields decreased and the precipitation onset increased with temperature, while the opposite occurred at temperatures over 140°C. Peramanu *et al.* (1999a) observed the same trend in asphaltene precipitation onsets from Athabasca and Cold Lake bitumens diluted with *n*-heptane. They reported a maximum in asphaltene solubility at approximately 90°C. In general, temperature appears to have only a small effect on asphaltene solubility and some of the contradictory trends may simply be the result of experimental error.

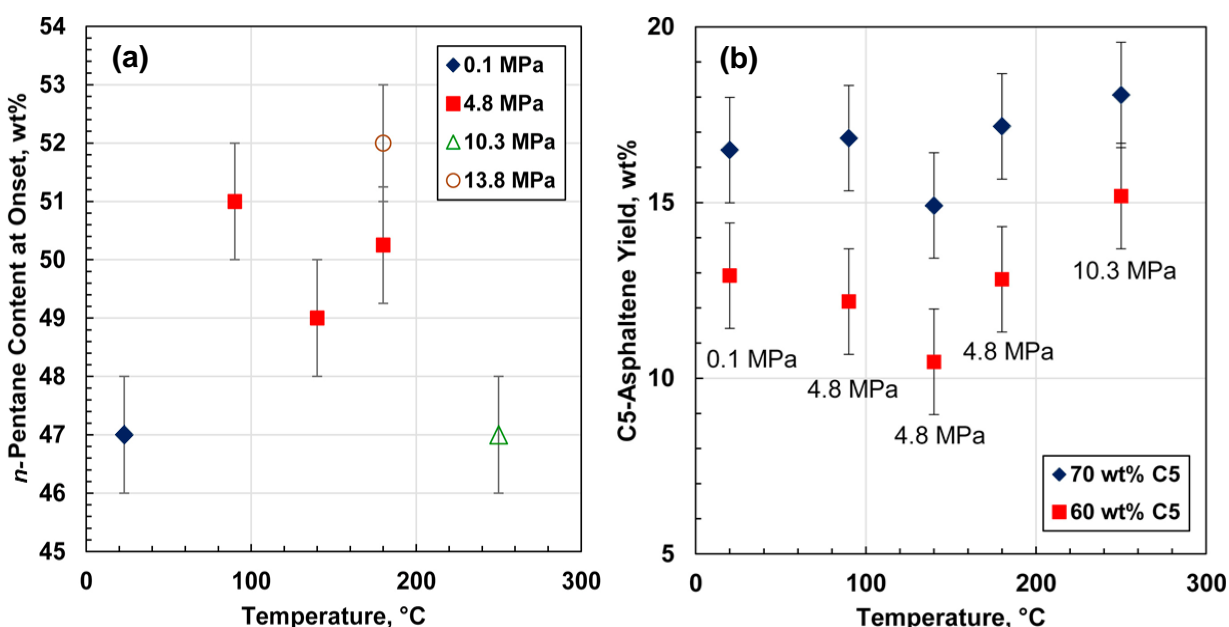


Figure 2.4 Effect of temperature on C5-asphaltene onsets and yields from a Western Canadian bitumen diluted with *n*-pentane: a) onset; b) yield. Figure adapted from Johnston *et al.* (2017b).

Effect of Pressure

Johnston *et al.* (2017b) investigated the effect of pressure on asphaltene precipitation from a Western Canadian bitumen diluted with *n*-pentane at pressures of up to 13.8 MPa. As shown in Figure 2.5, the asphaltene yields decreased with increasing pressure, indicating that the asphaltenes became more soluble as the pressure increased. Also, the extrapolated onsets of asphaltene precipitation increased from 49.5 wt% at 4.8 MPa to 52 wt% at 13.8 MPa. These results are consistent with measured asphaltene yields from Cold Lake and Athabasca bitumen diluted with *n*-

heptane at pressures ranging from 0.1 MPa to 6.9 MPa (Akbarzadeh *et al.*, 2005). The asphaltene yields decrease because the molar volume of the oil decreases and its solubility parameter increases with increasing pressure, which makes it a better solvent for asphaltenes at higher pressures (Hirschberg *et al.*, 1984; Nielsen *et al.*, 1994).

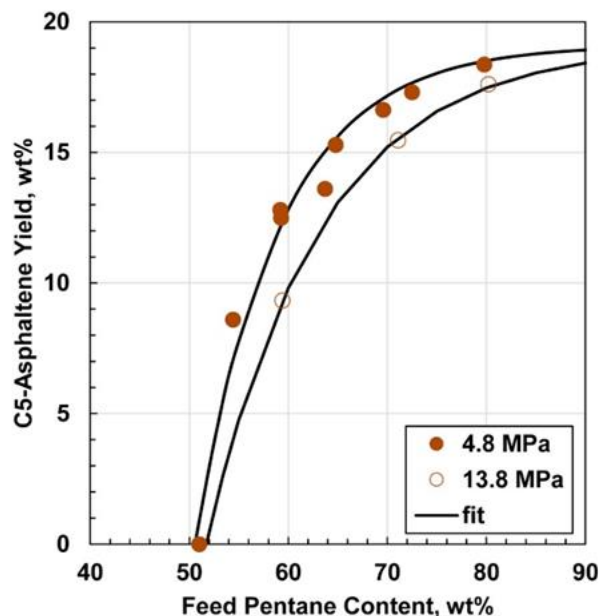


Figure 2.5 Effect of pressure on C5-asphaltene yield from Western Canadian bitumen diluted with *n*-pentane at 180°C. Figure from Johnston *et al.* (2017b).

Effect of Solvent Type and Composition

When a poor solvent (precipitant) is added to an oil, the asphaltene yield increases significantly just above the onset but eventually reaches a plateau as shown in Figure 2.6. The shape of the yield curve is related both to the change in the medium solubility parameters as the precipitant is added and to the distribution of solubility parameters within the asphaltenes. This pattern is observed for all solvents in which asphaltenes are insoluble, although the onset and maximum yield vary from solvent to solvent (Akbarzadeh *et al.*, 2005). Investigations with *n*-alkanes up to a carbon number of 12 have shown that the higher the *n*-alkane carbon number of the solvent, the more soluble are the asphaltenes (lower yields and higher onsets), including the following studies:

- a Peace River bitumen diluted with *n*-pentane, *n*-heptane, and *n*-octane at 22°C and 0.09 MPa (James and Mehrotra, 1988).
- a North Sea waxy crude oil diluted with *n*-pentane to *n*-octane at 0.69 MPa and temperatures from 33 to 100°C (Fuhr *et al.*, 1991).
- a Chinese crude oil diluted with the *n*-alkane series from *n*-pentane to *n*-dodecane, except *n*-undecane (Hu and Guo, 2001).
- two Mexican crude oils diluted with *n*-pentane, *n*-heptane, *n*-nonane, and *n*-dodecane at atmospheric pressure and 20°C (Buenrostro-Gonzalez *et al.*, 2004).
- Athabasca, Cold lake, Lloydminster, Russia, Indonesia, and two Venezuela heavy oils diluted with *n*-pentane to *n*-octane at temperatures between 0 and 100°C and pressures up to 6.9 MPa (Akbarzadeh *et al.*, 2005).
- a South American crude oil residue diluted with *n*-pentane, *n*-hexane, and *n*-heptane at temperatures from 25 to 98°C (Calles *et al.*, 2008).
- Alberta bitumens diluted with *n*-pentane, *n*-hexane, and *n*-heptane at temperatures between 25 and 80°C and pressures up to 2.76 MPa (Sattari *et al.*, 2016).

The decrease in the asphaltene yields with the carbon number of the *n*-alkanes shown in Figure 2.6 results from the decrease of the free energy of mixing. The lower the free energy of mixing, the more compatible the components in the mixture. The free energy of mixing decreases as the difference between the solubility parameters of the medium and the asphaltenes decreases (Barton, 1975; Wiehe *et al.*, 2005). The solubility parameter of the *n*-alkanes increases with carbon number (mainly because the molecules are bigger and have a higher heat of vaporization) and; therefore, the difference between the solubility parameters of the asphaltenes and the precipitant is smaller for higher carbon number *n*-alkanes.

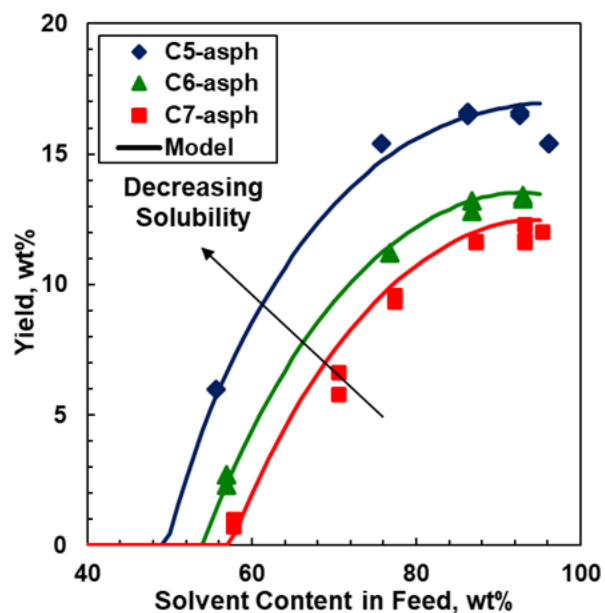


Figure 2.6 Effect of solvent type and composition on asphaltene precipitation yields from Athabasca bitumen diluted with different *n*-alkanes at 23°C and 0.1 MPa. Data from Akbarzadeh *et al.* (2005), figure adapted from Perez Claro (2019).

Studies encompassing higher carbon number *n*-alkanes have shown that the onset of asphaltene precipitation increases with increasing *n*-alkane carbon number up to a certain point, and then decreases with increasing carbon number. Wiehe *et al.* (2005) measured asphaltene precipitation onsets from bitumens and crude oils diluted with the series of *n*-alkanes from *n*-pentane to *n*-hexadecane at room temperature. They demonstrated that the onset of asphaltene precipitation has a maximum at about the carbon number of 9 or 10. Peramanu *et al.* (1999a) measured asphaltene precipitation onsets from Athabasca and Cold Lake bitumens diluted with *n*-heptane, *n*-octane, *n*-decane, and *n*-dodecane at 80°C. According to their results, a maximum in the onset of asphaltene precipitation occurs at approximately the carbon number of 10.

Asphaltene precipitation has also been studied with solvents other than *n*-alkanes, including mixed pure solvents and multicomponent solvents. Mannistu *et al.* (1997) reported asphaltene precipitation yields from solutions of Athabasca C7-asphaltenes dissolved in toluene and titrated with different nonpolar and slightly polar organic solvents. They demonstrated that asphaltene

solubility could be predicted based on solubility parameters for non-polar solvents but only qualitatively for polar solvents.

Andersen and Stenby (1996) measured asphaltene precipitation yields from Boscan and Kuwait crude oils diluted with binary blends of *n*-heptane and toluene at temperatures ranging from 24 to 80°C. They found that asphaltene precipitation decreased as the toluene content in the solvent blend increased. The toluene content increases the solvent "power" of the medium; hence, the solubility of the asphaltenes improves. Bjorøy *et al.* (2012) measured asphaltene yields and onset of precipitation from an Athabasca bitumen diluted with benzotrifluoride, an aromatic solvent structurally like toluene. They reported lower asphaltene yields and higher onset of precipitation compared to *n*-pentane, *n*-hexane, and *n*-heptane. Tharanivasan *et al.* (2009) measured asphaltene precipitation yields and onsets of precipitation from crude oil blends diluted with *n*-heptane or a mixture of toluene and *n*-heptane with similar results.

Hong and Watkinson (2004) reported asphaltene yields from an Athabasca atmospheric tower bottoms and a Cold Lake vacuum residue diluted with multicomponent solvents and their blends. The multicomponent solvents, in order of increasing aromatics content, included an aliphatic diluent, a heavy vacuum gas oil, and a resin enriched fraction. They showed that asphaltene yields decreased with increasing content of resins and aromatics in the solvent blend. The reduction of asphaltene precipitation was more pronounced with the resin enriched fraction.

Effect of Asphaltene Property Distributions

Asphaltenes are, by definition, a solubility class and, as such, consist of thousands of species with different molecular structures (McKenna *et al.*, 2019). Due to their polydispersity and self-association nature, their properties are not given by single values but rather as distribution of properties. A common approach to simplify the characterization is to fractionate the whole asphaltenes by solvent extraction and then measure the properties of the subfractions (Barrera *et al.*, 2013; Gawrys *et al.*, 2006a; Rogel *et al.*, 2015; Yarranton and Masliyah, 1996). A discussion of the distribution of properties from most to least soluble fractions follows.

Fuhr *et al.* (1991) measured the molecular weight and aromatic content of asphaltenes from a North Sea waxy crude. They suggested that the densest, most aromatic, and least soluble asphaltenes are the first ones to precipitate when crude oils are diluted with a poor solvent; therefore, they determine the onset of precipitation. Then, as the solvent content increases, the asphaltenes of lower molecular weight and density gradually precipitate. Barrera *et al.* (2013) fractionated C7-asphaltenes from three Western Canadian bitumens and an Arabian medium crude into two solubility fractions based on their solubility in blends of *n*-heptane and toluene (heptol). They recovered a light cut corresponding to the asphaltenes soluble in the solvent blend, and a heavy cut corresponding to the insoluble asphaltenes. They measured the density and molecular weight of the recovered fractions and constructed property distributions. The molecular weight measurements revealed that the denser fractions had a higher tendency to self-associate with increasing asphaltene concentrations than their less dense counterparts. Additionally, their measurements agreed with the observations that the asphaltenes at the onset of precipitation are the densest and least soluble (Andersen *et al.*, 1997; Fuhr *et al.*, 1991). Note that the average molecular weight of the most soluble cut was approximately 800 g/mol, which falls within the range of the asphaltene monomer molecular weight discussed in Section 2.2.3. Similarly, the density of the asphaltenes gradually increases from the most soluble fraction to the least soluble fraction (Yarranton *et al.*, 2013).

Powers *et al.* (2016) fractionated C7-asphaltenes from native and reacted oils in solutions of heptol. They measured the molecular weights and densities of the asphaltene subfractions. The experimental densities and molecular weights were used as inputs for a MRS model to calculate the asphaltene solubility parameter distribution. They determined the solubility parameters by tuning the model to match the experimental yields of asphaltene precipitation from solutions of heptol. They proposed a new correlation of the asphaltene solubility parameters to their cumulative mass frequency distribution. The solubility parameters increased from the most soluble to the least soluble asphaltenes. Rogel *et al.* (2015) determined the solubility profiles of asphaltenes from different petroleum-derived fluids. The asphaltenes were precipitated out of solution using *n*-heptane and retained in a packed column. They then eluted the asphaltenes using mixtures of dichloromethane and ethanol, obtaining different asphaltene fractions. In their approach, the asphaltenes were eluted from the most soluble (low solubility parameter) to the least soluble (high

solubility parameter). Aguiar *et al.* (2014) determined distributions of solubility parameters from solubilization heats measured using microcalorimetry. They found that asphaltenes with higher polarity had a higher upper limit in their solubility parameter distribution.

Andersen *et al.* (1997) studied the elemental composition of the C7-asphaltenes from a Boscan crude oil. The asphaltenes were obtained by precipitation and by solubility in blends with varying ratios of heptane and toluene. In the precipitation approach, they directly precipitated asphaltenes from the crude oil diluted with heptol. In the solubility methodology, the recovered asphaltenes were the undissolved fractions of asphaltenes in solutions of heptol. They found that the H/C ratio decreased, and the nitrogen-to-carbon (N/C) ratio increased from the most soluble to the least soluble fractions of the asphaltenes. In other words, the asphaltenes precipitated near the onset are the most polar and aromatic. Yang *et al.* (2004) precipitated asphaltenes from an Athabasca bitumen diluted with *n*-heptane and determined their elemental composition. Their H/C ratios followed the same trend reported by Andersen *et al.* (1997). However, they did not find significant differences in the N/C ratios among the asphaltene subfractions. They found that the metal and metalloporphyrin contents were lower in the most soluble fractions and higher in the least soluble fractions near the onset of precipitation. Similarly, Bjorøy *et al.* (2012) found that the sulfur content was slightly increased in the least soluble asphaltenes. Calles *et al.* (2008) measured asphaltene yields from a South American crude oil residue diluted with *n*-pentane, *n*-hexane, and *n*-heptane at temperatures ranging from 25 to 98°C. They found that diluting crude oil with heavier *n*-alkanes resulted in lower asphaltene yields. The elemental and nuclear magnetic resonance (NMR) spectroscopy analysis showed that heavier *n*-alkanes yield more aromatic asphaltenes, consistent with the least soluble material having the greatest aromaticity.

Asphaltene-Rich Phase Morphology

The morphology of precipitated asphaltenes has been found to be dependent on the proximity to their glass transition temperature. At low temperatures below their glass transition, asphaltenes precipitate out of solution as a glassy and highly viscous material that forms fractal-like aggregates. However, at higher temperatures above their glass transition temperature, asphaltenes precipitate as a liquid-like material with low viscosity (Sirota, 2005). Zhang *et al.* (2004) studied the glass transitions temperature of C7-asphaltenes from vacuum residues of Iranian, Khafji, Kuwait, and

Maya crude oils using differential scanning calorimetry. They reported glass transition temperatures in the range of 120 to 130°C. Furthermore, they observed that asphaltenes reached the liquid state at temperatures between 220 and 240°C.

Johnston *et al.* (2017b) examined the morphology of the asphaltene-rich phase from Western Canadian bitumen diluted with *n*-pentane using a high-pressure microscope. They found that the asphaltene-rich phase precipitated as glassy particles at temperatures below 90°C and as liquid droplets at temperatures above 140°C. They attributed the change in morphology to a gradual glass transition between 90 and 140°C. Similarly, Mancilla-Polanco *et al.* (2019) studied the morphology of the heavy pitch phase of Western Canadian bitumen diluted with propane. Phase composition measurements indicated that the pitch phase consisted of asphaltenes, maltenes, and propane. They observed that near the onset of precipitation, the pitch phase behaved as particles at temperatures below 50°C. At temperatures above 90°C, the pitch phase appeared as droplets that coalesced into a continuous liquid phase.

2.4 Asphaltene Precipitation Models

The main models to predict asphaltene precipitation include cubic equations of state (CEoS), the Cubic Plus Association equation of state (CPA EoS), the Perturbed-Chain Statistical Associating Fluid Theory equation of state (PC-SAFT EoS), and the regular solution theory. CEoS are the most common approach given the simplicity of the model. However, they require extensive tuning and composition dependent binary interaction parameters to model asphaltene precipitation from different solvents (Johnston *et al.*, 2017a; Mancilla-Polanco *et al.*, 2019). The CPA EoS and PC-SAFT EoS incorporate an association term to represent the self-association of asphaltene monomers. However, the PC-SAFT EoS typically neglects self-association under the assumption that dispersion forces are the dominant interactions in asphaltene precipitation. Both CPA EoS and PC-SAFT EoS can model asphaltene precipitation with conventional binary interaction parameters but must be tuned for each solvent. All of the above equations of state may be tuned to match saturation pressures, onsets of asphaltene precipitation, and to some extent, asphaltene yields.

An alternative to the equations of state (EoS) is the regular solution model. It has proven successful in modeling asphaltene yields and onsets of precipitation from crude oils diluted with *n*-alkanes

(Akbarzadeh *et al.*, 2005; Alboudwarej *et al.*, 2003). This approach can to some extent predict the effect of different solvents after tuning to precipitation data in one solvent. However, its application is limited to model liquid-liquid or liquid-solid equilibrium. When dealing with VLL equilibrium, a separate flash calculation to split the crude oil into vapor and liquid is required (Hirschberg *et al.*, 1984; Kawanaka *et al.*, 1991). However, using two different liquid phase models is thermodynamically inconsistent and may lead to multiple solutions of the flash calculation (Pedersen and Christensen, 2007). A more detailed review of the capabilities of each model follows.

2.4.1 Cubic Equation of State

Cubic equations of state are simple thermodynamic models widely used to predict the phase behaviour and properties of pure hydrocarbons and reservoir fluids (Riazi, 2005). They are able to represent the properties of liquid and vapor phases with a single equation, which guarantees thermodynamic consistency (Whitson and Brulé, 2000). Numerous cubic equations of state have been proposed, including those by van der Waals (1873), Redlich and Kwong (1949), Soave (1972), and Peng and Robinson (1976). The Peng-Robinson equation of state (PR EoS) (Peng and Robinson, 1976) is extensively used in petroleum engineering applications and is given by:

$$P = \frac{RT}{v-b} - \frac{a\alpha(T_r, \omega)}{v(v+b) + b(v-b)} \quad (2.1)$$

where P is the absolute pressure, R is the universal gas constant, T is the absolute temperature, v is the molar volume, a represents the intermolecular attraction forces, b represents the volume of the molecules, $\alpha(T_r, \omega)$ is a dimensionless function of the reduced temperature, T_r , and the acentric factor, ω .

One shortcoming of cubic equations of state is their poor estimation of liquid phase densities. Pénélox *et al.* (1982) addressed the inaccuracy of the density predictions with the introduction of the volume-shift or volume translation parameter to the Soave-Redlich-Kwong equation of state (SRK EoS). While the volume translation parameter corrects the molar volume and phase density predictions, it does not affect the phase equilibrium calculation. The concept of volume translation parameter was extended to the PR EoS by Jhaveri and Youngren (1988). The PR EoS including the volume translation parameter, c , is given by:

$$P = \frac{RT}{v-b} - \frac{a\alpha(T_r, \omega)}{(v+c)(v+2c+b) + (b+c)(v-b)} \quad (2.2)$$

Fahim *et al.* (2001) used the PR EoS to model asphaltene yields and onsets of asphaltene precipitation from a Kuwaiti crude oil diluted with *n*-alkanes from *n*-hexane to *n*-decane at temperatures from 25 to 45°C and pressures up to 28 MPa. The critical properties of the deasphalted oil, asphaltenes, and resins were estimated from the Joback group contribution method. They tested this methodology by comparing the molar volume from the estimated critical properties against the measured molar volume. The modeling results for the diluted crude oil were in good agreement with their experimental data. Additionally, their model was validated with a dataset of asphaltene precipitation from pressure depletion reported by Nghiem and Coombe (1997).

Tavakkoli *et al.* (2010) used a vapor-liquid-solid equilibrium model based on a cubic equation of state to model saturation pressures and asphaltene precipitation from an Iranian heavy oil under carbon dioxide injection and pressure depletion conditions. They treated the precipitated solid phase as pure asphaltenes. The fugacities of the components in the vapor and liquid phase were given by the PR EoS including the volume translation parameter. Their model was able to capture the trends of asphaltene precipitation of their measurements and the experimental data of Burke *et al.* (1990).

Johnston *et al.* (2017a) used the PR EoS with volume translation parameter to model saturation pressures, onsets, and yields of asphaltene precipitation from a Western Canadian bitumen diluted with *n*-pentane at temperatures from 23 to 280°C and pressures up to 13.8 MPa reported by Johnston *et al.* (2017b). They divided the maltenes into ten pseudo-components based on a Gaussian extrapolation of their distillation assay. They treated asphaltenes either as a single pseudo-component or five pseudo-components and reported that the modeling results were similar regardless of the assumption. The model performance was tested using several mixing rules. The best agreement with the experimental data was obtained with the compositionally dependent van der Waals mixing rules. This model was able to fit the trends of the asphaltene precipitation yields and phase boundaries.

2.4.2 Cubic Plus Association Equation of State

The Cubic Plus Association equation of state (CPA EoS) developed by Kontogeorgis *et al.* (1996) more accurately represents the phase equilibrium of associating fluids by the addition of an association term from the Wertheim perturbation theory to the physical term of the SRK EoS. The CPA EoS in terms of pressure (Kontogeorgis *et al.*, 2006) with the association term derived by Michelsen and Hendriks (2001) is given below:

$$P = \frac{RT}{v-b} - \frac{\alpha(T)}{v(v+b)} - \frac{1}{2} \left(\frac{RT}{v} \right) \left(1 + \frac{1}{v} \frac{\partial \ln g}{\partial (1/v)} \right) \sum_i x_i \sum_{A_i} (1 - X_{A_i}) \quad (2.3)$$

where P is the absolute pressure, R is the universal gas constant, T is the absolute temperature, v is the molar volume, $\alpha(T)$ is the energy parameter, b is a parameter for non-associating components, g is the radial distribution function, x_i is the mole fraction of component i , subscript A_i denotes sites of type A on molecules of component i , and X_{A_i} is the fraction of sites A on molecules i not bonded to other active sites. The radial distribution function, g , is given by:

$$g = \frac{1}{1 - \frac{1.9}{4} \left(\frac{b}{v} \right)} \quad (2.4)$$

The energy parameter, $\alpha(T)$, is given by:

$$\alpha(T) = a_0 \left[1 + c_1 (1 - \sqrt{T_r}) \right]^2 \quad (2.5)$$

where T_r is the reduced temperature. The last term on equation 2.3 is the association term and depends on the type and number of association sites on the molecules of each associating component. The associating components may have up to four association sites and must be classified as either proton donors or proton acceptors with a positive or negative sign, respectively. The fraction of unbonded sites, X_{A_i} , is given by:

$$X_{A_i} = \frac{1}{1 + \frac{1}{v} \sum_j x_j \sum_{B_j} X_{B_j} \Delta^{A_i B_j}} \quad (2.6)$$

The association due to hydrogen bonding of like ($i=j$) and unlike ($i \neq j$) components is known as self-association and cross-association, respectively. The association strength, $\Delta^{A_i B_j}$, between sites A and B on the molecules of components i and j is given by:

$$\Delta^{A_i B_j} = g \left[\exp \left(\frac{\epsilon^{A_i B_j}}{RT} \right) - 1 \right] b_{ij} \beta^{A_i B_j} \quad (2.7)$$

where $\epsilon^{A_i B_j}$ is the association energy and $\beta^{A_i B_j}$ is the association volume. There are three parameters for pure non-associating components (a_0 , b , c_1) and two parameters for pure associating components ($\epsilon^{A_i B_j}$, $\beta^{A_i B_j}$) required to solve the CPA EoS. All these parameters may be fitted using

experimental vapor pressure and saturated liquid density data. Alternatively, in the case of non-associating components, they may be determined from their critical properties and acentric factor (Kontogeorgis *et al.*, 2006).

Li and Firoozabadi (2010) used a CPA EoS to model saturation pressures and asphaltene precipitation from seven live oils due to carbon dioxide injection and pressure depletion. They assumed that the physical contribution term was given by the PR EoS and that the cross-association energy between the asphaltenes and heavy molecules was temperature-dependent. Their model captured the temperature and pressure effect on the experimental asphaltene yields and asphaltene onset pressures. Arya *et al.* (2017) applied the CPA EoS to model asphaltene precipitation yields and onsets from eight different light and heavy oils diluted with *n*-alkanes. They tested various characterization approaches for the asphaltenes and maltenes with different numbers of pseudo-components. They found that one asphaltene pseudo-component was sufficient to fit the onset of asphaltene precipitation. The number of maltenes pseudo-components did not affect the asphaltene solubility. Their model was also able to fit experimental asphaltene yields and onsets of diluted crude oil blends.

Zhang *et al.* (2019) tested the capability of the CPA EoS to fit phase behaviour data from bitumen diluted with *n*-alkanes at temperatures up to 250°C and pressures up to 13.8 MPa, including saturation pressures, phase compositions, asphaltene yields, and onsets of precipitation. The maltenes fraction was considered non-associating. They divided the asphaltenes into several pseudo-components that self-associated with other asphaltenes. Note that it was required to allow the cross-association of the asphaltenes with the maltene pseudo-components and the solvent to match the phase behavior data. Their model was able to fit the experimental data generally to within the error of the measurements, but it was not predictive for other solvents or oils without additional adjustments.

2.4.3 Perturbed-Chain Statistical Associating Fluid Theory

The Perturbed-Chain Statistical Associating Fluid Theory equation of state (PC-SAFT EoS) developed by Gross and Sadowski (2001) is founded on the Statistical Associating Fluid Theory equation of state (SAFT EoS) proposed by Chapman *et al.* (1990). The PC-SAFT EoS considers

the reference fluid consists of hard-chain molecules in place of the hard-spheres used for the dispersion contribution in other versions of the SAFT EoS. That is, the dispersion term accounts for attraction between chains rather than the attraction between unbonded spherical molecules. The chain and association contribution terms remain as in the original SAFT EoS and come from the Wertheim perturbation theory (Von Solms *et al.*, 2006). The PC-SAFT EoS in terms of residual Helmholtz free energy, A^{res} , is given by (Sadowski, 2011):

$$A^{res} = A^{hc} + A^{disp} + A^{assoc} \quad (2.8)$$

where A^{hc} is the hard-chain contribution which corresponds to sum of the hard-sphere and chain formation contributions, A^{disp} is the contribution due to non-specific attractive molecular interactions, and A^{assoc} is the association contribution due to very strong short-range attractive molecular interactions (*i.e.*, hydrogen bonding). There are three parameters used in the PC-SAFT EoS to describe pure non-associating components: the segment diameter (σ), the segment energy (ε/k), which accounts for the interactions between segments, and the segment number (m) that represents the departure from sphericity of the molecules. The PC-SAFT EoS requires two additional parameters to represent associating molecules, the association volume ($\kappa^{A_i B_i}$), and the association strength ($\varepsilon^{A_i B_i}/k$). The value of these parameters for several pure components were reported by Gross and Sadowski (2001, 2002).

Gonzalez *et al.* (2005) applied the PC-SAFT EoS to study the effect of gas injection (carbon dioxide, methane, and ethane) on the saturation pressures and onsets of asphaltene precipitation from a model live-oil and a recombined oil. They dropped the association term from the PC-SAFT EoS under the assumption that the molecular size and London dispersion forces dominated asphaltene aggregation and precipitation. Asphaltenes were a single pseudo-component instead of several self-associating components. The modeling results were in good agreement with the precipitation onsets. Additionally, the performance of the model was tested on asphaltene precipitation due to pressure depletion before and after nitrogen injection.

Panuganti *et al.* (2012) proposed an improved methodology to characterize crude oils for asphaltene precipitation modeling with the PC-SAFT EoS. They validated the robustness of the new characterization procedure by modeling the saturation pressures and onsets of asphaltene precipitation due to the pressure depletion of three different live oils. The proposed

characterization significantly improved the match to the experimental data compared to the modeling results obtained from the SRK EoS and the PC-SAFT EoS with the old methodology. Zúñiga-Hinojosa *et al.* (2014) modeled the yields and onsets of asphaltene precipitation from heavy oil diluted with *n*-alkanes reported by Sabbagh *et al.* (2006) using the PC-SAFT EoS. They treated asphaltenes as a distribution of nanoaggregates with molecular weights given by a gamma function rather than self-associating components. They proposed correlations of the asphaltenes non-associating PC-SAFT parameters (σ , ε/k , m) to their subfractions molecular weight. In this study, the precipitation was considered a LL phase separation, where only asphaltenes partitioned to the heavy phase.

2.4.4 Regular Solution Theory

Regular solutions are defined as the solutions whose components mix with no excess entropy at constant volume (Hildebrand *et al.*, 1970). These types of solutions have an ideal entropy of mixing despite having a non-ideal enthalpy of mixing. That is, regular solutions mix randomly even in the presence of specific solute-solvent interactions (Barton, 1975). The activity coefficients are determined from an enthalpic contribution only and are given by:

$$\ln \gamma_i^\alpha = \frac{v_i}{RT} (\delta_i - \delta^\alpha)^2 \quad (2.9)$$

where v_i and δ_i are the molar volume and solubility parameter of component i at the temperature and pressure of the system, δ^α is the volumetric average solubility parameter of all the components at the temperature and pressure of the system, R is the universal gas constant, T is the absolute temperature, and superscript α denotes the phase. The solubility parameter is defined as the positive square root of the cohesive energy density (Prausnitz *et al.*, 1999):

$$\delta_i = \sqrt{c} = \sqrt{\frac{\Delta u_{vap}}{v_i}} \quad (2.10)$$

where Δu_{vap} is the energy of complete vaporization. The cohesive energy density, c , refers to the energy associated with the molecular interactions between the different species in solution.

The entropic contribution term in the regular solution theory was modified to account for significant molecular size disparities using the Flory-Huggins lattice theory (Flory, 1941; Huggins, 1941). In this case, the activity coefficients are calculated as the sum of the Flory-Huggins entropic contribution and the original regular solution enthalpic contribution:

$$\ln \gamma_i^\alpha = \ln \left(\frac{v_i}{v^\alpha} \right) + 1 - \frac{v_i}{v^\alpha} + \frac{v_i}{RT} (\delta_i - \delta^\alpha)^2 \quad (2.11)$$

where v^α is the molar average of the molar volume of all the components at the temperature and pressure of the system. This approach was first applied by Hirschberg *et al.* (1984) to model the precipitation of asphaltenes from light crude oils diluted with various liquid *n*-alkanes and gases. They treated asphaltenes as a single pseudo-component and determined its molar volume and solubility parameter from titration experiments on dead oil. However, the assumption of a single asphaltene pseudo-component led to the underprediction of the asphaltene yields. Note that they used the SRK EoS to model the VL equilibrium and determine the composition of the liquid phase. Then, they applied the Flory-Huggins approach to model asphaltene precipitation in the resulting liquid phase.

Kawanaka *et al.* (1991) used a variation of the entropic term based on the polydisperse polymer theory of Scott and Magat (1945). They considered that asphaltenes consisted of a heterogeneous mixture of components and correlated their properties to their molecular weights obtained from a gamma function. They tested their model on asphaltene precipitation datasets of *n*-alkane diluted crude oil reported by Hirschberg *et al.* (1984). It predicted the asphaltene yields for the *n*-pentane and *n*-decane diluted crude oil but overpredicted it in the case of *n*-heptane.

Rassamdana *et al.* (1996) modeled asphaltene precipitation from an Iranian light crude oil diluted with the series of *n*-alkanes from *n*-pentane to *n*-decane, except *n*-nonane, using the modeling approach of Hirschberg *et al.* (1984). They treated asphaltene precipitation as solid-liquid phase separation and determined the solubility parameter of the liquid phase with the aid of the SRK EoS. The reported modeling results were in poor agreement with the experimental data, likely due to the assumption of a single asphaltene pseudo-component.

Yarranton and Masliyah (1996) modeled the solubility of Athabasca asphaltenes in solutions of toluene and *n*-hexane using a solid-liquid equilibrium model where the solid phase was considered to be an amorphous glass and thermodynamically equivalent to a liquid phase. Their model divided asphaltenes into several fractions and determined their distribution of properties from correlations of the molar volume and solubility parameter to the molar mass. They demonstrated that the implemented property distributions led to accurate predictions of the onset and amount of

asphaltene precipitation. Alboudwarej *et al.* (2003) adapted the regular solution approach of Yarranton and Masliyah (1996) to model asphaltene precipitation from heavy oil and bitumen diluted with *n*-alkanes at ambient conditions. They constrained their liquid-liquid equilibrium model to allow only the partition of asphaltenes to the heavy liquid phase.

Akbarzadeh *et al.* (2005) extended the application of this model to higher temperatures and pressures and allowed the resins to partition along with the asphaltenes. They reported that once their model was tuned to fit asphaltene precipitation data from bitumen diluted with an *n*-alkane, typically *n*-heptane, it was able to predict the effect of other *n*-alkanes without additional adjustment. The regular solution approach has also been validated to model asphaltene precipitation from crude oil blends, live oils, and reacted oils (Powers *et al.*, 2016; Rodriguez *et al.*, 2019; Tharanivasan *et al.*, 2009, 2011; Yarranton *et al.*, 2018). Very recently, this model was modified to allow partitioning of all components to both liquid phases (Ramos-Pallares and Yarranton, 2020). In this study, the MRS model from Akbarzadeh *et al.* (2005) is extended to multicomponent solvents. A more detailed description of the model and its assumptions is presented in Chapter 4.

CHAPTER 3: EXPERIMENTAL METHODS

This chapter describes the experimental methods and materials used to measure the onset and yield of asphaltene precipitation from bitumen diluted with multicomponent solvents. The onset of asphaltene precipitation is defined here as the lowest solvent content at which asphaltene precipitation occurs, as shown in Figure 3.1. Asphaltene yield is the mass of asphaltene precipitation relative to the mass of feed bitumen. Asphaltene precipitation onsets and yields at ambient conditions (21°C, 0.1 MPa) were measured gravimetrically in test tubes. Asphaltene onsets and yields at elevated temperature and pressure were measured in a high-pressure microscope (HPM) and a blind cell apparatus, respectively. The properties of the bitumens used in this thesis and a detailed description of each experimental method are presented below.

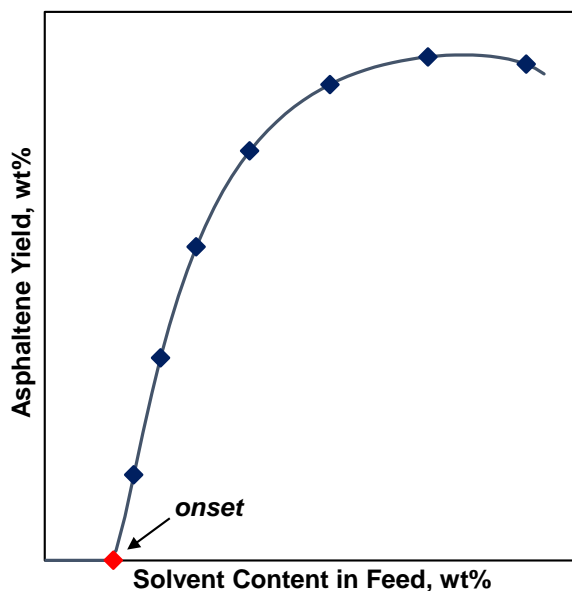


Figure 3.1 Schematic of a typical asphaltene solubility curve for an *n*-alkane diluted bitumen.

3.1 Materials

Two bitumen samples were used in this study: WC-B-A3 and WC-B-B5 bitumen, where WC indicates Western Canada, B indicates bitumen, and the final term indicates the source reservoir. The WC-B-A3 is a bitumen from a SAGD process supplied by CNOOC International Ltd. (JACOS). The bitumen sample originated from a commercial process and its water content was less than 1.5 wt%.

The WC-B-B5 is a well-head sample from a SAGD process from a Western Canadian reservoir provided by Shell. The sample had been dewatered prior to delivery and the water content was less than 1 wt%.

Table 3.1 lists selected properties and SARA assays of the two bitumen samples. The WC-B-B5 assay was previously reported by Perez Claro *et al.* (2019). The WC-B-A3 assay was measured in this study following the procedure from Tharanivasan *et al.* (2011). In the assay of the WC-B-B5 bitumen, distillates were first separated from the oil and the residue was fractionated into SARA cuts. In the SARA assay of the WC-B-A3 bitumen, the oil was fractionated directly into SARA cuts (conventional basis). The modeling uses the conventional basis as an input. Therefore, the SARA assay with distillates was converted to a conventional basis as shown in Appendix A.

The solvents considered include blended pure solvents and multicomponent petroleum solvents. Toluene ($\geq 99.5\%$ purity), *n*-pentane ($\geq 98\%$ purity), and *n*-heptane ($\geq 99\%$ purity) were purchased from Fisher Scientific. *n*-Hexane ($\geq 95\%$ purity) and cyclohexane ($\geq 99\%$ purity) were purchased from EMD Millipore and VWR International, LLC, respectively. The condensate samples (Condensate 1 and Condensate 2) used in this thesis were supplied by Nexen, the diesel samples (Diesel 1 and Diesel 3) were obtained from Shell, and the kerosene (Kerosene 1) and naphtha (Naphtha 1) were supplied by Suncor. A C30+ compositional analysis was performed on all of the petroleum solvents by Core Laboratories Canada Ltd. The GC assays of the petroleum solvents are provided in Appendix A.

Table 3.1 Selected properties and SARA assays of the WC-B-A3 and WC-B-B5 bitumens; data for the WC-B-B5 bitumen is from Perez Claro *et al.* (2019). “C5-asphaltenes” are the *n*-pentane insoluble asphaltenes.

Property	WC-B-A3 measured	WC-B-B5 measured	WC-B-B5 converted
Specific Gravity	-	1.020	-
Viscosity at 50°C, 1 atm, cP	-	7,600	-
Distillates, wt%	-	19.5	-
Saturates, wt%	20.0	7.7	17.4
Aromatics, wt%	37.9	29.8	39.6
Resins, wt%	21.9	18.9	18.9
C5-asphaltenes, wt%	20.1	23.5	23.5
Toluene Insolubles, wt%	0.1	0.6	0.6

3.2 Asphaltene Yield and Onset Measurement at Ambient Conditions

Yields for Blended Pure Solvents

To determine asphaltene yields at ambient conditions (21°C, 0.1 MPa), a series of solutions of bitumen and solvent with different solvent contents were prepared in 30 cm³ centrifuge tubes with known masses of bitumen and solvent. The solvents included *n*-pentane, *n*-hexane, *n*-heptane, toluene, cyclohexane, and blends of these components. The solutions were sonicated and agitated for 1 hour and left to settle for 24 hours. Each mixture was then centrifuged at 4000 rpm for 8 minutes and the supernatant was pipetted out of the tubes. The precipitate was washed with approximately 20 cm³ of the same pure solvent or solvent blend, sonicated and agitated for 1 hour, and left to settle for 24 hours. The samples were then centrifuged at 4000 rpm for 8 minutes and the supernatant was removed. Finally, the precipitate was dried in an oven under vacuum at a temperature of at least 60°C until the mass was constant.

The precipitate contains mineral solids and organic compounds that co-precipitate with the asphaltenes but are insoluble in toluene. The concentration of toluene insolubles (TI) in the bitumen was quantified in their SARA analysis. Asphaltene precipitation yields were calculated as the mass of precipitate divided by the initial mass of bitumen. The yields were then adjusted to a TI-free basis. The data are reported as an asphaltene solubility curve; that is, a plot of the yield

of precipitated TI-free asphaltenes versus the weight fraction of solvent. The repeatability of the yields is ± 0.5 wt%.

Yields for Multicomponent Solvents and their Blends

The same method was used with the following modifications. The precipitate from bitumen diluted with each of the petroleum solvents was washed with *n*-pentane in order to minimize the residue from the non-volatile part of the petroleum solvent. The precipitate from bitumen diluted with blends of kerosene and diesel with *n*-heptane was washed with the same solvent blend. In addition, the mass of wet precipitate before drying was determined for the kerosene blends and the diesel blends.

Note that at the experimental conditions, the heavy components of diesel and kerosene did not evaporate. Therefore, the dried mass of precipitate was corrected by deducting the residual solvent. The maximum percentage of the solvent blend that evaporated in the oven (E%) was determined in a separate experiment where a sample of the solvent blend was dried at the same conditions used to dry the precipitate. The initial mass of solvent in the precipitate was assumed to make up 85% of the wet precipitate mass based on previous work (Yarranton *et al.*, 2011). The mass of residual solvent is then (100-E%) of 85% of the wet precipitate mass. The maximum percentage of solvent blend that evaporated in the oven (E%) ranged between 98 and 100%. The mass correction method was validated by measuring the asphaltene yield from bitumen diluted with the heavy condensate (Condensate 1) using the above method. The asphaltene yield was compared to the asphaltene yield obtained with an *n*-pentane wash. Figure 3.2 shows that the asphaltene yield calculated using the residual solvent correction was within the error of the measurement of the asphaltene yield with *n*-pentane wash. Note that the asphaltene yield from Condensate 1 in Figure 3.2 does not level off at the higher solvent contents as the asphaltene yield from *n*-pentane shown in Figure 3.3. This trend is expected because the asphaltene yield from bitumen diluted with Condensate 1 is well below the total C5-asphaltene content of the bitumen. The plateau in the yield curves is more pronounced in poor solvents where the amount of precipitated asphaltene quickly approaches the total C5-asphaltene content of the bitumen near the onset of precipitation.

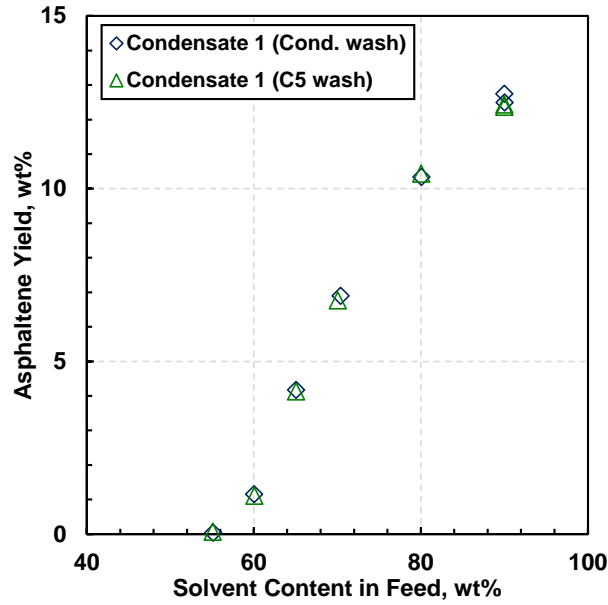


Figure 3.2 Asphaltene yield from WC-B-A3 bitumen diluted with condensate 1 at 21°C and 0.1 MPa using two different solvents to wash the precipitate: a) condensate; b) *n*-pentane.

Asphaltene Precipitation Onset

The precipitation onsets at ambient conditions were determined by fitting the yield data with the following expression,

$$Y_A = C[1 - \exp\{-D(w_S - w_{onset})\}] \quad (3.1)$$

where Y is the yield in wt%, w is mass fraction, the subscripts A , S , and $onset$, denote the asphaltenes, solvent content, and fitted solvent content at the onset of precipitation, respectively, and C and D are the fitted constants. Figure 3.3 shows the measured and fitted yield data for *n*-pentane diluted WC-B-A3 bitumen at 21°C and 0.1 MPa. The fitted onsets determined with this method have been shown to be within ± 1.5 wt% of the onsets determined from microscopic observation (Johnston *et al.*, 2017b), as long as there are sufficient yield data to establish a trend.

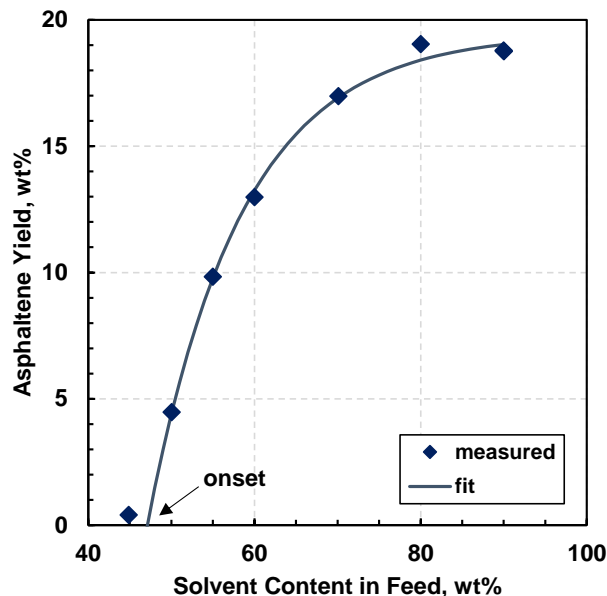


Figure 3.3 Determination of the onset of asphaltene precipitation from measured asphaltene yield curve for WC-B-A3 bitumen diluted with *n*-pentane at 21°C and 0.1 MPa. Note that the first data point appears to have a non-zero yield but is in fact below the onset of precipitation. It has a non-zero yield because some precipitation occurs in the mixing process due to localized areas of high solvent concentration.

3.3 Asphaltene Onset Measurement above Atmospheric Pressure

The asphaltene onset point above atmospheric pressure was measured by titrating the WC-B-A3 bitumen with solvent using a high-pressure microscope (HPM) coupled with a PVT apparatus. The solvents used to titrate the bitumen were a binary blend of 85 wt% *n*-pentane and 15 wt% toluene and a binary blend of 75 wt% *n*-pentane and 25 wt% cyclohexane. The onsets were determined at temperatures of 21 and 180°C and pressure of 10 MPa to maintain the solvent/bitumen mixture above its saturation pressure (liquid state). The experimental procedure to determine the saturation pressure is provided in Appendix B.

Figure 3.4 shows a schematic of the HPM system, which consists of a cell with two sapphire windows, a light source, and a high focal length camera connected to a computer in order to capture digital images and video. The gap between the windows was set to 100 μm. The HPM system was placed in-line between two high pressure cylinders equipped with floating pistons and magnetic

stirrers, both of which were connected to a computer-controlled pump and a back pressure regulator. The HPM is rated for temperatures from 20 to 200°C and pressures up to 138 MPa.

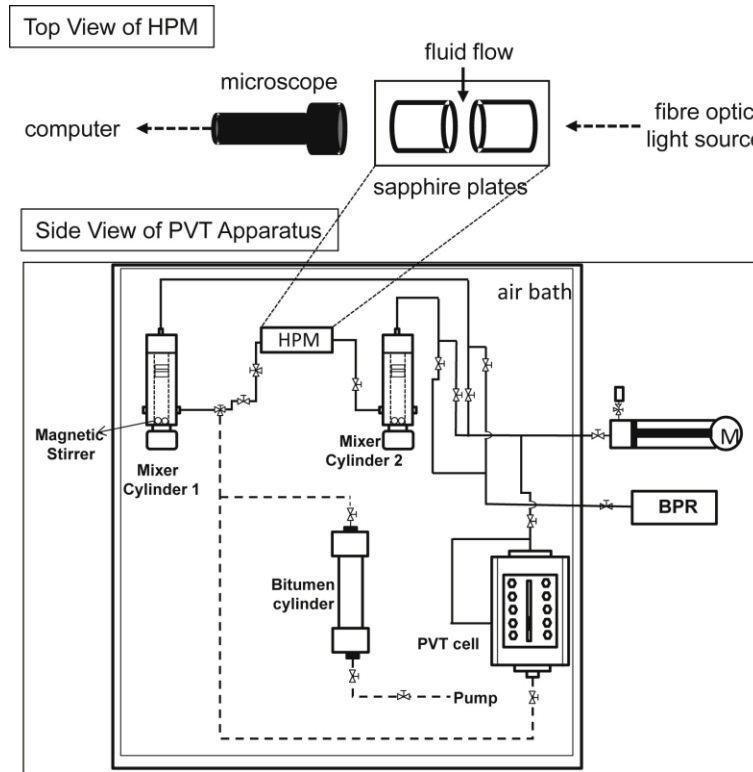


Figure 3.4 Schematic of the High-Pressure Microscope (HPM) system. Figure from Johnston *et al.* (2017b).

The onsets of asphaltene precipitation were determined as described by Agrawal *et al.* (2012). Before any measurement, the HPM system was flushed several times with toluene and then vacuum cleaned at 100°C. The floating pistons of both mixer cylinders were displaced to the bottom of each cylinder and the back pressure regulator (BPR) was set to the injection pressure. The initial pump reading, the mass of the hydraulic oil in the BPR container, the temperature, and the pressure of the system were recorded.

A target amount of WC-B-A3 bitumen was injected into the mixer cylinder 1. The final pump reading, the mass of hydraulic oil displaced to the BPR container, the temperature, and the pressure of the system after the injection were recorded. The volume of injected bitumen was determined in two ways: 1) from the difference between the initial and final pump readings; 2) from the volume

of displaced hydraulic oil plus the dead volume of the HPM system. The mass of injected bitumen was calculated from the average value determined from the two volumes mentioned above and the experimental density of the bitumen at the injection conditions. The volume of displaced hydraulic oil was in average within 3% of the volume from the pump readings.

The solvent blend was first injected into the PVT cell at a pressure above its saturation pressure (liquid state). The solvent from the PVT cell was then injected into the bitumen step-wise at a flow rate of 10 cm³/h for each step. This flow rate was chosen to avoid localized high concentrations of solvent which may trigger the premature precipitation of asphaltenes. The magnetic stirrer in the mixer cylinders was turned on for injections. After each injection, the volume of the injected solvent was determined from cathetometer readings on the sight glass of the PVT cell and verified with pump displacement volumes. The fluid was moved back and forth between the two cylinders until a uniform mixture was observed in the HPM cell and then an image was taken. This procedure was repeated for each incremental injection of solvent until an asphaltene-rich phase was observed. At temperatures below approximately 90°C (depending on the solvent), the asphaltene-rich phase usually appears as particles but at higher temperatures it appears as liquid droplets that settle into a continuous distinct liquid phase (Johnston *et al.*, 2017b).

The solvent content at the onset of the asphaltene-rich phase was taken to be the intermediate content between the highest content at which no phase was observed and the lowest content at which the second phase was observed, as shown in Figure 3.5. Figure 3.5a shows that even below the onset of asphaltene precipitation a small number of particles are observed in the micrographs, which correspond to the TI content. However, as shown in Figure 3.5b, the number of particles significantly increases when the onset of asphaltene precipitation is reached. In most cases, the injection steps were set at intervals of 2 wt% solvent and the uncertainty of the solvent content was ± 0.5 wt%; therefore, the uncertainty of the reported onset was ± 1.5 wt%.

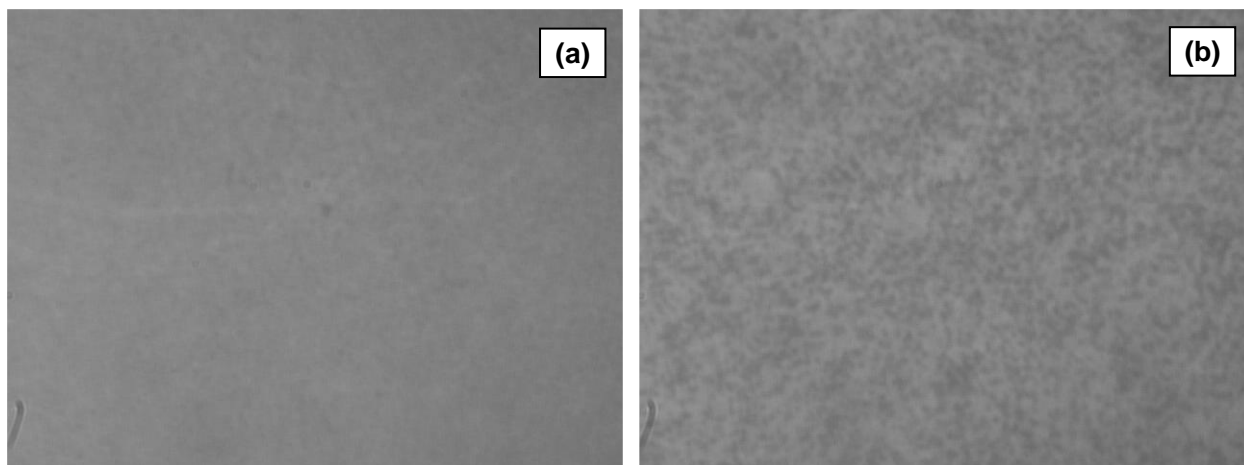


Figure 3.5 HPM micrographs from WC-B-A3 bitumen diluted with a binary blend of 85 wt% *n*-pentane and 15 wt% toluene at 21°C and 10 MPa: a) 60.0 wt% solvent; b) 61.9 wt% solvent. The onset was reported as 60.9 ± 1.5 wt% solvent.

3.4 Asphaltene Yield Measurement above Atmospheric Pressure

Asphaltene yields above atmospheric pressure were determined using a blind cell apparatus. The solvents used were a binary blend of 85 wt% *n*-pentane and 15 wt% toluene and a binary blend of 75 wt% *n*-pentane and 25 wt% cyclohexane. The asphaltene yields were determined at temperatures of 21 and 180°C and pressure of 10 MPa. The temperatures span the range of the HPM apparatus and the pressure was selected to maintain the solvent/bitumen mixture above its saturation pressure (liquid state). They also encompass most conditions encountered in heavy oil and solvent related processes. Figure 3.6 shows a schematic of the blind cell apparatus, which consists of five 100 cm³ stainless steel cylinders (PVT cells without a sight glass) with floating pistons but no mixers all housed in an air bath. The volume of each blind cell, and hence the pressure of the sample fluid under investigation, is controlled by hydraulic oil connected to a variable volume computer-controlled positive displacement pump. The blind cell apparatus is rated for temperatures from 20 to 300°C and pressures up to 70 MPa.

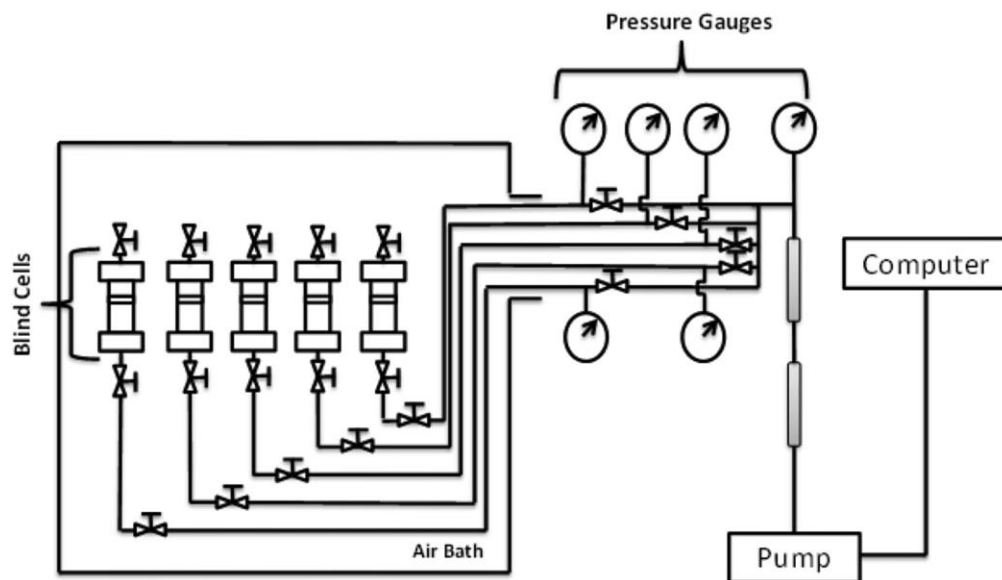


Figure 3.6 Schematic of the blind cell apparatus. Figure from Johnston *et al.* (2017b).

Only solvent-rich phase samples were collected from the blind cells because the location of the interface between the asphaltene-rich (heavy) and solvent-rich (light) phase was unknown. The asphaltene yield was determined from the solvent-rich phase composition and a mass balance following the procedure described by Johnston *et al.* (2017b) and Mancilla-Polanco *et al.* (2019). To prepare the mixtures, known masses of bitumen and solvent blend were injected into the blind cells at ambient conditions. For yield measurements at room temperature, the samples were mixed by inverting the blind cells at 21°C twice daily for 8 days to ensure complete mixing. For yield measurements at higher temperatures, the samples were mixed by inverting the blind cells at 180°C twice daily for 5 days. The blind cells were then oriented so that the asphaltene-rich phase settled on the floating piston. After mixing and orienting the blind cells for settling, the pressure and temperature were maintained for a minimum of 2 days to ensure equilibrium was reached. A sample of the solvent-rich phase was displaced at experimental pressure and temperature into a variable volume sample cylinder. The target volume was displaced from the blind cell to the sample cylinder and compressed nitrogen was used to maintain pressure in the sample cylinder at experimental conditions. The sample cylinders were allowed to cool down overnight and then at least two subsamples of the solvent-rich phase from each blind cell were transferred to centrifuge tubes.

Figure 3.7 summarizes the methodology used to determine the solvent-rich sample composition in terms of solvent, maltenes, and C5-asphaltenes. The solvent-rich phase subsamples were allowed to dry in a fumehood at 21°C and atmospheric pressure for at least 6 days and then were transferred to dry under vacuum at 60°C until their mass was constant. The solvent content of the solvent-rich phase subsamples was determined gravimetrically based on the mass loss during evaporation. The residue (bitumen components) from the solvent-rich phase subsamples was diluted with 90 wt% *n*-pentane to separate the pentane insoluble asphaltenes (C5-asphaltenes) from the maltenes. The mixture was sonicated and agitated for 1 hour until the residue was completely dispersed, then it was left to settle for 24 hours. The samples were then centrifuged for 8 minutes at 4000 rpm and the supernatant was pipetted out. The remaining residue (C5-asphaltenes in the solvent-rich phase subsamples) was washed with about 20 cm³ *n*-pentane, sonicated and agitated for 1 hour, and left to settle for 24 hours. The samples were then centrifuged for 8 minutes at 4000 rpm and the supernatant was removed. Finally, the C5-asphaltenes were left to dry in a vacuum oven at 60°C until the mass was constant. The C5-asphaltene content was the mass of the dried final residue divided by the initial mass of the solvent-rich phase subsample. The maltene content was determined by difference.

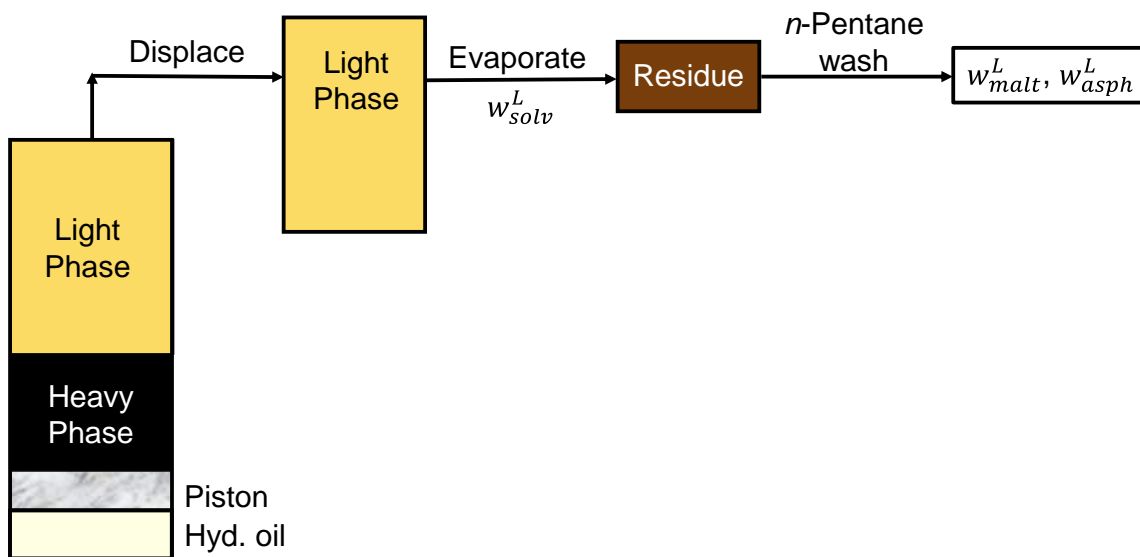


Figure 3.7 Sample collection methodology to measure light phase compositions and C5-Aphaltene yields in the blind cell apparatus.

Mass Balance and Asphaltene Yield Calculation

The C5-asphaltene yield was calculated as follows:

$$Y_A = \left(\frac{w_A^H}{1-w_S^F} \right) \frac{H}{F} \quad (3.2)$$

where Y is the yield, w is mass fraction, H/F is the mass ratio of heavy (asphaltene-rich) phase to feed, the superscripts F , and H denote the feed and heavy phase, respectively, and the subscripts A , and S , denote the asphaltenes and solvent, respectively. The feed and solvent-rich (L) phase compositions were known but mass balances were required to determine the asphaltene-rich (H) phase composition. Note that because the mass or volume of each phase was unknown, there was one unspecified degree of freedom. Therefore, the solvent content in the asphaltene-rich phase (w_S^H) was assumed so that the mass balances could be solved. A single component mass balance is given by:

$$w_i^F - w_i^L - \frac{H}{F} (w_i^H - w_i^L) = 0 \quad (3.3)$$

where subscript i denotes a component. The balance for the solvent was solved to determine the H/F mass ratio using known feed and solvent-rich phase compositions and the assumed solvent content in the asphaltene-rich phase (w_S^H). Once the H/F ratio was determined, the composition of the heavy phase were calculated from the component balances. The assumed solvent content was set to 25 wt% for all blind cell yields except for the binary toluene blend measured at 180°C that required 68 wt% to avoid negative compositions. Fortunately, the C5-asphaltene yields are relatively insensitive to the assumed solvent content with a combined uncertainty from this assumption and the error of the measurement of ± 1.5 wt% (Johnston *et al.*, 2017b).

CHAPTER 4: MODIFIED REGULAR SOLUTION MODEL

This chapter presents the Modified Regular Solution (MRS) model that was previously developed to model asphaltene onsets and yields from mixtures of heavy oil and a pure solvent. The main assumptions of the model and the fluid characterization methodology for the heavy oil and pure solvents are discussed. The heavy oil is characterized into four main pseudo-components based on a conventional SARA assay. The feed composition, molar volume, and solubility parameter of each pure solvent component and heavy oil pseudo-component are required inputs of the model. The correlations and previously established values used to calculate the inputs are provided. The updates made to the model and the oil characterization in order to fit and predict the onset and yield of asphaltene precipitation from heavy oil diluted with blended pure solvents and multicomponent petroleum-derived solvents will be discussed in Chapters 5 and 6, respectively.

4.1 Modified Regular Solution Model

The Modified Regular Solution theory is an activity coefficient model that has been successfully adapted to predict asphaltene precipitation from *n*-alkane diluted heavy oils and oil sands bitumen (Akbarzadeh *et al.*, 2005; Alboudwarej *et al.*, 2003). A liquid-liquid equilibrium is assumed between the asphaltene-rich (heavy) phase and the precipitant-rich (light) phase. The criterion for phase equilibrium between the two liquid phases is given by:

$$x_i^L \gamma_i^L f_i^0 = x_i^H \gamma_i^H f_i^0 \quad (4.1)$$

where x_i , γ_i , and f_i^0 are the mole fraction, activity coefficient, and the standard fugacity, respectively, of component i , and the superscripts L and H denote the light and heavy phase, respectively. It is also assumed that only asphaltenes and resins partition between the two phases. Hence, the partition coefficient, K_i , for a given component is calculated as follows:

$$\text{asphaltenes and resins:} \quad K_i = \frac{x_i^H}{x_i^L} = \frac{\gamma_i^L}{\gamma_i^H} \quad (4.2)$$

$$\text{other oil components and precipitant:} \quad K_i = 0 \quad (4.3)$$

The activity coefficient of the resins and asphaltene pseudo-components are determined as the sum of an entropic contribution term from the Flory-Huggins lattice theory (Flory, 1941; Huggins, 1941) and an enthalpic contribution term from the regular solution theory (Hildebrand *et al.*, 1970) as follows:

$$\ln \gamma_i^\alpha = \ln \left(\frac{v_i}{v^\alpha} \right) + 1 - \frac{v_i}{v^\alpha} + \frac{v_i}{RT} (\delta_i - \delta^\alpha)^2 \quad (4.4)$$

where v_i and δ_i are the molar volume and solubility parameter of component i at the temperature and pressure of the system, R is the universal gas constant, T is the absolute temperature, and the superscript α denotes the phase. The molar volume of a phase is determined as the molar average of all of the components in the phase and is given by,

$$v^\alpha = \sum x_i^\alpha v_i \quad (4.5)$$

The solubility parameter of a phase is calculated as a volumetric average,

$$\delta^\alpha = \sum \phi_i^\alpha \delta_i \quad (4.6)$$

where ϕ is the volume fraction.

If the mixture under study does not comply with the regular solution geometric mean assumption, *i.e.*, that the cohesive energy density of mixing of two different components is equal to the geometric mean of the two pure component cohesive energy densities, the activity coefficient is calculated as (Prausnitz *et al.*, 1999):

$$\ln \gamma_i^\alpha = \ln \frac{v_i}{v^\alpha} + 1 - \frac{v_i}{v^\alpha} + \frac{v_i}{RT} \sum_j^n \sum_k^n \phi_j^\alpha \phi_k^\alpha (D_{ij} - 0.5D_{jk}) \quad (4.7)$$

where

$$D_{jk} = (\delta_j - \delta_k)^2 + 2\lambda_{jk}\delta_j\delta_k \quad (4.8)$$

and λ_{jk} is the binary interaction parameter between components j and k , and n is the number of components in the mixture. λ_{jk} is an empirical parameter that is a function of temperature. Its magnitude is small compared to unity and typically increases with the difference in molecular size and chemical nature between components j and k (Funk and Prausnitz, 1970; Prausnitz *et al.*, 1999). When the binary interaction parameter is zero, Eq. 4.7 reduces to Eq. 4.4. In all previous work with this model, the binary interaction parameters were in effect set to zero.

In the version of the Modified Regular Solution model used in this study, the heavy oil is characterized based on a conventional SARA (saturates, aromatics, resins, and asphaltenes) assay. The inputs to the model are the feed composition, molar volume (in practice the density and molecular weight), and solubility parameter of each component. The MRS model is a function of a one-dimensional solubility parameter which represents the average contribution from all molecular interactions including London dispersion forces, polar forces, and hydrogen bonding.

The MRS model can represent mixtures with non-polar solvents where the dispersion forces are dominant: however, it does not accurately represent mixtures with polar solvents where polar forces and hydrogen bonding play a significant role (Mannistu *et al.*, 1997).

4.2 Fluid Characterization

Solvent Characterization

Solvents that cause asphaltene precipitation are more accurately described as precipitants. However, for convenience, all hydrocarbon liquids will be referred to as solvents. The molecular weights of the single component solvents used in this thesis are provided in Table 4.1. The *n*-alkane solvent densities were treated as effective densities where the effective density is defined as the density of a component when it is part of a liquid mixture. It is recommended for components which are a gas in their native state at the given temperature and pressure because the effective density can be used in a regular solution mixing rule to obtain an accurate mixture density whereas gas densities cannot. The effective densities were calculated from the following correlation (Saryazdi *et al.*, 2013):

$$\rho = (a_1 + a_2T) + [(b_1 + b_2T)P] \quad (4.9)$$

where a_1 , a_2 , b_1 , and b_2 are fluid-specific parameters, T is the absolute temperature in K, and P is the pressure in MPa. The fluid-specific parameters are provided in Appendix C. The densities of toluene and cyclohexane were calculated from the Tait-COSTALD correlation (Thomson *et al.*, 1982) and the modified Rackett correlation (Spencer and Danner, 1972) as described elsewhere (Ramos-Pallares and Yarranton, 2020) and in Appendix C.

Table 4.1 Molecular weights and solubility parameters at 25°C and 0.1 MPa for selected solvents. Solubility parameters taken from Barton’s handbook (Barton, 1991).

Solvent	<i>MW</i> g/mol	δ° MPa ^{0.5}
<i>n</i> -Pentane	72.15	14.40
<i>n</i> -Hexane	86.18	14.90
<i>n</i> -Heptane	100.20	15.20
Cyclohexane	84.16	16.60
Toluene	92.14	18.20

The solvent solubility parameters at the standard conditions of 25°C and 0.1 MPa (δ_i^o) were taken from Barton's handbook (Barton, 1991) and are provided in Table 4.1. The solubility parameters at non-standard conditions were calculated from the following correlation (Ramos-Pallares and Yarranton, 2020):

$$\delta_i = \delta_i^o \sqrt{\frac{\rho_{T_oP,i}}{\rho_i^o}} - k_i(T - 298.15) \quad (4.10)$$

where k is the temperature dependence of the solubility parameter in MPa^{0.5}/K, ρ_i^o is the density at standard conditions, and the subscript T_oP indicates standard temperature and actual pressure. The temperature dependence parameter for the solvents and for the oil fractions are provided elsewhere (Ramos-Pallares and Yarranton, 2020) and in Table 4.2.

Table 4.2 Values of temperature dependence parameter k in Eq. 4.10 for SAR fractions, C5-asphaltene pseudo-components, and solvents used in this thesis.

Fraction	k MPa ^{0.5} /K
Solvent	0.0232
Saturates	0.0222
Aromatics	0.0204
Resins	0.0191
C5-asphaltenes	0.0191

Heavy Oil Characterization

C5-Asphaltenes: The asphaltenes are defined as the n -pentane insoluble asphaltenes, termed C5-asphaltenes. The C5-asphaltenes are assumed to consist of asphaltene nanoaggregates and the molecular weights of the nanoaggregates are assumed to be distributed according to the gamma distribution function (Akbarzadeh *et al.*, 2005) given by,

$$f(MW) = \frac{(MW - MW_{mon})^{\beta-1}}{\Gamma(\beta)} \left(\frac{\beta}{MW_{avg} - MW_{mon}} \right)^{\beta} \exp\left(-\beta \frac{MW - MW_{mon}}{MW_{avg} - MW_{mon}}\right) \quad (4.11)$$

where MW is the molecular weight, MW_{mon} is the molecular weight of the monomer in the C5- asphaltene aggregate, MW_{avg} is the average molecular weight of the C5-asphaltene aggregate, and β is the shape factor. The gamma distribution is divided into pseudo-components of equal molecular weight interval. The recommended gamma distribution parameters are $MW_{mon} = 800$

g/mol, $MW_{avg} = 3000$ g/mol, $MW_{max} = 15,000$ g/mol and $\beta = 2.1$ (Powers *et al.*, 2016). In this thesis, 15 asphaltene pseudo-components were sufficient to eliminate any sensitivity to the number of pseudo-components.

The densities of each of the C5-asphaltene pseudo-component are given by:

$$\rho_{A,i} = \rho_{A,i}^o - m_i(T - 298.15) \quad (4.12)$$

where $\rho_{A,i}^o$ is the density of asphaltene pseudo-component i at the standard condition of 25°C and 0.1 MPa in kg/m³ and is given by (Ramos-Pallares and Yarranton, 2020),

$$\rho_{A,i}^o = 1047 + 151.4[1 - \exp(-9W_{A,i})] \quad (4.13)$$

where $\rho_{A,i}^o$ and $W_{A,i}$ are the density and cumulative mass fraction of pseudo-component i , respectively. The component specific constant, m , is given by:

$$m_i = 3.1635 - 0.00239\rho_{A,i}^o \quad (4.14)$$

The asphaltenes have been shown to be incompressible at temperatures and pressures up to 175°C and 10 MPa, respectively (Ramos-Pallares *et al.*, 2016). Hence, the effect of pressure on density is considered to be negligible.

The solubility parameter for each C5-asphaltene pseudo-component at 25°C and 0.1 MPa is determined as follows (Powers *et al.*, 2016),

$$\delta_{A,i}^o = \delta_{min}^o + (\delta_{max}^o - \delta_{min}^o)W_{A,i}^{1.2} \quad (4.15)$$

where $\delta_{A,i}^o$ is the solubility parameter at 25°C and 0.1 MPa, in MPa^{0.5}, and subscripts “*max*” and “*min*” denote the maximum and minimum solubility parameter of the distribution, respectively.

The values of δ_{min}^o and δ_{max}^o are determined by fitting the model to experimental yield data. The solubility parameters at non-standard conditions were calculated from Eq. 4.10.

Saturates, Aromatics, and Resins: The saturates, aromatics, and resins are assumed to contain only non-associated components and each fraction is represented as a single pseudo-component. The density, molecular weight, and solubility parameters at 25°C and 0.1 MPa for saturates, aromatics, and resins are provided elsewhere (Ramos-Pallares and Yarranton, 2020) and listed in Table 4.3. The saturate and aromatic densities at non-standard conditions were determined from the following correlation (Ramos-Pallares and Yarranton, 2020):

$$\rho_i = (a_{o,i} + b_{o,i}T + c_{o,i}T^2)\exp[(a_{1,i} + b_{1,i}T)P] \quad (4.16)$$

where ρ is the density in kg/m³ and a_o , b_o , c_o , a_1 , and b_1 are fluid-specific parameters, and subscript i indicates either the saturate or the aromatic pseudo-component. The $a_{o,i}$ value for each pseudo-component was adjusted to match the densities measured at 25°C and 0.1 MPa in Table 4.3 and are provided in Table 4.4. The density of the resin pseudo-component was determined as for the asphaltenes and is given by:

$$\rho_{R,i} = \rho_{R,i}^o - 0.659(T - 298.15) \quad (4.17)$$

The solubility parameters of the saturates, aromatics, and resins at non-standard conditions were calculated from Eq. 4.10.

Table 4.3 Density (ρ^o), molecular weight (MW) and solubility parameter (δ^o) at 25°C and 0.1 MPa for saturates, aromatics, and resins fractions for MRS model (Ramos-Pallares and Yarranton, 2020).

Fraction	ρ^o kg/m ³	MW g/mol	δ^o MPa ^{0.5}
Saturates	877	440	16.5
Aromatics	987	500	19.3
Resins	1047	1050	δ_{min}^o

Table 4.4 Parameters for the saturate and aromatic density correlation (Eq. 4.16).

Fraction	a_o (kg m ⁻³)	b_o (kg m ⁻³ K ⁻¹)	c_o (kg m ⁻³ K ⁻²)	$a_1 \times 10^4$ (MPa ⁻¹)	$b_1 \times 10^6$ (MPa ⁻¹ K ⁻¹)
Saturates	1053.44	-0.5457	-0.000150	-3.113	3.150
Aromatics	1163.45	-0.5457	-0.000150	-2.681	2.659

4.3 MRS Model Implementation

The Modified Regular Solution (MRS) model was implemented in a previously developed Visual Basic code by the Heavy Oil Properties and Processing Research Group. The required experimental data to use the MRS model are a SARA analysis, and an asphaltene yield curve from the heavy oil of interest diluted with a pure n -alkane, typically n -heptane at ambient conditions. The input properties are set using previously established average values and existing correlations

provided in section 4.2 or developed later in this thesis. The partition coefficient (K_i) of the asphaltenes and resins are initialized using the feed composition and assuming that the partition coefficients are equal to the activity coefficient of the light liquid phase. Flash calculations are performed until convergence is achieved (Alboudwarej *et al.*, 2003). The minimum and maximum solubility parameters of the asphaltenes are tuned against the experimental yield data. Once the model is tuned, it can be used to accurately predict asphaltene yields from other pure *n*-alkane solvents at different conditions.

CHAPTER 5: BLENDED PURE SOLVENTS RESULTS AND DISCUSSION

This chapter presents the experimental data from two Western Canadian bitumens diluted with single component solvents and blended pure solvents. The model performance for bitumen with a single component solvent and with binary solvent blends is examined. Binary interaction parameters (BIP) are fitted using onset and yield data from the binary solvent blends. A new correlation to calculate binary interaction parameters is proposed and tested on onset and yield data from bitumen diluted with ternary solvent blends. Finally, the application of the model to different bitumen and at higher temperatures and pressures is assessed. The following terminology is used to describe the blends: “XX:YY A:B” indicates XX wt% solvent A and YY wt% solvent B; C5, C6, C7, Tol, CH indicate *n*-pentane, *n*-hexane, *n*-heptane, toluene, and cyclohexane, respectively. The model deviations are assessed in terms of average absolute deviation (AAD), the maximum absolute deviation (MAD), and the bias (average deviation).

5.1 Bitumen with Single Component Solvent

For mixtures of bitumen and solvents, all of the binary interaction parameters were set to zero except for the binary interaction parameters between the asphaltene pseudo-components and each solvent, as will be discussed later. In addition, the binary interaction parameters with *n*-alkanes were set to zero. Of the single component solvents considered in this thesis, only the *n*-alkanes caused asphaltene precipitation when added to the bitumen on their own. Figure 5.1 presents asphaltene yields from the WC-B-A3 bitumen mixed with *n*-pentane, *n*-hexane, and *n*-heptane at 21°C and 0.1 MPa. These and all of the yields presented in this thesis are on a toluene insoluble-free basis. The onsets determined from the fitted yield data are provided in Table 5.1. As expected, the asphaltenes become more soluble (yields decreased and the onsets increased) as the carbon number of the *n*-alkane increased.

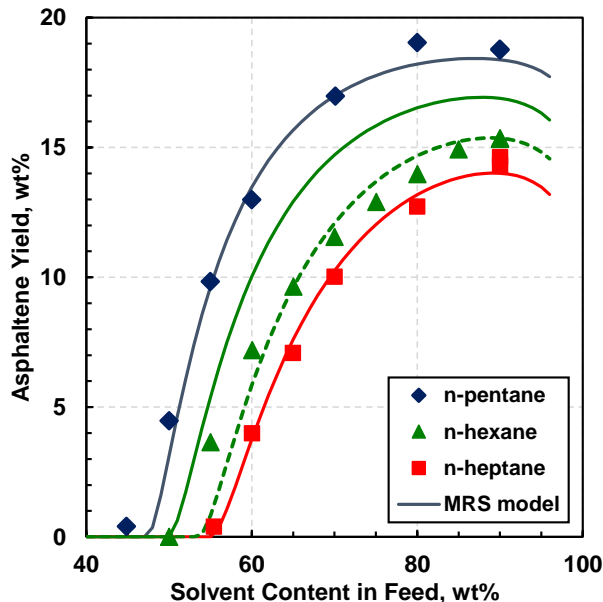


Figure 5.1 Measured and modeled asphaltene yields from WC-B-A3 bitumen diluted with *n*-pentane, *n*-hexane, and *n*-heptane at 21°C and 0.1 MPa. Solid lines are the model with default solubility parameters; dashed line is the model with an updated *n*-hexane solubility parameter.

The model was tuned to match the yields from the *n*-heptane diluted bitumen. The tuned asphaltene solubility parameters at standard conditions were $\delta_{min}^o = 19.81 \text{ MPa}^{0.5}$ and $\delta_{max}^o = 20.17 \text{ MPa}^{0.5}$. The model was then used to predict the onsets and yields for the bitumen diluted with the other *n*-alkane solvents. The deviations are summarized in Table 5.2. All of the modeled onsets in this thesis were determined as the lowest solvent content at which the model predicted an asphaltene yield of 0.01 wt%, which is the approximate detection limit of asphaltene precipitation in microscopic methods (Tharanivasan *et al.*, 2009). The model predicted the onset and yields from the *n*-pentane diluted bitumen to almost within the experimental errors of $\pm 1.5 \text{ wt\%}$ and $\pm 0.5 \text{ wt\%}$, respectively. The deviations were higher for the *n*-hexane diluted bitumen and the error is attributed to the default value for the *n*-hexane solubility parameter in the model ($14.80 \text{ MPa}^{0.5}$). Barton (1991) reports a value of $14.90 \text{ MPa}^{0.5}$ and using this value significantly reduces the deviation of the model. The updated value of $14.90 \text{ MPa}^{0.5}$ will be used to evaluate the solvent blends that contain *n*-hexane.

Table 5.1 Fitted and modeled asphaltene precipitation onsets from WC-B-A3 bitumen diluted with *n*-alkanes and blends of *n*-alkanes at 21°C and 0.1 MPa. The overall average absolute deviation and bias in the modeled onsets were 1.1 wt% and 0.7 wt%, respectively.

Solvent	Modeling	Fitted Onset wt%	Modeled Onset wt%	Deviation wt%
<i>n</i> -heptane	tuned	55.7	55.3	-0.4
<i>n</i> -hexane	predicted	50.9	50.2	-0.8
<i>n</i> -hexane	updated	50.9	53.8	2.9
<i>n</i> -pentane	predicted	47.1	47.5	0.4
50:50 C5:C7	predicted	51.2	51.3	0.1
50:50 C5:C6	predicted	48.7	50.5	1.8

Table 5.2 Deviations of the modeled asphaltene yields for WC-B-A3 bitumen diluted with *n*-alkanes and blends of *n*-alkanes at 21°C and 0.1 MPa. The overall average absolute deviation and bias in the modeled yields were 1.0 wt% and 0.5 wt%, respectively.

Solvent	Modeling	AAD wt%	MAD wt%	Bias wt%
<i>n</i> -heptane	tuned	0.4	0.6	0.0
<i>n</i> -hexane	predicted	2.4	3.3	2.4
<i>n</i> -hexane	updated	0.7	2.8	-0.2
<i>n</i> -pentane	predicted	0.5	1.3	-0.4
50:50 C5:C7	predicted	0.7	1.3	0.7
50:50 C5:C6	predicted	0.9	1.7	0.4

5.2 Bitumen with Binary Solvent Blends

First, consider blends of *n*-alkanes. Figures 5.2a and 5.2b show the measured and predicted asphaltene yields from WC-B-A3 bitumen diluted with 50:50 C5:C7 and 50:50 C5:C6, respectively, at 21°C and 0.1 MPa. The yields from the bitumen diluted with the single component solvents are provided for comparison. The fitted and predicted onsets are provided in Table 5.1. The deviations of the predicted yields are provided in Table 5.2. The model predicts the mixture yields and onsets with average deviations of less than 1.0 and 1.9 wt%, respectively.

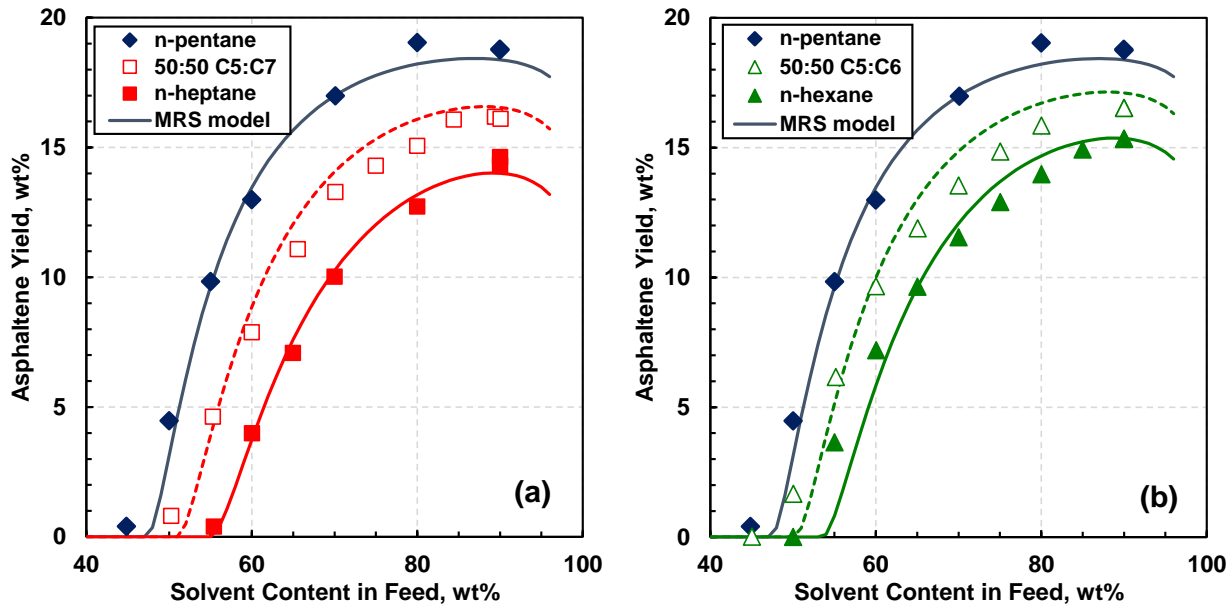


Figure 5.2 Measured and modeled asphaltene yields from WC-B-A3 bitumen diluted with binary blends of *n*-alkanes at 21°C and 0.1 MPa: a) *n*-pentane (C5) and *n*-heptane (C7); b) *n*-pentane (C5) and *n*-hexane (C6). The “50:50 X:Y” in the legend indicates a mixture of 50 wt% X and 50 wt% Y. Solid and dashed lines are the model results for a single component solvent and blended solvent, respectively.

Now consider blends of solvents from different chemical families. Figure 5.3 shows the measured and predicted asphaltene yields from WC-B-A3 bitumen diluted with mixtures of *n*-pentane and toluene at 21°C and 0.1 MPa. The model significantly under-predicts the measured yields. While not shown completely in Figure 5.3, the under-prediction becomes more severe as the blend approaches a 50:50 mix and this trend was observed for all of the blends. This type of deviation is consistent with a mixture where the cohesive energy density of the mixture departs from the geometric mean. In other words, where the internal energy of mixing of dissimilar species in solution is not exactly represented by the geometric mean of the internal energy of the components. In this case, the deviation can be corrected with a binary interaction parameter.

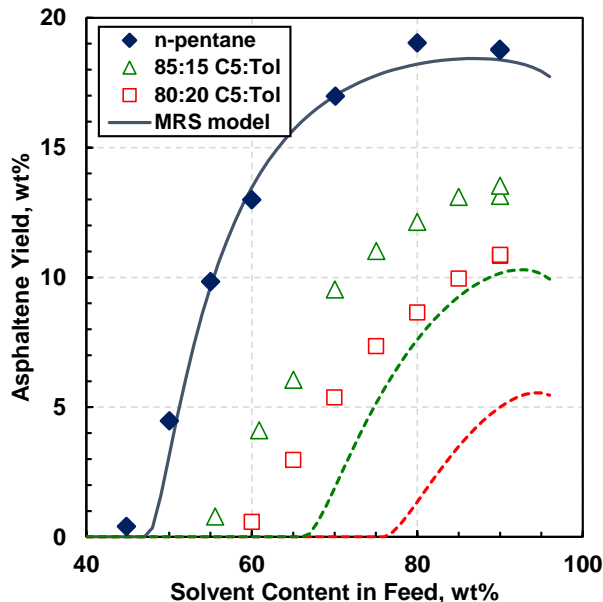


Figure 5.3 Measured and modeled asphaltene yields from WC-B-A3 bitumen diluted with binary blends of *n*-pentane and toluene at 21°C and 0.1 MPa; original version of model ($\lambda_{jk} = 0$). Solid and dashed lines are the model results for a single component solvent and blended solvent, respectively.

The yield data for the WC-B-A3 bitumen diluted with binary solvent blends were regressed using the least squares method to obtain binary interaction parameters. To minimize the number of parameters, the binary interaction parameters of all non-asphaltene component pairs and for the asphaltene pseudo-components with each other were all set to zero. The binary interaction parameters for *n*-alkane/asphaltene pairs were also set to zero; otherwise the tuned asphaltene solubility parameters were lower than the aromatic solubility parameters, a physically implausible outcome. It was also more straightforward to fit the data when the binary interaction parameters of the *n*-alkanes were set to zero; otherwise the asphaltene solubility parameters would have to be retuned each time the *n*-alkane/asphaltene binary interaction parameters were adjusted. Finally, the binary interaction parameters for asphaltene/toluene and asphaltene/cyclohexane pairs were set to increase monotonically along the asphaltene mass distribution according to the following expression:

$$\lambda_{jk} = \lambda_{min} + (\lambda_{max} - \lambda_{min})W_{A,i}^{1.2} \quad (5.1)$$

where λ_{min} is the minimum binary interaction parameter, λ_{max} is the maximum binary interaction parameter, and $W_{A,i}$ is the cumulative mass fraction of the asphaltene pseudo-component *i*. The fitted binary interaction parameters are provided in Table 5.3.

The measured and modeled asphaltene yields for all of the binary blends are shown in Figure 5.4. The fitted and modeled onsets are listed in Table 5.4. The deviations for the modeled yields are provided in Table 5.5. The model with the binary interaction parameters fit the yields with average deviations below 1 wt%. In general, the onsets were under-predicted but it is not clear if the systematic deviation is caused by the extrapolation used to obtain the experimental onset (Eq. 3.1) or by tuning the model to match yields without including the onsets. Nonetheless, the deviations of the modeled onsets were mainly below 2 wt% (slightly above the experimental error of ± 1.5 wt%) although some were as high as 4.6 wt%. The largest deviations were for low yield data where the fitted onset was least accurate.

Note that all of the modeled asphaltene yields in this thesis start decreasing at a solvent content of about 90 wt%, whereas the trends from the measured yields indicate that the asphaltene yields either reach a plateau or keep increasing at high dilutions. At high solvent contents, the system becomes dilute in bitumen and asphaltenes, and the model predicts that the asphaltenes are soluble. This deficiency has been observed in the past not only with the MRS approach (Akbarzadeh *et al.*, 2005; Ramos-Pallares and Yarranton, 2020) but also with EoS modeling (Johnston *et al.*, 2017a; Sabbagh *et al.*, 2006). No asphaltene yields were measured to confirm what happens above the solvent content of 90 wt% due to the difficulty of getting an accurate measurement at such high dilutions. Akbarzadeh *et al.* (2005) suggested that the increased solubility of asphaltenes predicted by the MRS approach at high solvent contents is not observed in experimental measurements because, at high dilutions, the asphaltenes may self-associate to a greater extent decreasing their solubility in the mixture.

Table 5.3 Fitted binary interaction parameters for asphaltene/toluene and asphaltene/cyclohexane pairs at 21°C and 0.1 MPa.

Solvent	λ_{min}	λ_{max}
Toluene	0.0093	0.0259
Cyclohexane	0.0123	0.0177

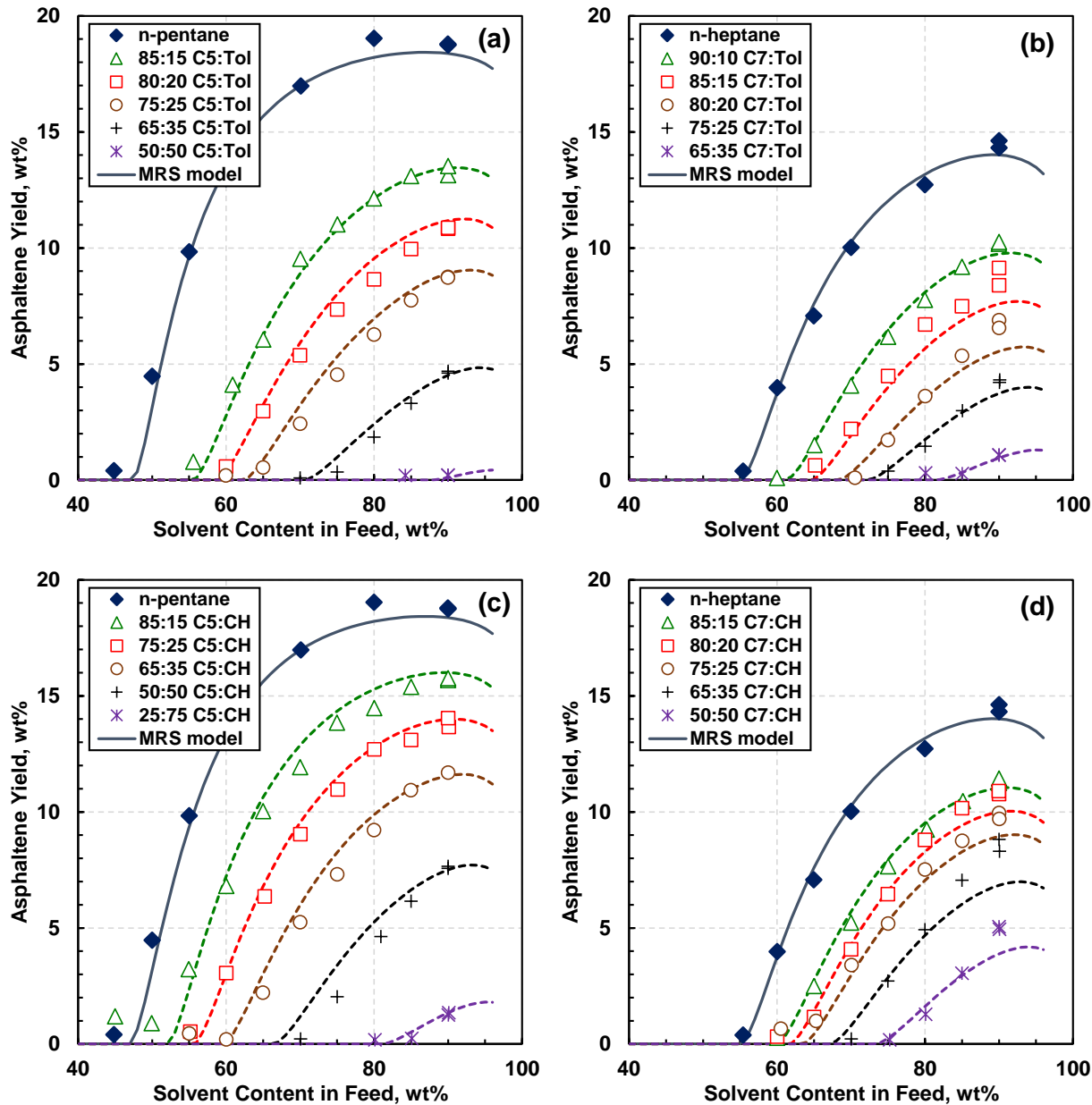


Figure 5.4 Measured and modeled asphaltene yields from WC-B-A3 bitumen diluted with binary blends of solvents from different chemical families at 21 °C and 0.1 MPa: a) *n*-pentane and toluene; b) *n*-heptane and toluene; c) *n*-pentane and cyclohexane; d) *n*-heptane and cyclohexane. Solid and dashed lines are the model results for a single component solvent and blended solvent, respectively.

Table 5.4 Fitted and modeled asphaltene onsets from WC-B-A3 bitumen diluted with binary blends of solvents from different chemical families at 21°C and 0.1 MPa. The overall average absolute deviation and bias in the modeled onsets were 2.0 wt% and -1.9 wt%, respectively.

Blend	Fitted Onset wt%	Modeled Onset wt%	Deviation wt%
85:15 C5:Tol	56.9	55.8	-1.1
80:20 C5:Tol	60.1	59.0	-1.1
75:25 C5:Tol	64.1	62.6	-1.6
65:35 C5:Tol	73.9	70.9	-3.1
50:50 C5:Tol	-	88.2	-
90:10 C7:Tol	62.6	61.5	-1.1
85:15 C7:Tol	66.6	64.9	-1.7
80:20 C7:Tol	71.2	68.6	-2.6
75:25 C7:Tol	75.9	72.6	-3.4
65:35 C7:Tol	83.5	81.9	-1.7
85:15 C5:CH	52.0	52.3	0.3
75:25 C5:CH	56.9	55.9	-1.0
65:35 C5:CH	61.9	59.8	-2.0
50:50 C5:CH	71.3	66.7	-4.6
25:75 C5:CH	84.0	81.4	-2.6
85:15 C7:CH	61.7	60.2	-1.5
80:20 C7:CH	63.6	61.9	-1.7
75:25 C7:CH	63.7	63.7	0.0
65:35 C7:CH	70.2	67.4	-2.8
50:50 C7:CH	76.8	73.7	-3.1

Table 5.5 Deviations of the modeled asphaltene yields for WC-B-A3 bitumen diluted with binary blends of solvents from different chemical families at 21°C and 0.1 MPa. The overall average absolute deviation and bias in the modeled yields were 0.5 wt% and -0.1 wt%, respectively.

Blend Set	AAD wt%	MAD wt%	Bias wt%
<i>n</i> -pentane:toluene	0.4	0.9	0.2
<i>n</i> -pentane:cyclohexane	0.4	1.4	0.3
<i>n</i> -heptane:toluene	0.4	1.5	-0.3
<i>n</i> -heptane:cyclohexane	0.6	2.0	-0.4

5.3 Testing the Predictive Capability of the Model with Binary Interaction Parameters

Same Bitumen with Ternary Solvent Blends

To test the predictive ability of the proposed binary interaction parameters, the model with the proposed binary interaction parameters was applied without adjustment to predict yield data from the same bitumen with ternary blends of solvents. Figures 5.5a and 5.5b show the measured and predicted yields from WC-B-A3 bitumen diluted with ternary solvent blends of *n*-pentane/toluene/cyclohexane and *n*-heptane/toluene/cyclohexane, respectively, at 21°C and 0.1 MPa. The data for the ternary solvent blends with 75 wt% *n*-pentane and 75 wt% *n*-heptane are not shown in Figure 5.5 to avoid crowding but are provided in Appendix D and are included in the error analysis. The fitted and modeled onsets are listed in Table 5.6. The deviations for the modeled yields are provided in Table 5.7. The deviations are similar to the fitted binary blend results, confirming that the proposed binary interaction parameters can be used to predict asphaltene yields from multicomponent solvent blends.

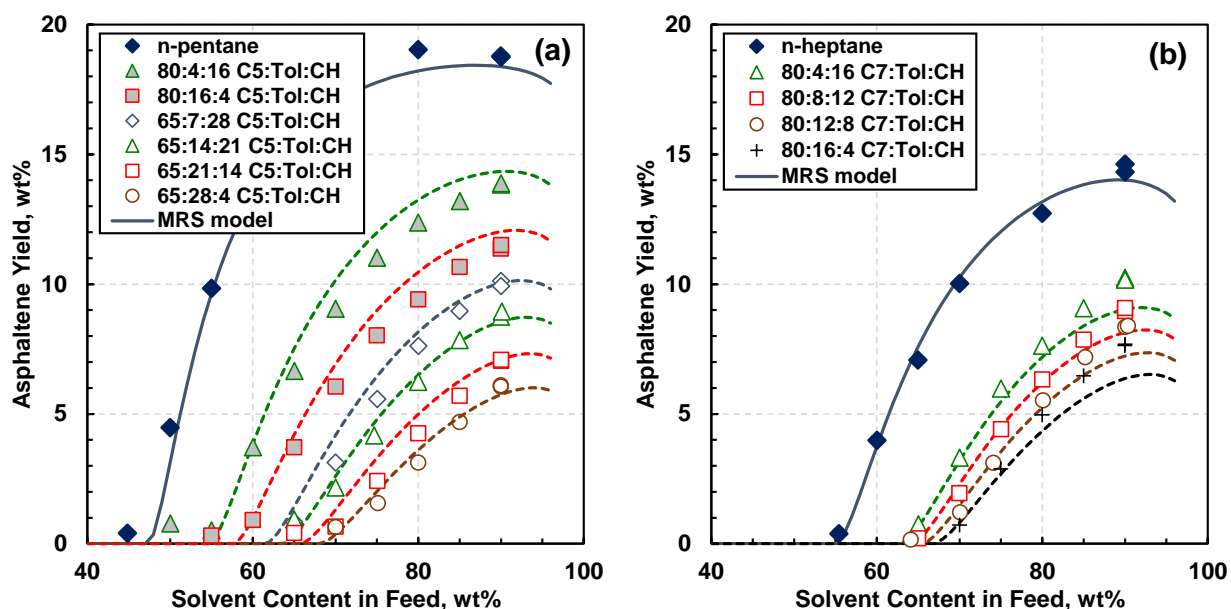


Figure 5.5 Measured and predicted asphaltene yields from WC-B-A3 bitumen diluted with ternary blends of solvents from different chemical families at 21°C and 0.1 MPa: a) mixtures of *n*-pentane, toluene, and cyclohexane; b) mixtures of *n*-heptane, toluene, and cyclohexane. The model results for the ternary blends are predictions using the binary interaction parameters determined from the binary blends.

Table 5.6 Fitted and predicted asphaltene onsets from WC-B-A3 bitumen diluted with ternary blends of solvents from different chemical families at 21°C and 0.1 MPa. The overall average absolute deviation and bias in the modeled onsets were 1.7 wt% and -1.7 wt%, respectively.

Blend	Fitted Onset wt%	Predicted Onset wt%	Deviation wt%
80:4:16 C5:Tol:CH	55.7	55.0	-0.7
80:16:4 C5:Tol:CH	58.7	58.0	-0.8
75:5:20 C5:Tol:CH	58.0	57.1	-0.9
75:20:5 C5:Tol:CH	62.4	61.1	-1.3
65:7:28 C5:Tol:CH	63.8	61.8	-2.0
65:14:21 C5:Tol:CH	66.2	63.9	-2.4
65:21:14 C5:Tol:CH	68.4	66.1	-2.4
65:28:7 C5:Tol:CH	70.6	68.4	-2.2
80:4:16 C7:Tol:CH	64.0	63.2	-0.8
80:8:12 C7:Tol:CH	66.8	64.4	-2.3
80:12:8 C7:Tol:CH	67.9	65.8	-2.2
80:16:4 C7:Tol:CH	68.7	67.1	-1.6
75:5:20 C7:Tol:CH	67.3	65.3	-2.0
75:20:5 C7:Tol:CH	73.1	70.7	-2.4

Table 5.7 Deviations of the predicted asphaltene yields for WC-B-A3 bitumen diluted with ternary blends of solvents from different chemical families at 21°C and 0.1 MPa. The overall average absolute deviation and bias in the modeled yields were 0.6 wt% and 0.1 wt%, respectively.

Blend Set	AAD wt%	MAD wt%	Bias wt%
<i>n</i> -pentane:toluene:cyclohexane	0.6	1.3	0.5
<i>n</i> -heptane:toluene:cyclohexane	0.6	1.3	-0.4

A Different Bitumen with Binary Solvent Blends

The model was also tested on a different bitumen (WC-B-B5) with binary solvent blends. The model was tuned to match the yield data from the WC-B-B5 bitumen diluted with *n*-heptane as shown in Figure 5.6a. The tuned minimum and maximum asphaltene parameters at standard conditions were 19.66 and 20.18 MPa, respectively. The fitted parameters are similar to those

determined from the WC-B-A3 bitumen (19.81 and 20.17 MPa^{0.5}, respectively). The small difference may reflect real physical differences in the asphaltenes or may be compensating for small errors in the estimated properties or SARA assays of the bitumens. No other tuning was performed and the model results for the other solvents and blends discussed below are predictions.

Figure 5.6a also shows the measured asphaltene yields from WC-B-B5 bitumen diluted with *n*-pentane and 50:50 C5:C7. Figure 5.6b shows the measured and predicted yields from WC-B-B5 bitumen diluted with binary blends of *n*-pentane/toluene and *n*-pentane/cyclohexane at 21°C and 0.1 MPa. The fitted and modeled onsets are listed in Table 5.8. The deviations for the modeled yields are provided in Table 5.9. The deviations are similar to the fitted binary blend results, confirming that the proposed binary interaction parameters can be used to predict asphaltene yields from other bitumens with solvent blends. Based on previous experience with the modified regular solution model (Akbarzadeh *et al.*, 2005), the model is expected to perform similarly for other crude oils.

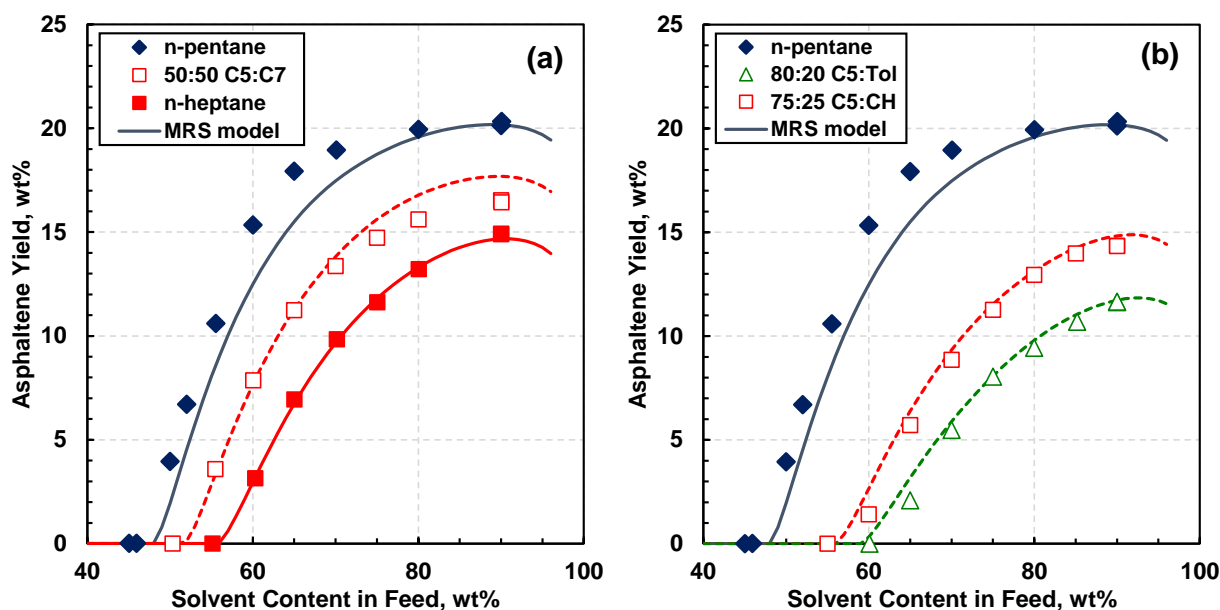


Figure 5.6 Measured and modeled asphaltene yields from WC-B-B5 bitumen diluted with: a) *n*-pentane, *n*-heptane, and a binary blend of *n*-pentane and *n*-heptane at 21°C and 0.1 MPa; b) a binary blend of *n*-pentane and toluene and a binary blend of *n*-pentane and cyclohexane. The model results for the blends are predictions using the binary interaction parameters determined from the binary blends of WC-B-A3 bitumen.

Table 5.8 Fitted and modeled asphaltene precipitation onsets from WC-B-B5 bitumen diluted with *n*-alkanes and blends of *n*-alkanes at 21°C and 0.1 MPa. The overall average absolute deviation and bias in the predicted onsets were 1.8 wt% and -1.8 wt%, respectively.

Solvent	Modeling	Fitted Onset wt%	Modeled Onset wt%	Deviation wt%
<i>n</i> -heptane	tuned	57.2	55.8	-1.4
<i>n</i> -pentane	predicted	48.3	48.1	-0.3
50:50 C5:C7	predicted	52.8	51.8	-1.0
80:20 C5:Tol	predicted	62.6	59.1	-3.5
75:25 C5:CH	predicted	58.8	56.1	-2.7

Table 5.9 Deviations of the modeled asphaltene yields for WC-B-B5 bitumen diluted with *n*-alkanes and blends of *n*-alkanes at 21°C and 0.1 MPa. The overall average absolute deviation and bias in the predicted yields were 0.6 wt% and 0.0 wt%, respectively.

Solvent	Modeling	AAD wt%	MAD wt%	Bias wt%
<i>n</i> -heptane	tuned	0.2	0.2	-0.1
<i>n</i> -pentane	predicted	1.5	2.8	-1.5
50:50 C5:C7	predicted	0.7	1.3	0.6
80:20 C5:Tol	predicted	0.3	1.1	0.3
75:25 C5:CH	predicted	0.5	1.2	0.5

5.4 Bitumen with Solvent Blends at Elevated Temperatures and Pressures

Figures 5.7a and 5.7b show the measured and predicted onsets and yields from WC-B-A3 bitumen diluted with binary solvent blends of 85:15 C5:Tol and 75:25 C5:CH, respectively, at 21°C and pressures of 0.1 and 10 MPa. The deviations for the modeled onsets and yields are provided in Table 5.10. As expected, the solubility of the asphaltenes increased with pressure (yields decreased and the onsets increased) because oils become a better solvents for asphaltenes at higher pressures, as discussed in Chapter 2. The model predicts the effect of pressure almost to within the error of the measurements.

Figures 5.8a and 5.8b show the measured and predicted onsets and yields from the same respective mixtures at temperatures of 21°C and 180°C and pressure of 10 MPa. At the higher temperature,

the onsets shift to lower values indicating that the asphaltenes become less soluble but the yields decrease indicating that the asphaltenes become more soluble. The reason for this apparent contradiction is not clear. One possibility is that the asphaltenes nano-aggregates partially dissociate at the higher temperature leading to a different distribution of molar volumes and solubility parameters and hence a different yield curve. The model predicts the effect of temperature on the yields at high dilution but fails to predict the effect of temperature on the onset. It is likely that the binary interaction parameters are temperature dependent. Therefore, the binary interaction parameters were retuned at 180°C to fit both yields and onsets. The adjusted binary interaction parameters at 180°C are provided in Table 5.11 and the tuned model is shown in Figure 5.8. The tuned model matches the onsets but over-predicts the yields. The deviations are summarized in Table 5.12. The highest deviation is for the yield measured at 180°C, 10 MPa, and 70 wt% 75:25 C5:CH. The yield measurements are least reliable near the onset of precipitation and this point may be an outlier. The onset is a direct measurement and is more reliable than the high temperature and pressure yields which were determined from a material balance. Therefore, it is recommended to include the temperature dependence of the binary interaction parameters in the model.

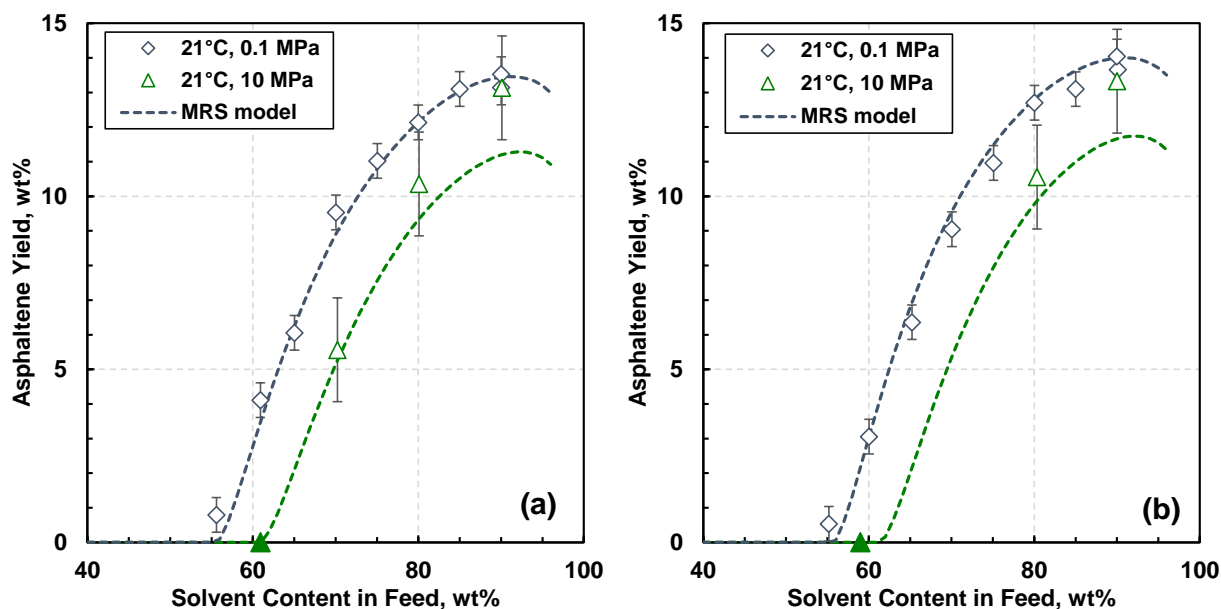


Figure 5.7 Measured and predicted asphaltene onsets and yields from WC-B-A3 bitumen diluted with binary blends of solvents at 21°C and pressures of 0.1 and 10 MPa: a) blend of 85:15 C5:Tol; b) blend of 75:25 C5:CH. The solid symbols are measured onsets (HPM) and the open symbols are measured yields (blind cell apparatus).

Table 5.10 Deviations of the modeled onsets and yields for WC-B-A3 bitumen diluted with binary blends of solvents from different chemical families at temperatures of 21 and 180°C and pressure of 10 MPa. The overall average absolute deviation and bias in the yields after adjustment were 1.1 wt% and 0.3 wt%, respectively.

Solvent	Temperature °C	Modeling	AAD wt%	MAD wt%	Bias wt%
85:15 C5:Tol	21	predicted	0.8	1.9	-0.8
85:15 C5:Tol	180	predicted	0.5	1.5	-0.5
85:15 C5:Tol	180	adjusted	0.8	2.2	0.8
75:25 C5:CH	21	predicted	0.8	1.7	-0.8
75:25 C5:CH	180	predicted	0.6	1.1	-0.1
75:25 C5:CH	180	adjusted	2.0	5.3	2.0

Table 5.11 Fitted binary interaction parameters for asphaltene/toluene and asphaltene/cyclohexane pairs at 180°C and 10 MPa.

Solvent	λ_{min}	λ_{max}
Toluene	0.0000	0.0687
Cyclohexane	0.0000	0.0466

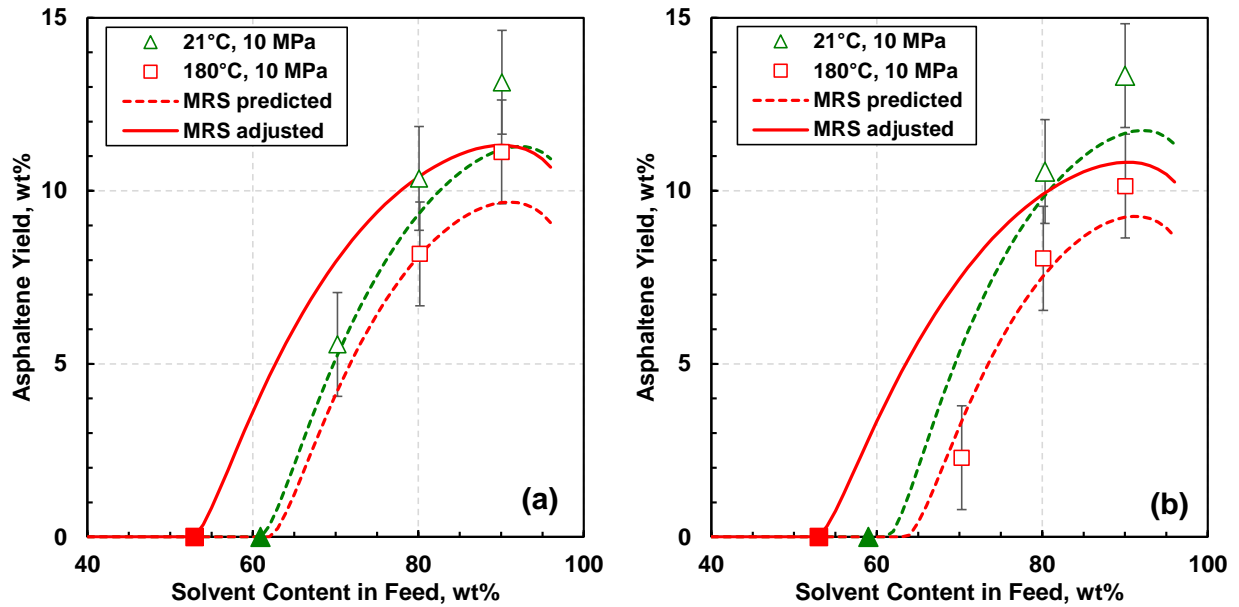


Figure 5.8 Measured, predicted, and adjusted asphaltene onsets and yields from WC-B-A3 bitumen diluted with binary blends of solvents at temperatures of 21 and 180°C and pressure of 10 MPa: a) blend of 85:15 C5:Tol; b) blend of 75:25 C5:CH. The dashed lines are the predicted yields with the original BIPs and the solid line is the modeled yield with the adjusted BIPs from Table 5.11. The solid symbols are measured onsets (HPM) and the open symbols are measured yields (blind cell apparatus).

Table 5.12 Measured and modeled asphaltene precipitation onsets from WC-B-A3 bitumen diluted with binary blends of solvents from different chemical families at temperatures of 21 and 180°C and pressure of 10 MPa. The overall average absolute deviation and bias in the onsets after adjustment were 0.7 wt% and 0.7 wt%, respectively.

Solvent	Temperature °C	Modeling	Measured Onset wt%	Modeled Onset wt%	Deviation wt%
85:15 C5:Tol	21	predicted	60.9	61.1	0.2
85:15 C5:Tol	180	predicted	52.9	62.2	9.3
85:15 C5:Tol	180	adjusted	52.9	52.9	0.0
75:25 C5:CH	21	predicted	59.0	61.5	2.6
75:25 C5:CH	180	predicted	53.0	63.8	10.8
75:25 C5:CH	180	adjusted	53.0	53.0	0.0

CHAPTER 6: PETROLEUM SOLVENTS RESULTS AND DISCUSSION

This chapter presents a new fluid characterization methodology based on gas chromatography assays to determine the solvent properties required for asphaltene precipitation modeling. The MRS model performance with the new characterization methodology is assessed on asphaltene precipitation data from bitumen diluted with petroleum solvents and with binary blends of petroleum solvents and *n*-heptane. The experimental data was measured for a Western Canadian bitumen diluted with petroleum solvents and their blends with *n*-heptane. The solvents included two condensate samples (Condensate 1 and Condensate 2), two diesel samples (Diesel 1 and Diesel 3), a kerosene (Kerosene 1), and a naphtha (Naphtha 1). The following terminology is used to describe the blends: “XX:YY A:B” indicates XX wt% solvent A and YY wt% solvent B; C7, D1, D3, and KER, indicate *n*-heptane, Diesel 1, Diesel 3, and Kerosene 1, respectively. The model deviations are assessed in terms of average absolute deviation (AAD), the maximum absolute deviation (MAD), and the bias (average deviation).

6.1 Petroleum Solvent Characterization Based on Gas Chromatography

As discussed in Chapter 5, the bitumens used in this thesis were characterized based on a SARA analysis. However, SARA fractionation is not appropriate to characterize petroleum solvents. One of the main drawbacks of the SARA analysis is the loss of volatile material, corresponding to saturates and aromatics, which are the main components of the petroleum solvents of interest in this thesis (Bissada *et al.*, 2016; Fan and Buckley, 2002). In addition, the SARA assay cannot provide a composition of the solvents that is detailed enough to predict their properties (Broad *et al.*, 2001; Riazi, 2005). The solvents typically consist of a mixture of light components which would appear merely as a saturate and an aromatic fraction in the SARA assay. Gas chromatography provides a much more detailed description of such fluids, including the mass fractions of: pure normal and iso-alkanes up to a carbon number of 5, selected aromatic and cyclic components, and single carbon number fractions often up to a carbon number of 30 (Pedersen and Christensen, 2007).

6.1.1 Generation of Pseudo-Components

The petroleum solvents used in this thesis, including condensates, diesel, kerosene, and naphtha, were characterized into single carbon number (SCN) pseudo-components based on their GC assay. A SCN fraction includes all of the species with that carbon number. These solvents were characterized into SCN pseudo-components with carbon numbers of up to 29, while heavier components with a carbon number higher than 29 were lumped into a single C30+ pseudo-component. The aromatic and naphthenic components were lumped into the SCN of the same carbon number, whereas the iso-paraffins were treated as individual components. The measured and lumped GC assay of Condensate 1 is provided in Table 6.1 as an example. The assays for the other petroleum solvents are provided in Appendix A.

Table 6.1 Measured and lumped GC assay of Condensate 1.

Component	Carbon Number	Measured wt%	Lumped wt%
Methane	C ₁	0.00	0.00
Ethane	C ₂	0.00	0.00
Propane	C ₃	0.00	0.00
Iso Butane	iC ₄	0.05	0.05
Normal Butane	C ₄	3.75	3.75
Iso Pentane	iC ₅	18.36	18.36
Normal Pentane	C ₅	17.29	17.29
Hexanes	C ₆	16.83	24.03
Heptanes	C ₇	9.20	14.84
Octanes	C ₈	6.48	8.14
Nonanes	C ₉	3.96	4.16
Decanes	C ₁₀	2.68	2.68
Undecanes	C ₁₁	1.68	1.68
Dodecanes	C ₁₂	0.80	0.80
Tridecanes	C ₁₃	0.63	0.63
Tetradecanes	C ₁₄	0.51	0.51
Pentadecanes	C ₁₅	0.40	0.40
Hexadecanes	C ₁₆	0.33	0.33
Heptadecanes	C ₁₇	0.21	0.21
Octadecanes	C ₁₈	0.26	0.26
Nonadecanes	C ₁₉	0.30	0.30
Eicosanes	C ₂₀	0.20	0.20
Heneicosanes	C ₂₁	0.18	0.18
Docosanes	C ₂₂	0.18	0.18
Tricosanes	C ₂₃	0.16	0.16
Tetracosanes	C ₂₄	0.14	0.14
Pentacosanes	C ₂₅	0.13	0.13
Hexacosanes	C ₂₆	0.12	0.12
Heptacosanes	C ₂₇	0.10	0.10
Octacosanes	C ₂₈	0.10	0.10
Nonacosanes	C ₂₉	0.06	0.06
Triacontanes Plus	C ₃₀₊	0.21	0.21
Benzene	C ₆ H ₆	0.93	
Toluene	C ₇ H ₈	1.69	
Ethylbenzene, p+m-Xylene	C ₈ H ₁₀	1.32	
o-Xylene	C ₈ H ₁₀	0.34	
1,2,4 Trimethylbenzene	C ₉ H ₁₂	0.20	
Cyclopentane	C ₅ H ₁₀	0.00	
Methylcyclopentane	C ₆ H ₁₂	3.42	
Cyclohexane	C ₆ H ₁₂	2.85	
Methylcyclohexane	C ₇ H ₁₄	3.95	

6.1.2 Pseudo-Component Properties at Standard Conditions

Up to Carbon Number of 5

The properties required for the pseudo-components are their molecular weight, effective density, and solubility parameter. The properties of the SCN pseudo-components with carbon numbers of up to five were set equal to the pure component properties of the *n*-alkanes with the same carbon number. The properties of isobutane and isopentane were also set equal to their pure component properties. The molecular weights were reported values from the literature.

The *n*-alkane liquid densities were determined as effective densities because the lighter *n*-alkanes are gases at standard conditions. The *n*-alkane effective densities at standard conditions were calculated from the following correlation (Saryazdi *et al.*, 2013):

$$\rho = (a_1 + a_2T) + [(b_1 + b_2T)P] \quad (6.1)$$

where a_1 , a_2 , b_1 , and b_2 are fluid-specific parameters, T is the absolute temperature in K, and P is the pressure in MPa. The fluid-specific parameters are provided in Appendix C. The effective densities of isobutane and isopentane at standard conditions (ρ_{iCX}^o) were calculated from the ratio of molecular weight to molar volume, and the molar volumes were determined from the modified Rackett correlation (Spencer and Danner, 1972) as follows:

$$\rho_{iCX}^o = \frac{MW}{\frac{RT_c Z_{RA}}{P_c} [1 + (1 - T_r)^{2/7}]} \quad (6.2)$$

where MW is the molecular weight, R is gas constant, T_c is the critical temperature in K, P_c is the critical pressure in MPa, Z_{RA} is the Rackett compressibility factor, and T_r is the reduced temperature. The Rackett compressibility factor was tuned to experimental saturated liquid densities (*NIST Standard Reference Database*, n.d.). The tuned Z_{RA} for isobutane and isopentane are provided in Appendix C.

The solvent solubility parameters at the standard conditions of 25°C and 0.1 MPa (δ_i^o) were taken from Barton (1991) and are provided in Appendix C. However, the standard condition solubility parameters of the isobutane and isopentane were set to 0.995 times the equivalent carbon number *n*-alkane solubility parameter, as will be discussed later.

Carbon Number > 5

The higher carbon number fractions consist of a number of isomers including aromatic and naphthenic components. Therefore, the properties of the SCN pseudo-components with carbon numbers from six to thirty were scaled between *n*-alkane reference properties and the equivalent carbon number aromatic properties using an aromaticity factor (A_F). The densities, molecular weights, and solubility parameters of the SCN pseudo-components were adjusted using a correlation of the form:

$$X_{adj}^o = X_{ref}^o(1 + k_X A_F) \quad (6.3)$$

where X^o is a given property at the standard conditions of 25°C and 0.1 MPa, k_X is a coefficient specific to the property X , the subscript *adj* indicates any SCN pseudo-component with a carbon number higher than five, and the subscript *ref* indicates the reference *n*-alkane with the same carbon number as the SCN pseudo-component. A_F is the aromaticity factor of the solvent and is set to scale between the *n*-alkane reference density, molecular weight, and solubility parameter when $A_F = 0$ and the equivalent carbon number aromatic density, molecular weight, and solubility parameter when $A_F = 1$. It is well established that the density at a fixed molecular weight increases as the aromaticity of the fraction increases (Pedersen and Christensen, 2007). Therefore, the aromaticity factor (A_F) is tuned for each solvent to fit the measured density at the standard conditions of 25°C and 0.1 MPa. The measured densities of the petroleum solvents used in this thesis are provided in Appendix C. The correlations used to determine the properties of the SCN pseudo-components with carbon numbers higher than five are provided below.

Molecular Weight

Figure 6.1 shows the relationship of molecular weight to single carbon number for different chemical families. The relationship is linear for each family and the molecular weight decreases as the aromaticity of the fraction increases. Therefore, the molecular weights of the SCN pseudo-components with carbon numbers higher than five were calculated as follows:

$$MW_{adj} = MW_{ref}(1 - 0.0732A_F) \quad (6.4)$$

where MW_{ref} is the molecular weight of the reference *n*-alkane with the same carbon number as the SCN pseudo-component. The *n*-alkane reference molecular weights were set to the reported values from the literature. The reference molecular weight of the C30+ pseudo-component was set equal to the molecular weight of the *n*-alkane with a carbon number of 30. The coefficient of -

0.0732 in Eq. 6.4 was set to give the molecular weight of the aromatic component with the same carbon number as the reference *n*-alkane when $A_F=1$ (dashed line on Figure 6.1).

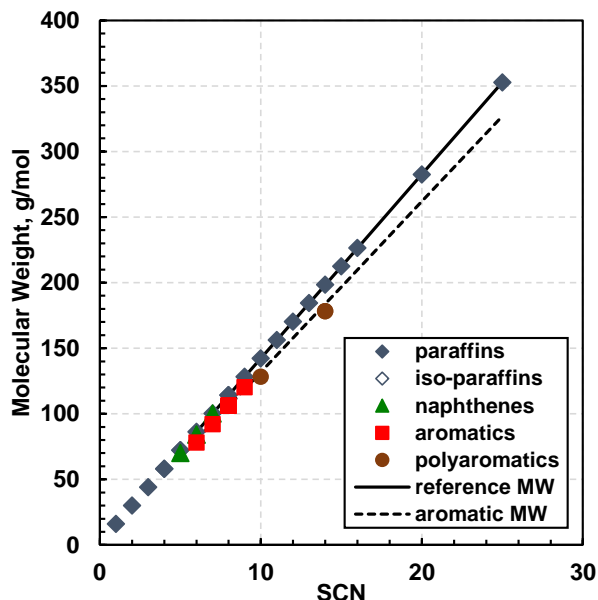


Figure 6.1 Molecular weights of selected hydrocarbons from different chemical families. The solid line is a best fit of the molecular weights of paraffins with carbon numbers higher than five, provided as visual aid. The dashed line is the proposed correlation (Eq. 6.4) to calculate the molecular weights of SCN pseudo-components with carbon numbers higher than five when $A_F = 1$.

Density

Figure 6.2 shows the relationship of density to carbon number for different chemical families. Above a carbon number of 5, density increases gradually with increasing carbon number for the *n*-alkanes and naphthenes. The naphthene curve is approximately parallel to the *n*-alkane curve. The aromatic curve is not exactly parallel because some of the aromatic compounds include *n*-alkyl side chains (*e.g.*, ethylbenzene). The purely aromatic curve was assumed to be parallel to the *n*-alkane curve and the density at standard conditions of the SCN pseudo-components with carbon numbers higher than five were then calculated as follows:

$$\rho_{adj}^o = \rho_{ref}^o(1 + 0.4A_F) \quad (6.5)$$

where ρ_{ref}^o is the density at standard conditions of the reference *n*-alkane with the same carbon number as the SCN pseudo-component. The coefficient of 0.4 in Eq. 6.5 was set to give the density

of the aromatic component with the same carbon number as the reference n -alkane when $A_F=1$ (dashed line on Figure 6.2).

The n -alkane reference densities at standard conditions of the SCN pseudo-components with carbon numbers from 6 to 29 were calculated with Eq. 6.1. The n -alkane reference density at standard conditions of the C30+ pseudo-component was linearly extrapolated from the n -alkane reference densities at standard conditions of the SCN pseudo-components with carbon numbers from 25 to 29. The following correlations were proposed to calculate the fluid-specific parameters used in Eq. 6.1 for n -alkanes with carbon numbers higher than seven:

$$a_1 = A_{a_1} + B_{a_1}[1 - \exp(-C_{a_1}MW_{ref})] \quad (6.6)$$

$$a_2 = A_{a_2} + B_{a_2}[1 - \exp(-C_{a_2}MW_{ref})] \quad (6.7)$$

$$b_1 = A_{b_1} + B_{b_1}[1 - \exp(-C_{b_1}MW_{ref})] \quad (6.8)$$

$$b_2 = A_{b_2} + (B_{b_2}MW_{ref}) \quad (6.9)$$

where a_1 , a_2 , b_1 , and b_2 are the fluid-specific parameters in Eq. 6.1, MW_{ref} is the n -alkane reference molecular weight, and A_i , B_i , and C_i are fitted constants. The correlations were developed using the fluid-specific parameters of n -pentane to n -heptane from Saryazdi *et al.* (2013) and values fitted to experimental saturated liquid densities (*NIST Standard Reference Database*, n.d.) for n -octane, n -decane, n -dodecane, n -tetradecane, and n -hexadecane. The correlation of these fluid-specific parameters to the molecular weight of n -alkanes is shown in Figure 6.3. The fitted constants for Equations 6.6 to 6.9 are provided in Table 6.2. Figure 6.3 shows the fitted and predicted fluid-specific parameters for the effective liquid density of n -alkanes with a carbon number of up to sixteen.

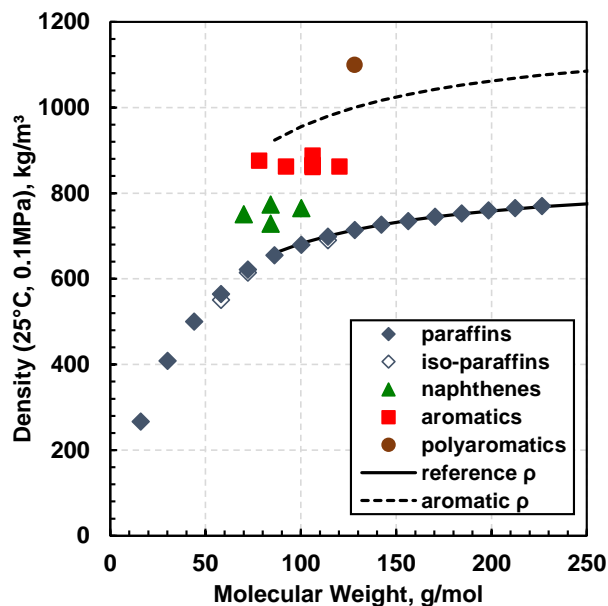


Figure 6.2 Effective liquid densities at standard conditions of selected hydrocarbons from different chemical families. The solid line represents the density of selected *n*-alkanes with carbon numbers higher than five calculated with Eq. 6.1. The dashed line is the proposed correlation (Eq. 6.5) to calculate the density of SCN pseudo-components with carbon numbers higher than five when $A_F = 1$.

Table 6.2 Fitted constants for the effective liquid density fluid-specific parameters for SCN pseudo-components with carbon numbers higher than seven.

Parameter	A_i	B_i	C_i
a_1	582.128	399.776	0.018608
a_2	-0.889137	0.791902	0.001228
b_1	0.012399	-0.286667	0.010706
b_2	0.002649	4.57555×10^{-7}	-

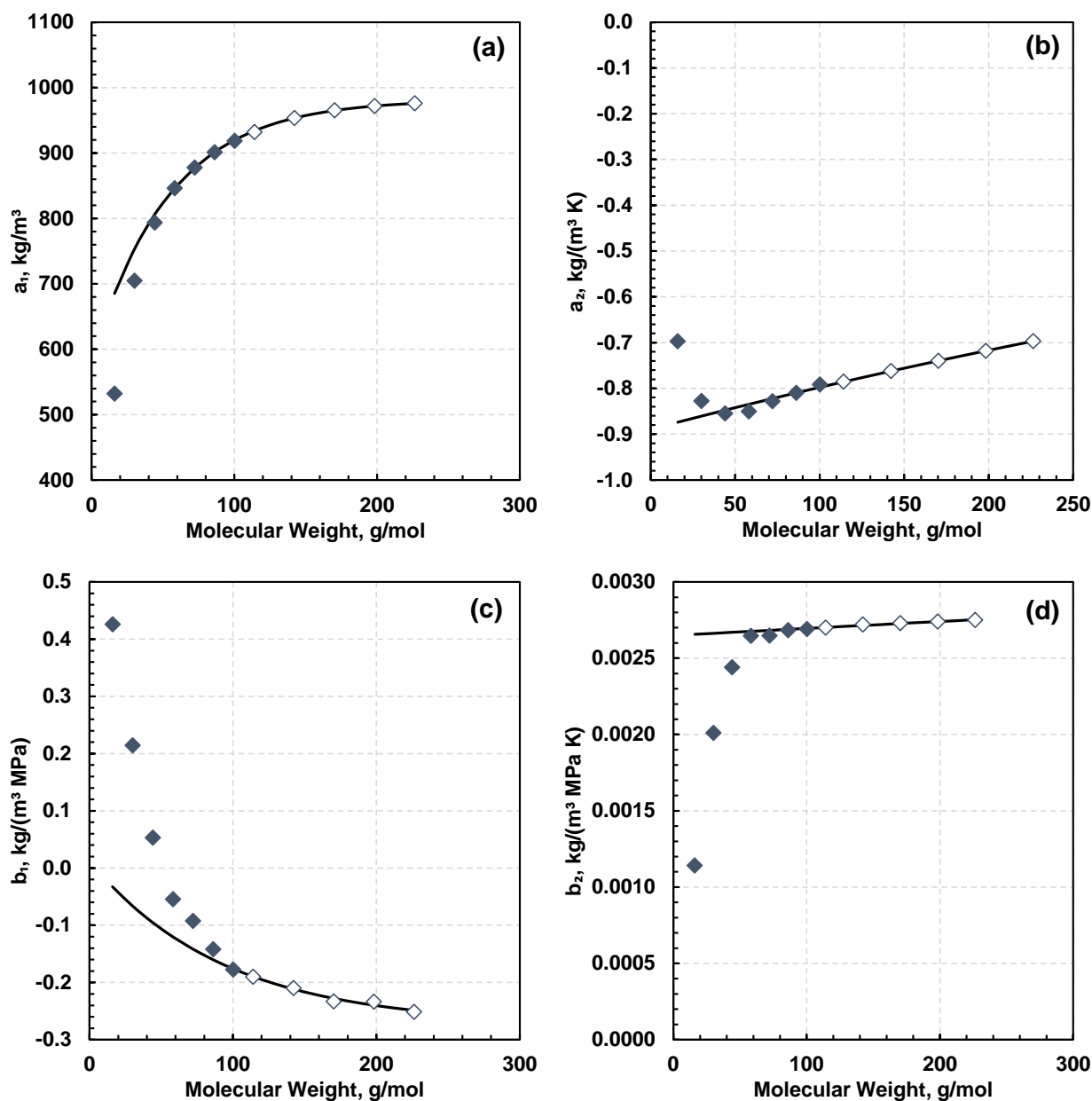


Figure 6.3 Fluid-specific parameters for the effective liquid density of *n*-alkanes. The closed symbols are the parameters for methane to *n*-heptane from Saryazdi *et al.* (2013). The open symbols are the fitted parameters for *n*-octane to *n*-hexadecane tuned in this thesis. The solid lines are the proposed correlations (Eq. 6.6 to 6.9) to calculate the fluid-specific parameters for the effective liquid density of *n*-alkanes with carbon numbers higher than seven.

Solubility Parameter

Figure 6.5 shows the relationship of solubility parameter to carbon number for different chemical families. The pattern is similar to the density trends. Above a carbon number of 5, the solubility parameter increases gradually with increasing carbon number for the *n*-alkanes and naphthenes. The naphthene curve is approximately parallel to the *n*-alkane curve and the aromatic curve is again not parallel because some of the aromatic compounds include *n*-alkyl side chains. The purely aromatic curve was assumed to be parallel to the *n*-alkane curve and the solubility parameters at standard conditions of the SCN pseudo-components with carbon numbers higher than five were initially calculated using the following empirical correlation:

$$\delta_{adj}^o = \delta_{ref}^o (1 + 0.29A_F) \quad (6.10)$$

where δ_{ref}^o is the solubility parameter at standard conditions of the reference *n*-alkane with the same carbon number as the SCN pseudo-component. The coefficient of 0.29 in Eq. 6.10 was set to calculate the solubility parameter of the aromatic component with the same carbon number as the reference *n*-alkane when $A_F=1$. The coefficient was adjusted, as will be discussed later, to obtain the following final correlation:

$$\delta_{adj}^o = \delta_{ref}^o (1 + 0.11A_F) \quad (6.11)$$

The *n*-alkane reference solubility parameters of the SCN pseudo-components with carbon numbers higher than five at the standard conditions of 25°C and 0.1 MPa were calculated from the following correlation (Ramos-Pallares *et al.*, 2020):

$$\delta_{ref}^o = -0.979 + 17.79119[1 - \exp(-0.00646T_b)] \quad (6.12)$$

where T_b is the normal boiling point in K. The normal boiling points of *n*-alkanes were correlated to their molecular weight as follows:

$$T_b = 41.8916MW_{ref}^{0.4770} \quad (6.13)$$

Note that the reference solubility parameter for the C30+ pseudo-component was calculated from the normal boiling point and molecular weight of the *n*-alkane with carbon number of 30. Figure 6.4 shows the normal boiling points of selected *n*-alkanes with carbon numbers higher than five calculated from Eq. 6.13. Figure 6.5 compares the *n*-alkane reference solubility parameters calculated with Eq. 6.12 and the equivalent carbon number aromatic solubility parameters for selected SCN pseudo-components calculated from Eqs. 6.10 and 6.11 when $A_F = 1$.

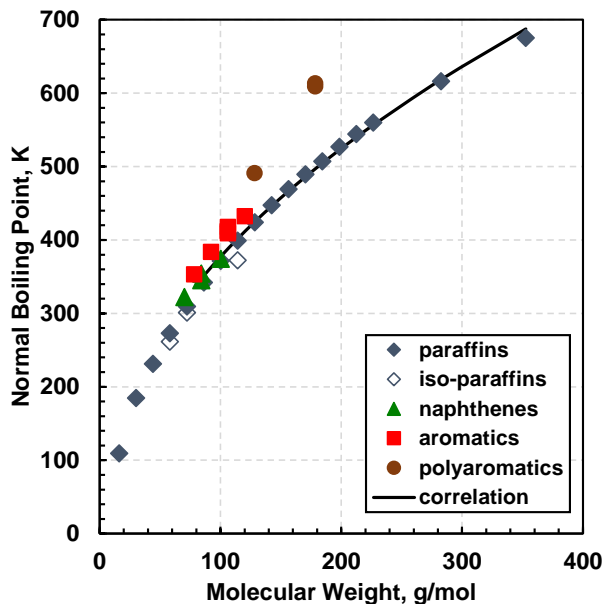


Figure 6.4 Normal boiling points of selected hydrocarbons from different chemical families. Solid line is the empirical correlation (Eq. 6.13) to calculate the normal boiling points of *n*-alkanes with carbon numbers higher than five.

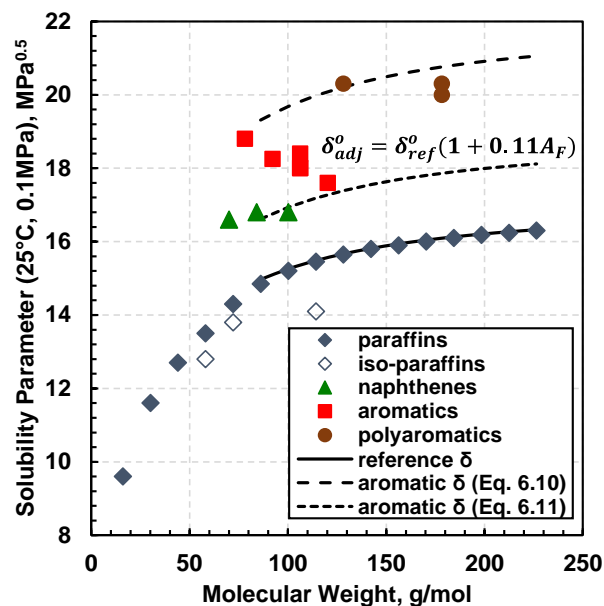


Figure 6.5 Solubility parameters at standard conditions of selected hydrocarbons from different chemical families. The solid line represents the solubility parameters of selected *n*-alkanes with carbon numbers higher than five at standard conditions calculated with Eq. 6.12. The dashed lines are the proposed correlations (Eq. 6.10 and 6.11) to calculate the solubility parameters of SCN pseudo-components with carbon numbers higher than five when $A_F = 1$.

6.1.3 Pseudo-Component Properties at non-Standard Conditions

The density at non-standard conditions of the SCN pseudo-components with carbon numbers of up to five were set equal to the effective density of the *n*-alkanes with the same carbon number. The densities at non-standard conditions of the SCN pseudo-components with carbon numbers higher than five were calculated as follows:

$$\rho_{adj} = \rho_{ref}(1 + 0.4A_F) \quad (6.14)$$

where ρ_{ref} is the density at non-standard conditions of the reference *n*-alkane with the same carbon number as the SCN pseudo-component. The *n*-alkane reference densities at non-standard conditions of the SCN pseudo-components with carbon numbers up to 29 were calculated from Eq. 6.1. The *n*-alkane reference density at non-standard conditions of the C30+ pseudo-component was linearly extrapolated from the *n*-alkane reference densities at non-standard conditions of the SCN pseudo-components with carbon numbers from 25 to 29.

The densities at non-standard conditions of isobutane and isopentane were calculated as follows:

$$\rho_{iCX} = \left(\frac{\rho_{iCX}^o}{\rho_{ref}^o} \right) \rho \quad (6.15)$$

where ρ_{iCX}^o is the density at standard conditions of the iso-paraffin calculated from Eq. 6.2, ρ_{ref}^o is the effective density at standard conditions of the equivalent carbon number paraffin calculated from Eq. 6.1, and ρ is the effective density at non-standard conditions of the equivalent carbon number paraffin calculated from Eq. 6.1.

The solubility parameters at non-standard conditions of the iso-paraffins and of any SCN pseudo-component were calculated from the following correlation (Ramos-Pallares and Yarranton, 2020):

$$\delta_i = \delta_i^o \sqrt{\frac{\rho_{TOP,i}}{\rho_i^o}} - 0.0232(T - 298.15) \quad (6.16)$$

where δ_i^o is the solubility parameter at standard conditions, ρ_i^o is the density at standard conditions, $\rho_{TOP,i}$ is the density at standard temperature and actual pressure, and T is the absolute temperature.

6.1.4 Model Implementation

The model is implemented exactly as described in Chapter 4 except that the molecular weight, density, and solubility parameters of the petroleum solvents were calculated using the characterization methodology presented in the previous sections. The modified implementation is shown in Figure 6.6. The mixing rules, MRS model, and flash calculations are unchanged.

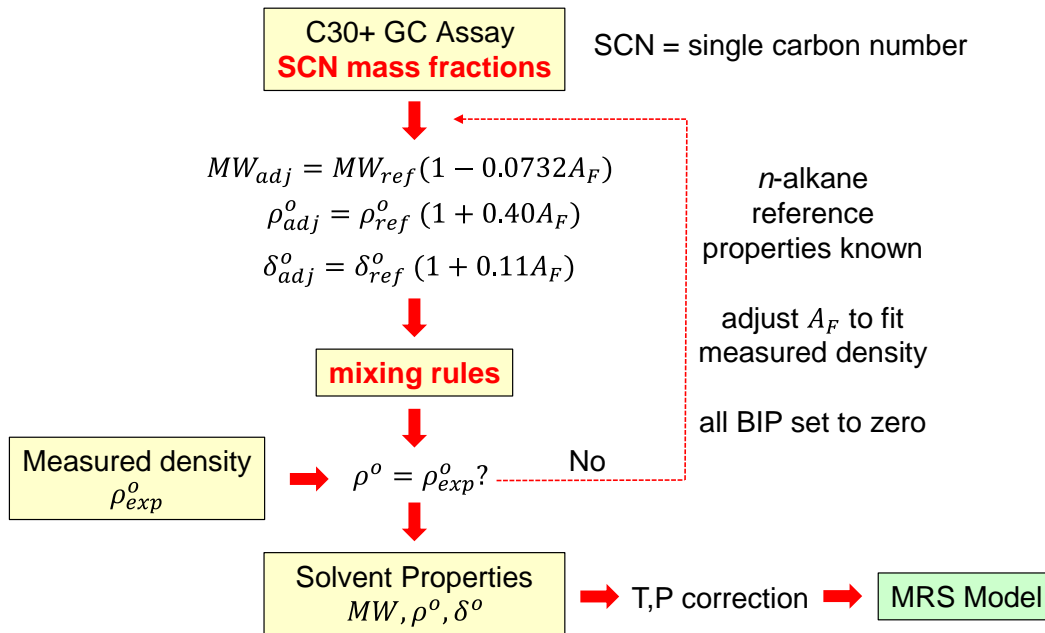


Figure 6.6 Schematic of the fluid characterization methodology.

6.2 Asphaltene Precipitation Data

The asphaltene yields from bitumen diluted with petroleum solvents and binary blends of petroleum solvents and *n*-heptane at 21°C and 0.1 MPa are summarized in Figure 6.7. The yields are on a toluene insoluble-free basis and their repeatability is ± 0.5 wt%. The asphaltene precipitation data are also provided in Tables 6.3 to 6.7. Figure 6.7 shows that the only petroleum solvents that precipitated asphaltenes upon their addition to the bitumen were the condensates and the naphtha. Diesel 1, Diesel 3, and Kerosene 1 were blended with *n*-heptane to trigger a measurable amount of asphaltene precipitation to which the MRS model could be fitted.

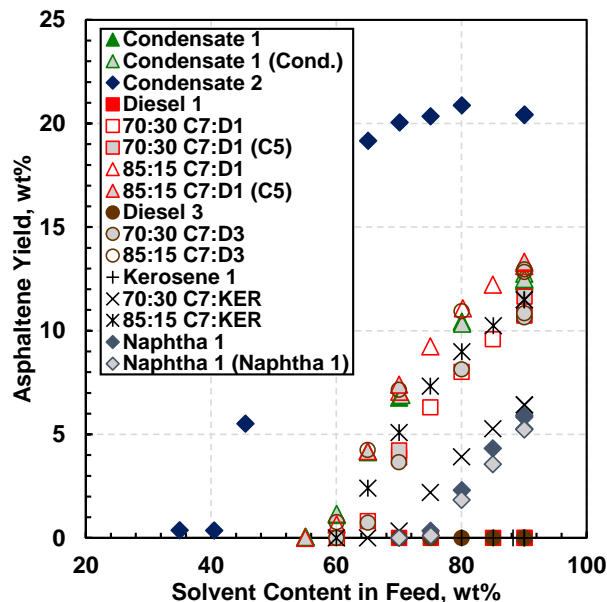


Figure 6.7 Asphaltene yields from WC-B-A3 bitumen diluted with petroleum solvents and binary blends of petroleum solvents and *n*-heptane at 21°C and 0.1 MPa. The precipitate from bitumen diluted with petroleum solvents and solvent blends was washed with *n*-pentane and the same solvent blend, respectively, unless otherwise noted. The solvent in parenthesis indicates the solvent used to wash the precipitate.

Recall that the asphaltene precipitate from petroleum solvents was washed with *n*-pentane whereas the precipitate from solvent blends was washed with the same solvent blend and the residual solvent was deducted, as described in Chapter 3. To validate the mass correction method, the asphaltene yields from Condensate 1 and Naphtha 1 obtained with an *n*-pentane wash were compared to the yields obtained with a petroleum solvent wash. The collected yields are provided in Tables 6.3 and 6.7. The yields measured using the petroleum solvent wash were within the error of the measurement of the asphaltene yield obtained with the *n*-pentane wash.

The residual solvent in the precipitate from the bitumen diluted with binary blends of *n*-heptane and Diesel 1 was not quantified. Therefore, to validate the measurements, the asphaltene yields at selected solvent contents were repeated using an *n*-pentane wash. The methodology with the *n*-pentane wash was used because the drying times are significantly shorter compared to the procedure with the solvent blend wash. The asphaltene yields from bitumen diluted with Diesel 1 and the binary blends of *n*-heptane and Diesel 1 are provided in Table 6.4. Similarly to the Naphtha 1 yields, the yields from the diesel blends washed with *n*-pentane were slightly higher than the

yields obtained with the solvent blend wash. Note that the asphaltene yields obtained with the *n*-pentane wash are higher because the addition of the excess of *n*-pentane triggers the precipitation of all the asphaltenes from the residual bitumen trapped in the precipitate.

Table 6.3 Asphaltene yields from WC-B-A3 bitumen diluted with Condensate 1 and Condensate 2 at 21°C and 0.1 MPa. The precipitate was washed with *n*-pentane unless otherwise noted. The solvent in parenthesis indicates the solvent used to wash the precipitate.

Solvent	Solvent Content	Asphaltene Yield
	wt%	wt%
Condensate 1	55.1	0.1
	60.1	1.1
	65.1	4.1
	70.0	6.8
	80.0	10.4
	90.0	12.4
	90.0	12.4
Condensate 1 (Condensate 1)	55.1	0.0
	60.0	1.2
	65.0	4.2
	70.4	6.9
	80.1	10.3
	90.0	12.8
	90.0	12.5
Condensate 2	35.0	0.4
	40.5	0.4
	45.5	5.5
	50.1	11.2
	55.1	14.4
	60.2	17.5
	65.1	19.2
	70.1	20.1
	75.0	20.3
	80.0	20.9
	90.0	20.4
90.0	20.4	

Table 6.4 Asphaltene yields from WC-B-A3 bitumen diluted with Diesel 1 and binary blends of Diesel 1 and *n*-heptane at 21°C and 0.1 MPa. The precipitate from bitumen diluted with Diesel 1 and the solvent blends was washed with *n*-pentane and the same solvent blend, respectively, unless otherwise noted. The solvent in parenthesis indicates the solvent used to wash the precipitate.

Solvent	Solvent Content	Asphaltene Yield
	wt%	wt%
Diesel 1	70.0	0.0
	75.1	0.0
	85.0	0.0
	90.1	0.0
	90.0	0.0
70:30 C7:D1	60.1	0.0
	65.0	0.8
	70.0	3.9
	75.0	6.3
	80.0	8.0
	85.0	9.6
	90.0	10.8
	90.0	10.7
70:30 C7:D1 (<i>n</i> -pentane)	70.0	4.2
	90.1	11.6
85:15 C7:D1	55.0	0.0
	60.0	0.7
	65.0	4.2
	70.0	7.1
	75.0	9.3
	80.2	11.1
	85.0	12.2
	90.0	13.1
	90.0	13.3
85:15 C7:D1 (<i>n</i> -pentane)	70.0	7.4
	90.0	13.3

Table 6.5 Asphaltene yields from WC-B-A3 bitumen diluted with Diesel 3 and binary blends of Diesel 3 and *n*-heptane at 21°C and 0.1 MPa. The precipitate from bitumen diluted with Diesel 3 and the solvent blends was washed with *n*-pentane and the same solvent blend, respectively.

Solvent	Solvent Content	Asphaltene Yield
	wt%	wt%
Diesel 3	70.0	0.0
	75.0	0.0
	80.0	0.0
	85.0	0.0
	90.0	0.0
	90.0	0.0
70:30 C7:D3	60.0	0.0
	65.0	0.7
	70.0	3.7
	80.0	8.1
	90.0	10.7
	90.0	10.9
85:15 C7:D3	60.1	0.8
	65.0	4.3
	70.0	7.2
	80.0	10.9
	90.0	12.8
	90.0	13.0

Table 6.6 Asphaltene yields from WC-B-A3 bitumen diluted with Kerosene 1 and binary blends of Kerosene 1 and *n*-heptane at 21°C and 0.1 MPa. The precipitate from bitumen diluted with Kerosene 1 and the solvent blends was washed with *n*-pentane and the same solvent blend, respectively.

Solvent	Solvent Content	Asphaltene Yield
	wt%	wt%
Kerosene 1	80.0	0.0
	85.1	0.0
	88.2	0.0
	90.0	0.0
	90.0	0.0
70:30 C7:KER	65.0	0.0
	70.0	0.3
	75.0	2.2
	80.0	3.9
	85.0	5.3
	90.0	6.4
	90.1	6.4
85:15 C7:KER	60.0	0.0
	65.0	2.4
	70.0	5.1
	75.0	7.3
	80.0	9.0
	85.1	10.2
	90.0	11.5
90.0	11.5	

Table 6.7 Asphaltene yields from WC-B-A3 bitumen diluted with Naphtha 1 at 21°C and 0.1 MPa. The solvent in parenthesis indicates the solvent used to wash the precipitate.

Solvent	Solvent Content	Asphaltene Yield
	wt%	wt%
Naphtha 1	75.1	0.3
(n-pentane)	80.0	2.3
	85.0	4.3
	90.0	5.9
	90.0	5.8
	90.0	5.8
Naphtha 1	70.0	0.0
(Naphtha 1)	75.1	0.1
	80.0	1.8
	85.0	3.6
	90.0	5.3
	90.0	5.2

6.3 Asphaltene Precipitation Modeling Results

6.3.1 Initial Testing

The MRS model was first tested on the measured asphaltene yields from the WC-B-A3 bitumen at ambient conditions. The initial correlation for the SCN solubility parameters (Eq. 6.10) was used in this test. The model was previously tuned to match the yield from *n*-heptane diluted bitumen. The tuned asphaltene solubility parameters at standard conditions were $\delta_{min}^o = 19.81 \text{ MPa}^{0.5}$ and $\delta_{max}^o = 20.17 \text{ MPa}^{0.5}$.

Figure 6.8a shows the measured and predicted asphaltene yields from the WC-B-A3 bitumen diluted with Condensate 1 and Condensate 2 at 21°C and 0.1 MPa. Condensate 2 is a highly paraffinic condensate and Condensate 1 is a less paraffinic condensate. Therefore, the measured yield of asphaltene precipitation from the bitumen diluted with Condensate 2 was higher than the yield from Condensate 1. Figure 6.8a shows that the model under-predicted the asphaltene yield from Condensate 1 and over-predicted the asphaltene yield from Condensate 2. This deviation may occur because the characterization methodology does not accurately give the proportion of components from different chemical families within the petroleum solvents.

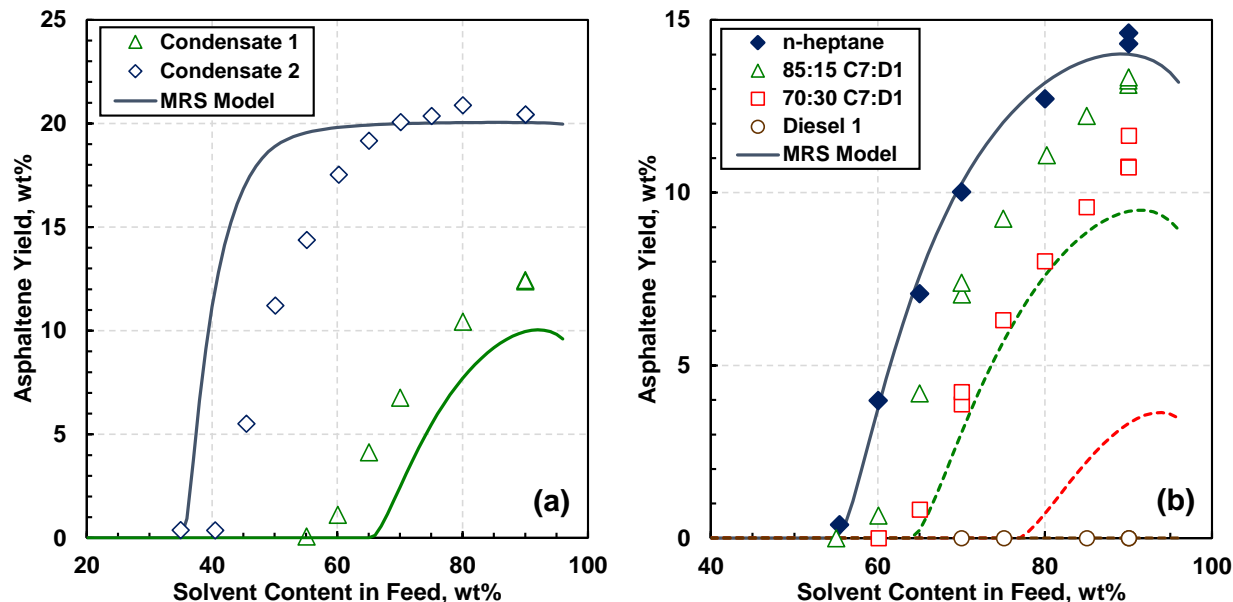


Figure 6.8 Measured and modeled asphaltene yields from WC-B-A3 bitumen diluted at 21°C and 0.1 MPa: a) Condensate 1 and Condensate 2; b) binary blends of *n*-heptane and Diesel 1. The solid lines are the model results for the single or multicomponent component solvent and the dashed lines are the blended solvents.

Figure 6.8b shows the measured and predicted yield from the WC-B-A3 bitumen diluted with 85:15 C7:D1 and 70:30 C7:D1 at 21°C and 0.1 MPa. The asphaltene yield from the bitumen diluted with *n*-heptane is provided for comparison. The measured asphaltene yield decreased as the content of diesel in the binary blend increased indicating that the diesel was a better solvent for asphaltenes than *n*-heptane. Figure 6.8b shows that the model over-predicted the asphaltene onsets and under-predicted all of the yields for both solvent blends. While not shown here, the model also under-predicted the asphaltene yields from the bitumen diluted with the naphtha and all of the binary blends of petroleum solvents and *n*-heptane.

6.3.2 Updated Characterization

The model deviation may be due to a departure in the cohesive energy density of the mixture from the geometric mean as described in Chapter 5. However, in this case, the chemical family of the SCN pseudo-components is ill-defined and there is no way to determine the binary interaction parameters. For the sake of simplicity, all the binary interaction parameters were set to zero, and, instead, the solubility parameter property correlation (Eq. 6.10) was modified to match the

experimental data. The coefficient of 0.29 in the solubility parameter correlation (Eq. 6.10) was adjusted to 0.11. The new coefficient was determined by fitting the MRS model to yield data collected for bitumen diluted with all of the petroleum solvents. In addition, the standard condition solubility parameters of the iso-paraffins (isobutane and isopentane) were set to 0.995 times the equivalent carbon number n -alkane solubility parameter. The tuning of the iso-paraffins was required to better fit the condensate data. The predicted molecular weight, density, and solubility parameter of each petroleum solvent are provided in Table 6.8.

Table 6.8 Predicted molecular weight, density, and solubility parameter of petroleum solvents at temperatures of 21 and 25°C and pressure of 0.1 MPa.

Solvent	MW g/mol	$\rho_{21^\circ C}$ kg/m ³	$\delta_{21^\circ C}$ MPa ^{0.5}	$\rho_{25^\circ C}$ kg/m ³	$\delta_{25^\circ C}$ MPa ^{0.5}
Condensate 1	87.18	682.11	15.08	678.79	14.99
Condensate 2	70.08	618.91	14.32	615.64	14.23
Diesel 1	192.60	839.33	16.74	836.17	16.65
Diesel 3	194.64	842.61	16.77	839.45	16.67
Kerosene 1	226.39	905.08	17.20	901.87	17.10
Naphtha 1	103.16	748.11	15.77	744.69	15.67

Figures 6.9 and 6.10 show the measured and modeled yield data for the WC-B-A3 bitumen diluted with petroleum solvents and binary blends of petroleum solvents and n -heptane at 21°C and 0.1 MPa. The fitted and modeled onsets are listed in Table 6.9. The deviations for the modeled yields are provided in Table 6.10. The model captured the onsets of asphaltene precipitation with deviations within the experimental error of ± 1.5 wt% (Johnston *et al.*, 2017b). The adjusted model matched the asphaltene yields with AAD and bias of 1.1 wt% and -0.8 wt%, respectively. The modeled asphaltene yields were slightly higher than the repeatability of the yields of ± 0.5 wt%.

In general, the adjusted model was able to match the asphaltene precipitation onsets and yields for bitumen diluted with petroleum solvents and their blends with n -heptane to almost within the error of the measurement. In other words, the characterization approach captured the proportion of components from different chemical families within petroleum solvents. The exception was

naphtha; the model significantly under-predicted the asphaltene yield from the bitumen diluted with Naphtha 1. The reason for this error is unknown but one possibility is that the binary interaction parameters for bitumen and naphtha cannot be neglected. More data on petroleum solvents with a range of chemical compositions would be required to establish a binary interaction parameter correlation. If naphtha is excluded, the deviations of the modeled yields reduce to an AAD of 0.7 wt% and a bias of -0.3 wt%.

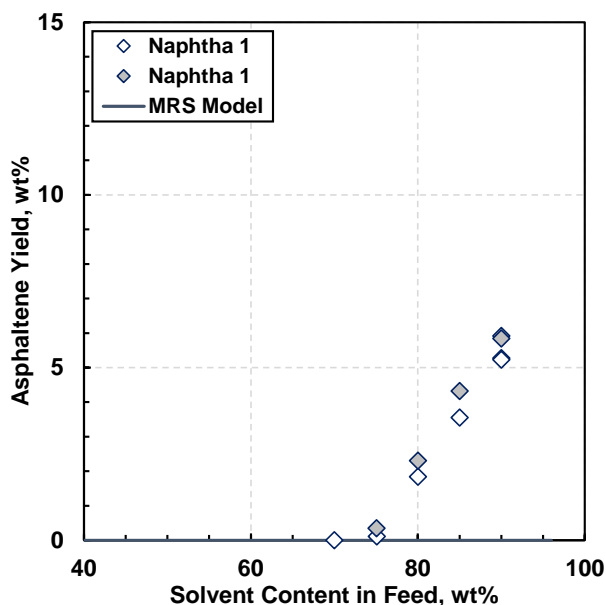


Figure 6.9 Measured and modeled asphaltene yields from WC-B-A3 bitumen diluted with Naphtha 1 at 21°C and 0.1 MPa. The open symbols indicate that the precipitate was washed with naphtha and the closed symbols that it was washed with *n*-pentane.

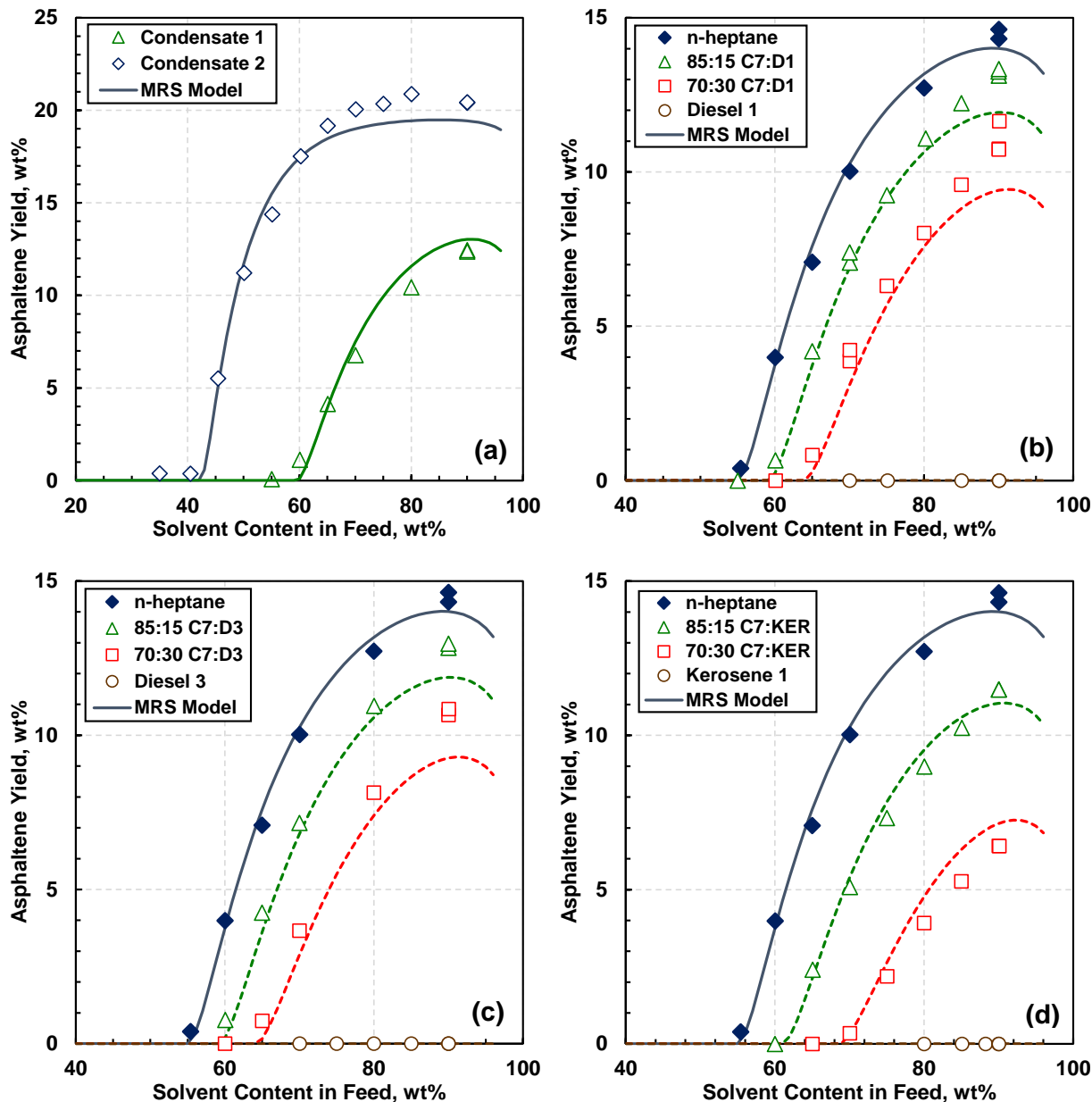


Figure 6.10 Measured and modeled asphaltene yields from WC-B-A3 bitumen diluted with petroleum solvents and binary blends of petroleum solvents and *n*-heptane at 21°C and 0.1 MPa: a) Condensate 1 and Condensate 2; b) binary blends of *n*-heptane and Diesel 1; c) binary blends of *n*-heptane and Diesel 3; d) binary blends of *n*-heptane and Kerosene 1. The solid lines are the model results for the single or multicomponent component solvent and the dashed lines are the blended solvents.

Table 6.9 Fitted and modeled asphaltene onsets from WC-B-A3 bitumen diluted with petroleum solvents and binary blends of petroleum solvents and *n*-heptane at 21°C and 0.1 MPa. The overall average absolute deviation and bias in the modeled onsets after adjustment were 0.3 wt% and 0.2 wt%, respectively. Naphtha 1 and the solvents with no measured yield are not included in the overall deviation calculation.

Solvent	Fitted Onset wt%	Modeled Onset wt%	Deviation wt%
Condensate 1	58.7	59.8	1.1
Condensate 2	42.5	42.5	0.0
Diesel 1	-	-	-
85:15 C7:D1	59.3	59.4	0.1
70:30 C7:D1	63.8	64.2	0.3
Diesel 3	-	-	-
85:15 C7:D3	59.2	59.5	0.3
70:30 C7:D3	64.0	64.5	0.4
Kerosene 1	-	-	-
85:15 C7:KER	61.4	61.3	0.0
70:30 C7:KER	69.3	68.9	-0.4
Naphtha 1	75.6	-	-

Table 6.10 Deviations of the modeled asphaltene yields from WC-B-A3 bitumen diluted with petroleum solvents and binary blends of petroleum solvents and *n*-heptane at 21°C and 0.1 MPa. The overall average absolute deviation and bias in the modeled yields were 1.1 wt% and -0.8 wt%, respectively. The petroleum solvents with no measured yield are not included in the overall deviation calculations.

Solvent	AAD wt%	MAD wt%	Bias wt%
Condensate 1	0.7	1.1	0.3
Condensate 2	0.8	1.4	-0.5
Diesel 1	-	-	-
85:15 C7:D1	0.6	1.3	-0.6
70:30 C7:D1	0.8	1.3	-0.8
Diesel 3	-	-	-
85:15 C7:D3	0.7	1.1	-0.7
70:30 C7:D3	1.0	1.6	-1.0
Kerosene 1	-	-	-
85:15 C7:KER	0.4	0.5	0.1
70:30 C7:KER	0.6	1.0	0.6
Naphtha 1	4.6	5.9	-4.6

CHAPTER 7: CONCLUSIONS AND RECOMMENDATIONS

The main contributions of this thesis are 1) measuring yields and onsets of asphaltene precipitation from Western Canadian bitumens diluted with blended pure solvents, petroleum solvents, and binary blends of *n*-heptane and petroleum solvents; 2) extending the Modified Regular Solution (MRS) approach to model asphaltene precipitation from bitumen diluted with multicomponent solvents. The updated model can be used to predict asphaltene stability in field applications that rely on solvent blends and multicomponent petroleum solvents such as condensates or refinery distillation fractions. The major conclusions and recommendations for future research projects are listed below.

7.1 Conclusions

7.1.1 Experimental Methods

The benchtop procedure previously reported by Johnston *et al.* (2017b) for asphaltene yield measurements from bitumen diluted with *n*-pentane was successfully applied with a few modifications to measure asphaltene yields from bitumen diluted with multicomponent solvents. In the modified procedure, when solvent blends were used for precipitation, the precipitate was washed with the same solvent blend. However, if a petroleum solvent was added to the bitumen on its own, the precipitate was washed with *n*-pentane. Also, in the case of binary blends of *n*-heptane and petroleum solvents, the residual solvent that did not evaporate at experimental conditions was deducted from the precipitate for the yield calculation.

The blind cell methodology to determine asphaltene yields from light-phase compositions and a material balance developed by Johnston *et al.* (2017b) was applied for bitumen diluted with blended pure solvents at temperatures of 21 and 180°C and pressure of 10 MPa. A few modifications from the standard procedure were implemented. Instead of mixing for 1-2 days at room temperature in a roller mixer before bringing the blind cells to the target temperature, the samples were mixed by inverting the blind cells at experimental conditions twice daily for several days to ensure complete mixing. The samples at 21 and 180°C were mixed for 8 and 5 days, respectively. After mixing, the pressure and temperature were maintained for a minimum of 2 days to ensure equilibrium was reached.

A new procedure to measure saturation pressures was tested on a limited set of mixtures of WC-B-A3 bitumen diluted with binary solvent blends at 180°C. The saturation pressures were detected based on the behavior of the pump in pressure mode after isothermal expansions. The new methodology allowed for significantly lower equilibration times and was found to be consistent with the previously validated volume expansion method (Perez Claro *et al.*, 2019).

7.1.2 Experimental Results

The asphaltene yield from bitumen diluted with *n*-alkanes and petroleum solvents were measured at the ambient conditions of 21°C and 0.1 MPa. The asphaltene yields decreased, and the onsets increased as the carbon number of the *n*-alkane increased, as reported in other studies (Akbarzadeh *et al.*, 2005; Buenrostro-Gonzalez *et al.*, 2004; Calles *et al.*, 2008; Fuhr *et al.*, 1991; Hu and Guo, 2001). In the case of multicomponent petroleum solvents, the asphaltene yields were higher for highly paraffinic fluids, whereas aromatic petroleum solvents such as diesel and kerosene did not trigger precipitation when added to the bitumen on their own.

The asphaltene yield from bitumen diluted with solvent blends made up from *n*-alkanes, cyclohexane, toluene, and petroleum solvents were measured at 21°C and 0.1 MPa. It was found that the asphaltene yields decreased as the solvent content of toluene, cyclohexane, or aromatic petroleum solvent in the solvent blend increased. This trend is in agreement with the findings of other studies (Andersen and Stenby, 1996; Hong and Watkinson, 2004) and may be explained as a result of the increment of the solvent "power" of the medium, which makes asphaltenes more soluble in the bitumen.

In addition, the onset and yield of asphaltene precipitation from mixtures of bitumen and selected binary solvent blends (85:15 C5:Tol and 75:25 C5:CH) were measured at temperatures of 21 and 180°C and pressure of 10 MPa. As expected (Akbarzadeh *et al.*, 2005; Johnston *et al.*, 2017b), the asphaltenes became more soluble (yields decreased, and the onsets increased) with the pressure increment. Similarly, the asphaltene yields decreased as the temperature increased from 21 to 180°C. However, the measured onsets decreased.

7.1.3 Modeling

It was demonstrated that binary interaction parameters are required when using the Modified Regular Solution approach to model the onset and yield of asphaltene precipitation heavy oil diluted with blended pure solvents. Temperature dependent binary interaction parameters for the cyclohexane/asphaltene and toluene/asphaltene pseudo-component pairs were sufficient to match all of the data collected with binary solvent blends. All other binary interaction parameters were set to zero. The model with the binary interaction parameters obtained from the binary solvent blends predicted the asphaltene onsets and yields from heavy oil with ternary solvent blends, generally to within the error of the measurements. The model with these binary interaction parameters was also able to predict asphaltene yields from mixtures of a different heavy oil and binary solvent blends.

It is not yet known if the binary interaction parameters for cyclohexane can be extended to other cyclic components or those for toluene to other aromatics. Asphaltene data with a broader set of solvent blends and temperatures are required to establish a set of binary interaction parameters or correlations to better generalize the model. While the need for binary interaction parameters reduces the simplicity and general applicability of the model; the flash procedure remains straight forward, and the model remains well suited for heavy oil applications.

A new petroleum solvent characterization methodology was developed to predict the required properties for asphaltene precipitation modeling. The molecular weight, density, and solubility parameter of the SCN pseudo-components were correlated to the properties of the equivalent carbon number reference *n*-alkane and to an aromaticity factor adjusted to fit the measured density at standard conditions. The asphaltene yields modeled using the proposed correlations as input to the MRS model matched the experimental data for various petroleum solvents and their blends with *n*-heptane with an overall average absolute deviation and bias of 1.1 wt% and -0.8 wt%, respectively. However, the MRS model did not match the asphaltene yield from the naphtha.

7.2 Recommendations

The new experimental methodology to detect the saturation pressures was only tested on a couple of mixtures of diluted bitumen at a single temperature. Therefore, it is recommended to assess the

repeatability and uncertainty of saturation pressure measurements from the pump displacement method at different temperatures and solvent contents.

It is recommended to test the binary interaction parameters tuned for toluene and cyclohexane on solvent blends with *n*-alkanes other than *n*-pentane and *n*-heptane used for development. Similarly, it is further recommended to examine the application of the binary interaction parameters to solvent blends with other aromatic and naphthenic solvents.

The Modified Regular Solution model was not able to match the asphaltene yield from the bitumen diluted with naphtha. This deviation may occur because the characterization methodology does not accurately give the proportion of components from different chemical families within all petroleum solvents. Another possibility is that the binary interaction parameters for mixtures of bitumen and naphtha cannot be neglected. In either case, it is recommended to test the capability of the new characterization methodology to predict the onset and yield of asphaltene precipitation from mixtures of bitumen and other petroleum solvents. It is further recommended to validate the applicability of the characterization methodology to model yields at higher temperatures and pressures.

It is recommended to collect phase behavior data for bitumen diluted with other solvent blends and petroleum solvents at temperature and pressure conditions relevant to field applications. Future work on this area should be focused on studying the effect of temperature and pressure on the onset and yield of asphaltene precipitation from bitumen diluted with multicomponent solvents. A better phase behavior dataset will allow the development of a more robust characterization methodology.

References

- Acevedo, S., Gutierrez, L. B., Negrin, G., Pereira, J. C., Mendez, B., Delolme, F., Dessalces, G., and Broseta, D. (2005). Molecular Weight of Petroleum Asphaltenes : A Comparison between Mass Spectrometry and Vapor Pressure Osmometry. *Energy & Fuels*, 19(4), 1548–1560.
- Agrawal, P., Schoeggl, F. F., Satyro, M. A., Taylor, S. D., and Yarranton, H. W. (2012). Measurement and modeling of the phase behavior of solvent diluted bitumens. *Fluid Phase Equilibria*, 334, 51–64.
- Agrawala, M., and Yarranton, H. W. (2001). An Asphaltene Association Model Analogous to Linear Polymerization. *Industrial & Engineering Chemistry Research*, 40(21), 4664–4672.
- Aguiar, J. I. S., Garreto, M. S. E., González, G., Lucas, E. F., and Mansur, C. R. E. (2014). Microcalorimetry as a new technique for experimental study of solubility parameters of crude oil and asphaltenes. *Energy & Fuels*, 28(1), 409–416.
- Akbarzadeh, K., Alboudwarej, H., Svrcek, W. Y., and Yarranton, H. W. (2005). A generalized regular solution model for asphaltene precipitation from n-alkane diluted heavy oils and bitumens. *Fluid Phase Equilibria*, 232(1–2), 159–170.
- Akbarzadeh, K., Dhillon, A., Svrcek, W. Y., and Yarranton, H. W. (2004). Methodology for the characterization and modeling of asphaltene precipitation from heavy oils diluted with n-alkanes. *Energy & Fuels*, 18(5), 1434–1441.
- Akbarzadeh, K., Hammami, A., Kharrat, A., Zhang, D., Allenson, S., Creek, J., Kabir, S., Jamaluddin, A., Marshall, A., Rodgers, R., Mullins, O., and Solbakken, T. (2007). Asphaltenes - problematic but rich in potential. *Oilfield Review*, 19(2), 22–43.
- Akmaz, S., Iscan, O., Gurkaynak, M. A., and Yasar, M. (2011). The structural characterization of saturate, aromatic, resin, and asphaltene fractions of Batiraman crude oil. *Petroleum Science and Technology*, 29(2), 160–171.
- Alboudwarej, H., Akbarzadeh, K., Beck, J., Svrcek, W. Y., and Yarranton, H. W. (2003). Regular Solution Model for Asphaltene Precipitation from Bitumens and Solvents. *AIChE Journal*, 49(11), 2948–2956.
- Alomair, O. A., and Almusallam, A. S. (2013). Heavy crude oil viscosity reduction and the impact of asphaltene precipitation. *Energy & Fuels*, 27(12), 7267–7276.

- Altgelt, K. H., and Boduszynski, M. M. (1993). *Composition and analysis of heavy petroleum fractions*. CRC Press.
- Andersen, S. I. (1994). Effect of precipitation temperature on the composition of *n*-heptane asphaltenes. *Fuel Science and Technology International*, 12(1), 51–74.
- Andersen, S. I., and Birdi, K. S. (1990). Influence of temperature and solvent on the precipitation of asphaltenes. *Fuel Science and Technology International*, 8(6), 593–615.
- Andersen, S. I., Keul, A., and Stenby, E. (1997). Variation in composition of subfractions of petroleum asphaltenes. *Petroleum Science and Technology*, 15(7–8), 611–645.
- Andersen, S. I., and Speight, J. G. (2001). Petroleum resins: Separation, character, and role in petroleum. *Petroleum Science and Technology*, 19(1–2), 1–34.
- Andersen, S. I., and Stenby, E. I. (1996). Thermodynamics of asphaltene precipitation and dissolution investigation of temperature and solvent effects. *Fuel Science and Technology International*, 14(1–2), 261–287.
- Arya, A., Liang, X., Von Solms, N., and Kontogeorgis, G. M. (2017). Modeling of Asphaltene Precipitation from Crude Oil with the Cubic Plus Association Equation of State. *Energy & Fuels*, 31(2), 2063–2075.
- Azinfar, B., Haddadnia, A., Zirrahi, M., Hassanzadeh, H., and Abedi, J. (2018). Phase behaviour of butane/bitumen fractions: Experimental and modeling studies. *Fuel*, 220, 47–59.
- Badamchi-Zadeh, A., Yarranton, H. W., Svrcek, W. Y., and Maini, B. B. (2009a). Phase behaviour and physical property measurements for VAPEX solvents: Part I. propane and Athabasca bitumen. *Journal of Canadian Petroleum Technology*, 48(1), 54–61.
- Badamchi-Zadeh, A., Yarranton, H. W., Maini, B. B., and Satyro, M. A. (2009b). Phase Behavior and Physical Property Modeling for Vapex Solvents: Part II. Propane, Carbon Dioxide, and Athabasca Bitumen. *Journal of Canadian Petroleum Technology*, 48(3), 57–65.
- Barrera, D. M., Ortiz, D. P., and Yarranton, H. W. (2013). Molecular weight and density distribution of asphaltenes from crude oils. *Energy & Fuels*, 27(5), 2474–2487.
- Bartholomew, C. H. (2001). Mechanisms of catalyst deactivation. *Applied Catalysis A: General*, 212(1–2), 17–60.
- Barton, A. F. M. (1975). Solubility Parameters. *Chemical Reviews*, 75(6), 731–753.

- Barton, A. F. M. (1991). *CRC Handbook of Solubility Parameters and Other Cohesion Parameters*. CRC Press.
- Bayestehparvin, B., Ali, S. M. F., and Abedi, J. (2019). Solvent-based and solvent-assisted recovery processes: State of the art. *SPE Reservoir Evaluation & Engineering*, 22(1), 29–49.
- Bissada, K. K., Tan, J., Szymczyk, E., Darnell, M., and Mei, M. (2016). Group-type characterization of crude oil and bitumen. Part I: Enhanced separation and quantification of saturates, aromatics, resins and asphaltenes (SARA). *Organic Geochemistry*, 95, 21–28.
- Bjorøy, Ø., Fotland, P., Gilje, E., and Høiland, H. (2012). Asphaltene precipitation from Athabasca bitumen using an aromatic diluent: A comparison to standard *n*-alkane liquid precipitants at different temperatures. *Energy & Fuels*, 26(5), 2648–2654.
- Boduszynski, M. M. (1987). Composition of heavy petroleums. 1. Molecular weight, hydrogen deficiency, and heteroatom concentration as a function of atmospheric equivalent boiling point up to 1400°F (760°C). *Energy & Fuels*, 1(1), 2–11.
- Boduszynski, M. M. (2015). Petroleum molecular composition continuity model. In C. Ovalles and C. E. Rechsteiner Jr. (Eds.), *Analytical methods in petroleum upstream applications* (pp. 3–30). Taylor & Francis Group.
- Broad, T. J., Varotsis, N., and Pasadakis, N. (2001). The Compositional Characterization of Gas Condensate Fluids - A Review Featuring the Impact of the Analysis Data Quality on the Accuracy of Equation of State Based PVT Predictions. *Proceedings of the SPE Middle East Oil Show*, 885–892.
- Buenrostro-Gonzalez, E., Lira-Galeana, C., Gil-Villegas, A., and Wu, J. (2004). Asphaltene precipitation in crude oils: Theory and experiments. *AIChE Journal*, 50(10), 2552–2570.
- Burke, N. E., Hobbs, R. E., and Kashou, S. F. (1990). Measurement and modeling of asphaltene precipitation. *Journal of Petroleum Technology*, 42(11), 1440–1446.
- Calles, J. A., Dufour, J., Marugán, J., Peña, J. L., Giménez-Aguirre, R., and Merino-García, D. (2008). Properties of asphaltenes precipitated with different *n*-Alkanes. A study to assess the most representative species for modeling. *Energy & Fuels*, 22(2), 763–769.
- Castro, L. V., and Vazquez, F. (2009). Fractionation and characterization of Mexican crude oils. *Energy & Fuels*, 23(3), 1603–1609.

- Chacón-Patiño, M. L., Rowland, S. M., and Rodgers, R. P. (2017). Advances in asphaltene petroleomics. Part 1: Asphaltenes are composed of abundant island and archipelago structural motifs. *Energy & Fuels*, 31(12), 13509–13518.
- Chacón-Patiño, M. L., Rowland, S. M., and Rodgers, R. P. (2018a). Advances in Asphaltene Petroleomics. Part 2: Selective Separation Method That Reveals Fractions Enriched in Island and Archipelago Structural Motifs by Mass Spectrometry. *Energy & Fuels*, 32(1), 314–328.
- Chacón-Patiño, M. L., Rowland, S. M., and Rodgers, R. P. (2018b). Advances in Asphaltene Petroleomics. Part 3. Dominance of Island or Archipelago Structural Motif Is Sample Dependent. *Energy & Fuels*, 32(9), 9106–9120.
- Chandio, Z. A., Ramasamy, M., and Mukhtar, H. B. (2015). Temperature effects on solubility of asphaltenes in crude oils. *Chemical Engineering Research and Design*, 94, 573–583.
- Chapman, W. G., Gubbins, K. E., Jackson, G., and Radosz, M. (1990). New reference equation of state for associating liquids. *Industrial and Engineering Chemistry Research*, 29(8), 1709–1721.
- Cronquist, C. (2000). *Estimation and Classification of Reserves of Crude Oil, Natural Gas, and Condensate*. Society of Petroleum Engineers.
- Da Silva Oliveira, E. C., Neto, Á. C., Júnior, V. L., De Castro, E. V. R., and De Menezes, S. M. C. (2014). Study of Brazilian asphaltene aggregation by Nuclear Magnetic Resonance spectroscopy. *Fuel*, 117(Part A), 146–151.
- Derakhshesh, M., Gray, M. R., and Dechaine, G. P. (2013). Dispersion of asphaltene nanoaggregates and the role of Rayleigh scattering in the absorption of visible electromagnetic radiation by these nanoaggregates. *Energy & Fuels*, 27(2), 680–693.
- Diallo, M. S., Cagin, T., Faulon, J. L., and Goddard III, W. A. (2000). Thermodynamic properties of asphaltenes: A predictive approach based on computer assisted structure elucidation and atomistic simulations. In G. V. Chilingarian and T. F. Yen (Eds.), *Asphaltenes and Asphalts, 2: Part B* (Vol. 40, pp. 103–127). Elsevier.
- Dini, Y., Becerra, M., and Shaw, J. M. (2016). Phase behavior and thermophysical properties of Peace River bitumen + propane mixtures from 303 K to 393 K. *Journal of Chemical and Engineering Data*, 61(8), 2659–2668.
- Duran, J. A., Casas, Y. A., Xiang, L., Zhang, L., Zeng, H., and Yarranton, H. W. (2019). Nature of asphaltene aggregates. *Energy & Fuels*, 33(5), 3694–3710.

- Durand, E., Clemancey, M., Lancelin, J.-M., Verstraete, J., Espinat, D., and Quoineaud, A.-A. (2010). Effect of chemical composition on asphaltenes aggregation. *Energy & Fuels*, 24(2), 1051–1062.
- Eastick, R. R., Svrcek, W. Y., and Mehrotra, A. K. (1992). Phase Behaviour of CO₂-Bitumen Fractions. *The Canadian Journal of Chemical Engineering*, 70(1), 159–164.
- Eyssautier, J., Levitz, P., Espinat, D., Jestin, J., Gummel, J., Grillo, I., and Barré, L. (2011). Insight into asphaltene nanoaggregate structure inferred by small angle neutron and X-ray scattering. *Journal of Physical Chemistry B*, 115(21), 6827–6837.
- Fahim, M. A., Al-Sahhaf, T. A., and Elkilani, A. S. (2001). Prediction of asphaltene precipitation for Kuwaiti crude using thermodynamic micellization model. *Industrial and Engineering Chemistry Research*, 40(12), 2748–2756.
- Fan, T., and Buckley, J. S. (2002). Rapid and accurate SARA analysis of medium gravity crude oils. *Energy & Fuels*, 16(6), 1571–1575.
- Flory, P. J. (1941). Thermodynamics of high polymer solutions. *The Journal of Chemical Physics*, 9(8), 660.
- Forte, E., and Taylor, S. E. (2015). Thermodynamic modelling of asphaltene precipitation and related phenomena. *Advances in Colloid and Interface Science*, 217, 1–12.
- Fuhr, B. J., Cathrea, C., Coates, L., Kalra, H., and Majeed, A. I. (1991). Properties of asphaltenes from a waxy crude. *Fuel*, 70(11), 1293–1297.
- Funk, E. W., and Prausnitz, J. M. (1970). Thermodynamic Properties of Liquid Mixtures: Aromatic-Saturated Hydrocarbon Systems. *Industrial and Engineering Chemistry*, 62(9), 8–15.
- Gao, J., Okuno, R., and Li, H. A. (2017). An experimental study of multiphase behavior for *n*-butane/bitumen/water mixtures. *SPE Journal*, 22(3), 783–798.
- Gawrys, K. L., Blankenship, G. A., and Kilpatrick, P. K. (2006a). On the distribution of chemical properties and aggregation of solubility fractions in asphaltenes. *Energy & Fuels*, 20(2), 705–714.
- Gawrys, K. L., Blankenship, G. A., and Kilpatrick, P. K. (2006b). Solvent entrainment in and flocculation of asphaltenic aggregates probed by small-angle neutron scattering. *Langmuir*, 22(10), 4487–4497.

- Gharbi, K., Benyounes, K., and Khodja, M. (2017). Removal and prevention of asphaltene deposition during oil production: A literature review. *Journal of Petroleum Science and Engineering*, 158, 351–360.
- Ghloum, E. F., Al-Qahtani, M., and Al-Rashid, A. (2010). Effect of inhibitors on asphaltene precipitation for Marrat Kuwaiti reservoirs. *Journal of Petroleum Science and Engineering*, 70(1–2), 99–106.
- Gonzalez, D. L., Ting, P. D., Hirasaki, G. J., and Chapman, W. G. (2005). Prediction of asphaltene instability under gas injection with the PC-SAFT equation of state. *Energy & Fuels*, 19(4), 1230–1234.
- Gray, M. R. (1994). *Upgrading Petroleum Residues and Heavy Oils*. CRC Press.
- Gray, M. R. (2003). Consistency of asphaltene chemical structures with pyrolysis and coking behavior. *Energy & Fuels*, 17(6), 1566–1569.
- Gray, M. R. (2015). *Upgrading oilsands bitumen and heavy oil*. University of Alberta Press.
- Gray, M. R., Tykwinski, R. R., Stryker, J. M., and Tan, X. (2011). Supramolecular assembly model for aggregation of petroleum asphaltenes. *Energy & Fuels*, 25(7), 3125–3134.
- Gray, M. R., and Yarranton, H. W. (2019). Quantitative modeling of formation of asphaltene nanoaggregates. *Energy & Fuels*, 33(9), 8566–8575.
- Groenzin, H., and Mullins, O. C. (1999). Asphaltene molecular size and structure. *Journal of Physical Chemistry A*, 103(50), 11237–11245.
- Groenzin, H., and Mullins, O. C. (2000). Molecular size and structure of asphaltenes from various sources. *Energy & Fuels*, 14(3), 677–684.
- Gross, J., and Sadowski, G. (2001). Perturbed-chain SAFT: An equation of state based on a perturbation theory for chain molecules. *Industrial and Engineering Chemistry Research*, 40(4), 1244–1260.
- Gross, J., and Sadowski, G. (2002). Application of the perturbed-chain SAFT equation of state to associating systems. *Industrial and Engineering Chemistry Research*, 41(22), 5510–5515.
- Haghighat, P., and Maini, B. B. (2010). Role of asphaltene precipitation in VAPEX process. *Journal of Canadian Petroleum Technology*, 49(3), 14–21.

- Hammami, A., Phelps, C. H., Monger-McClure, T., and Little, T. M. (2000). Asphaltene precipitation from live oils: An experimental investigation of onset conditions and reversibility. *Energy & Fuels*, *14*(1), 14–18.
- Hao, J., Che, Y., Tian, Y., Li, D., Zhang, J., and Qiao, Y. (2017). Thermal cracking characteristics and kinetics of oil sand bitumen and its SARA fractions by TG-FTIR. *Energy & Fuels*, *31*(2), 1295–1309.
- Hashmi, S. M., and Firoozabadi, A. (2012). Controlling nonpolar colloidal asphaltene aggregation by electrostatic repulsion. *Energy & Fuels*, *26*(7), 4438–4444.
- Hemmati-Sarapardeh, A., Alipour-Yeganeh-Marand, R., Naseri, A., Safiabadi, A., Gharagheizi, F., Ilani-Kashkouli, P., and Mohammadi, A. H. (2013). Asphaltene precipitation due to natural depletion of reservoir: Determination using a SARA fraction based intelligent model. *Fluid Phase Equilibria*, *354*, 177–184.
- Hildebrand, J. H., Prausnitz, J. M., and Scott, R. L. (1970). *Regular and Related Solutions*. Van Nostrand Reinhold Co.
- Hirschberg, A., DeJong, L. N. J., Schipper, B. A., and Meijer, J. G. (1984). Influence of Temperature and Pressure on Asphaltene Flocculation. *Society of Petroleum Engineers Journal*, *24*(3), 283–293.
- Hollebone, B. P. (2015). Oil physical properties: Measurement and correlation. In M. Fingas (Ed.), *Handbook of Oil Spill Science and Technology* (pp. 38–50). John Wiley & Sons.
- Hong, E., and Watkinson, P. (2004). A study of asphaltene solubility and precipitation. *Fuel*, *83*(14–15), 1881–1887.
- Hortal, A. R., Hurtado, P., Martínez-Haya, B., and Mullins, O. C. (2007). Molecular-weight distributions of coal and petroleum asphaltenes from Laser Desorption/Ionization experiments. *Energy & Fuels*, *21*(5), 2863–2868.
- Hosseini-Dastgerdi, Z., Tabatabaei-Nejad, S. A. R., Khodapanah, E., and Sahraei, E. (2015). A comprehensive study on mechanism of formation and techniques to diagnose asphaltene structure; molecular and aggregates: a review. *Asia-Pacific Journal of Chemical Engineering*, *10*(1), 1–14.
- Hsu, C., and Robinson, P. (2019). *Petroleum science and technology*. Springer International Publishing.

- Hu, Y.-F., and Guo, T.-M. (2001). Effect of temperature and molecular weight of n-alkane precipitants on asphaltene precipitation. *Fluid Phase Equilibria*, 192(1–2), 13–25.
- Huggins, M. L. (1941). Solutions of long chain compounds. *The Journal of Chemical Physics*, 9(5), 440.
- Jamaluddin, A., Law, D. H.-S., Taylor, S. D., and Andersen, S. I. (2018). *Heavy oil exploitation*. PennWell Corporation.
- James, N. E., and Mehrotra, A. K. (1988). V-L-S multiphase equilibrium in bitumen-diluent systems. *The Canadian Journal of Chemical Engineering*, 66(5), 870–878.
- Javanbakht, G., Sedghi, M., Welch, W. R. W., Goual, L., and Hoepfner, M. P. (2018). Molecular polydispersity improves prediction of asphaltene aggregation. *Journal of Molecular Liquids*, 256, 382–394.
- Jhaveri, B. S., and Youngren, G. K. (1988). Three-parameter modification of the Peng-Robinson equation of state to improve volumetric predictions. *SPE Reservoir Engineering*, 3(3), 1033–1040.
- Johnston, K. A., Satyro, M. A., Taylor, S. D., and Yarranton, H. W. (2017a). Can a Cubic Equation of State model bitumen-solvent phase behavior? *Energy & Fuels*, 31(8), 7967–7981.
- Johnston, K. A., Schoeggl, F. F., Satyro, M. A., Taylor, S. D., and Yarranton, H. W. (2017b). Phase behavior of bitumen and n-pentane. *Fluid Phase Equilibria*, 442, 1–19.
- Joseph, D. D., Kamp, A. M., and Bai, R. (2002). Foamy oil flow in porous media. In J. Chadam, A. Cunningham, R. E. Ewing, P. Ortoleva, and M. F. Wheeler (Eds.), *Resource recovery, confinement, and remediation of environmental hazards* (pp. 81–113). Springer-Verlag.
- Joshi, N. B., Mullins, Jamaluddin, A., Creek, J., and McFadden, J. (2001). Asphaltene precipitation from live crude oil. *Energy & Fuels*, 15(4), 979–986.
- Juyal, P., McKenna, A. M., Fan, T., Cao, T., Rueda-Velásquez, R. I., Fitzsimmons, J. E., Yen, A., Rodgers, R. P., Wang, J., Buckley, J. S., Gray, M. R., Allenson, S. J., and Creek, J. (2013). Joint industrial case study for asphaltene deposition. *Energy & Fuels*, 27(4), 1899–1908.
- Karimi, A., Qian, K., Olmstead, W. N., Freund, H., Yung, C., and Gray, M. R. (2011). Quantitative evidence for bridged structures in asphaltenes by thin film pyrolysis. *Energy & Fuels*, 25(8), 3581–3589.

- Kawanaka, S., Park, S. J., and Mansoori, G. A. (1991). Organic deposition from reservoir fluids: a thermodynamic predictive technique. *SPE Reservoir Engineering*, 6(2), 185–192.
- Kharrat, A. M. (2009). Characterization of Canadian heavy oils using sequential extraction approach. *Energy & Fuels*, 23(2), 828–834.
- Kontogeorgis, G. M., Michelsen, M. L., Folas, G. K., Derawi, S., Von Solms, N., and Stenby, E. H. (2006). Ten Years with the CPA (Cubic-Plus-Association) equation of state. Part 1. Pure compounds and self-associating systems. *Industrial and Engineering Chemistry Research*, 45(14), 4855–4868.
- Kontogeorgis, G. M., Voutsas, E. C., Yakoumis, I. V., and Tassios, D. P. (1996). An equation of state for associating fluids. *Industrial and Engineering Chemistry Research*, 35(11), 4310–4318.
- Langevin, D., and Argillier, J.-F. (2016). Interfacial behavior of asphaltenes. *Advances in Colloid and Interface Science*, 233, 83–93.
- Li, Z., and Firoozabadi, A. (2010). Cubic-plus-association equation of state for asphaltene precipitation in live oils. *Energy & Fuels*, 24(5), 2956–2963.
- Lian, H., Lin, J.-R., and Yen, T. F. (1994). Peptization studies of asphaltene and solubility parameter spectra. *Fuel*, 73(3), 423–428.
- Long, J., Xu, Z., and Masliyah, J. H. (2007). Single molecule force spectroscopy of asphaltene aggregates. *Langmuir*, 23(11), 6182–6190.
- Macchietto, S., Hewitt, G. F., Coletti, F., Crittenden, B. D., Dugwell, D. R., Galindo, A., Jackson, G., Kandiyoti, R., Kazarian, S. G., Luckham, P. F., Matar, O. K., Millan-Agorio, M., Müller, E. A., Paterson, W., Pugh, S. J., Richardson, S. M., and Wilson, D. I. (2011). Fouling in crude oil preheat trains: A systematic solution to an old problem. *Heat Transfer Engineering*, 32(3–4), 197–215.
- Malone, K., Aman, Z. M., Pesch, S., Schlüter, M., and Krause, D. (2020). Jet Formation at the Spill Site and Resulting Droplet Size Distributions. In S. Murawski, C. Ainsworth, S. Gilbert, D. Hollander, C. Paris, M. Schlüter, and D. Wetzel (Eds.), *Deep Oil Spills: Facts, Fate, and Effects*. Springer International Publishing.
- Mancilla-Polanco, A., Johnston, K. A., Richardson, W. D. L., Schoeggl, F. F., Zhang, Y., Yarranton, H. W., and Taylor, S. D. (2019). Phase Behavior of Heavy-Oil/Propane Mixtures. *SPE Journal*, 24(2), 596–617.

- Mannistu, K. D., Yarranton, H. W., and Masliyah, J. H. (1997). Solubility Modeling of Asphaltenes in Organic Solvents. *Energy & Fuels*, 11(3), 615–622.
- Martínez-Palou, R., Mosqueira, M. de L., Zapata-Rendón, B., Mar-Juárez, E., Bernal-Huicochea, C., de la Cruz Clavel-López, J., and Aburto, J. (2011). Transportation of heavy and extra-heavy crude oil by pipeline: A review. *Journal of Petroleum Science and Engineering*, 75(3–4), 274–282.
- Marufuzzaman, M., and Henni, A. (2015). Solubility of CO₂ and C₂H₆ in heavy oil and its SARA fractions. *Canadian Journal of Chemical Engineering*, 93(3), 553–564.
- McKenna, A. M., Chacón-Patiño, M. L., Weisbrod, C. R., Blakney, G. T., and Rodgers, R. P. (2019). Molecular-Level Characterization of Asphaltenes Isolated from Distillation Cuts. *Energy & Fuels*, 33(3), 2018–2029.
- McKenna, A. M., Donald, L. J., Fitzsimmons, J. E., Juyal, P., Spicer, V., Standing, K. G., Marshall, A. G., and Rodgers, R. P. (2013). Heavy petroleum composition. 3. Asphaltene aggregation. *Energy & Fuels*, 27(3), 1246–1256.
- Mehrotra, A. K., and Svrcek, W. Y. (1988). Properties of cold lake bitumen saturated with pure gases and gas mixtures. *The Canadian Journal of Chemical Engineering*, 66(4), 656–665.
- Michelsen, M. L., and Hendriks, E. M. (2001). Physical properties from association models. *Fluid Phase Equilibria*, 180(1–2), 165–174.
- Mitchell, D. L., and Speight, J. G. (1973). The solubility of asphaltenes in hydrocarbon solvents. *Fuel*, 52(2), 149–152.
- Mullins, O. C., and Groenzin, H. (2007). Asphaltene molecular size and weight by time-resolved fluorescence depolarization. In O. C. Mullins, E. Y. Sheu, A. Hammami, and A. G. Marshall (Eds.), *Asphaltenes, heavy oils, and petroleomics* (pp. 17–62). Springer.
- Mullins, O. C., Sabbah, H., Eyssautier, J., Pomerantz, A. E., Barré, L., Andrews, A. B., Ruiz-Morales, Y., Mostowfi, F., McFarlane, R., Goual, L., Lepkowicz, R., Cooper, T., Orbulescu, J., Leblanc, R. M., Edwards, J., and Zare, R. N. (2012). Advances in asphaltene science and the Yen-Mullins model. *Energy & Fuels*, 26(7), 3986–4003.
- Nghiem, L. X., and Coombe, D. A. (1997). Modeling asphaltene precipitation during primary depletion. *SPE Journal*, 2(2), 170–176.

- Nielsen, B. B., Svrcek, W. Y., and Mehrotra, A. K. (1994). Effects of Temperature and Pressure on Asphaltene Particle Size Distributions in Crude Oils Diluted with *n*-Pentane. *Industrial and Engineering Chemistry Research*, 33(5), 1324–1330.
- NIST Standard Reference Database. (n.d.). NIST/TRC Source Database; WinSource, Version 2008.
- Nourozieh, H., Kariznovi, M., and Abedi, J. (2015). Experimental and modeling studies of phase behavior for propane/Athabasca bitumen mixtures. *Fluid Phase Equilibria*, 397, 37–43.
- Ovalles, C. (2019). *Subsurface Upgrading of Heavy Crude Oils and Bitumen (1st ed.)*. CRC Press.
- Painter, P., Veytsman, B., and Youtcheff, J. (2015). Guide to asphaltene solubility. *Energy & Fuels*, 29(5), 2951–2961.
- Panuganti, S. R., Vargas, F. M., Gonzalez, D. L., Kurup, A. S., and Chapman, W. G. (2012). PC-SAFT characterization of crude oils and modeling of asphaltene phase behavior. *Fuel*, 93, 658–669.
- Pedersen, K. S., and Christensen, P. L. (2007). *Phase behavior of petroleum reservoir fluids*. CRC/Taylor & Francis.
- Péneloux, A., Rauzy, E., and Fréze, R. (1982). A consistent correction for Redlich-Kwong-Soave volumes. *Fluid Phase Equilibria*, 8(1), 7–23.
- Peng, D. Y., and Robinson, D. B. (1976). A New Two-Constant Equation of State. *Industrial and Engineering Chemistry Fundamentals*, 15(1), 59–64.
- Peramanu, S., Clarke, P. F., and Pruden, B. B. (1999a). Flow loop apparatus to study the effect of solvent, temperature and additives on asphaltene precipitation. *Journal of Petroleum Science and Engineering*, 23(2), 133–143.
- Peramanu, S., Pruden, B. B., and Rahimi, P. (1999b). Molecular weight and specific gravity distributions for Athabasca and Cold Lake bitumens and their saturate, aromatic, resin, and asphaltene fractions. *Industrial and Engineering Chemistry Research*, 38(8), 3121–3130.
- Perez Claro, Y. A. (2019). *Phase Behaviour of Mixtures of Heavy Oil and n-Butane*. University of Calgary.
- Perez Claro, Y. A., Schoeggl, F. F., Taylor, S. D., and Yarranton, H. W. (2019). Phase behavior of mixtures of bitumen and *n*-butane. *Energy & Fuels*, 33(9), 8530–8543.

- Pomerantz, A. E., Wu, Q., Mullins, O. C., and Zare, R. N. (2015). Laser-based mass spectrometric assessment of asphaltene molecular weight, molecular architecture, and nanoaggregate number. *Energy & Fuels*, 29(5), 2833–2842.
- Powers, D. P., Sadeghi, H., Yarranton, H. W., and Van Den Berg, F. G. A. (2016). Regular solution based approach to modeling asphaltene precipitation from native and reacted oils: Part 1, molecular weight, density, and solubility parameter distributions of asphaltenes. *Fuel*, 178, 218–233.
- Prakoso, A., Punase, A., Klock, K., Rogel, E., Ovalles, C., and Hascakir, B. (2016). Determination of the stability of asphaltenes through physicochemical characterization of asphaltenes. *SPE Western Regional Meeting, 23-26 May, Anchorage, Alaska, USA*.
- Prausnitz, J. M., Lichtenthaler, R. N., and Gomes de Azevedo, E. (1999). *Molecular Thermodynamics of Fluid-Phase Equilibria (3rd ed.)*. Prentice Hall PTR.
- Punase, A., and Hascakir, B. (2017). Stability determination of asphaltenes through dielectric constant measurements of polar oil fractions. *Energy & Fuels*, 31(1), 65–72.
- Punnapala, S., and Vargas, F. M. (2013). Revisiting the PC-SAFT characterization procedure for an improved asphaltene precipitation prediction. *Fuel*, 108, 417–429.
- Qi, Z., Abedini, A., Sharbatian, A., Pang, Y., Guerrero, A., and Sinton, D. (2018). Asphaltene deposition during bitumen extraction with natural gas condensate and naphtha. *Energy & Fuels*, 32(2), 1433–1439.
- Rahimi, P. M., and Gentzis, T. (2006). The chemistry of bitumen and heavy oil processing. In Chang S. Hsu and P. R. Robinson (Eds.), *Practical Advances in Petroleum Processing* (pp. 597–634). Springer.
- Ramirez-Corredores, M. M. (2017). *Science and technology of unconventional oils: Finding refining opportunities*. Elsevier.
- Ramos-Pallares, F., Santos, D., and Yarranton, H. W. (2020). Application of the Modified Regular Solution Model to Crude Oils Characterized from a Distillation Assay. *Energy & Fuels*, 34(12), 15270–15284.
- Ramos-Pallares, F., Taylor, S. D., Satyro, M. A., Marriott, R. A., and Yarranton, H. W. (2016). Prediction of viscosity for characterized oils and their fractions using the expanded fluid model. *Energy & Fuels*, 30(9), 7134–7157.

- Ramos-Pallares, F., and Yarranton, H. W. (2020). Extending the Modified Regular Solution model to predict component partitioning to the asphaltene-rich phase. *Energy & Fuels*, 34(5), 5213–5230.
- Rao, F., and Liu, Q. (2013). Froth treatment in Athabasca oil sands bitumen recovery process: A review. *Energy & Fuels*, 27(12), 7199–7207.
- Rassamdana, H., Dabir, B., Nematy, M., Farhani, M., and Sahimi, M. (1996). Asphalt Flocculation and Deposition: I. The Onset of Precipitation. *AIChE Journal*, 42(1), 10–22.
- Redlich, O., and Kwong, J. N. S. (1949). On the thermodynamics of solutions. V. An equation of state. Fugacities of gaseous solutions. *Chemical Reviews*, 44(1), 233–244.
- Riazi, M. R. (2005). *Characterization and Properties of Petroleum Fractions (1st ed.)*. ASTM International.
- Rodriguez, S., Baydak, E. N., Schoeggl, F. F., Taylor, S. D., Hay, G., and Yarranton, H. W. (2019). Regular solution based approach to modeling asphaltene precipitation from native and reacted oils: Part 3, visbroken oils. *Fuel*, 257.
- Rogel, E. (1997). Theoretical estimation of the solubility parameter distributions of asphaltenes, resins, and oils from crude oils and related materials. *Energy & Fuels*, 11(4), 920–925.
- Rogel, E., and Carbognani, L. (2003). Density estimation of asphaltene using molecular dynamics simulations. *Energy & Fuels*, 17(2), 378–386.
- Rogel, E., Ovalles, C., Bake, K. D., Zuo, J. Y., Dumont, H., Pomerantz, A. E., and Mullins, O. C. (2016). Asphaltene densities and solubility parameter distributions: Impact on asphaltene gradients. *Energy & Fuels*, 30(11), 9132–9140.
- Rogel, E., Roye, M., Vien, J., and Miao, T. (2015). Characterization of asphaltene fractions: Distribution, chemical characteristics, and solubility behavior. *Energy & Fuels*, 29(4), 2143–2152.
- Sabbagh, O., Akbarzadeh, K., Badamchi-Zadeh, A., Svrcek, W. Y., and Yarranton, H. W. (2006). Applying the PR-EoS to asphaltene precipitation from *n*-alkane diluted heavy oils and bitumens. *Energy & Fuels*, 20(2), 625–634.
- Sabbah, H., Morrow, A. L., Pomerantz, A. E., Mullins, O. C., Tan, X., Gray, M. R., Azyat, K., Tykwinski, R. R., and Zare, R. N. (2010). Comparing Laser Desorption / Laser Ionization mass spectra of asphaltenes and model compounds. *Energy & Fuels*, 24(6), 3589–3594.

- Sabbah, H., Morrow, A. L., Pomerantz, A. E., and Zare, R. N. (2011). Evidence for island structures as the dominant architecture of asphaltenes. *Energy & Fuels*, 25(4), 1597–1604.
- Sadowski, G. (2011). Modeling of Polymer Phase Equilibria Using Equations of State. In S. Enders and B. A. Wolf (Eds.), *Polymer Thermodynamics: Liquid Polymer-Containing Mixtures* (pp. 389–418). Springer-Verlag Berlin Heidelberg.
- Saryazdi, F., Motahhari, H., Schoeggl, F. F., Taylor, S. D., and Yarranton, H. W. (2013). Density of hydrocarbon mixtures and bitumen diluted with solvents and dissolved gases. *Energy & Fuels*, 27(7), 3666–3678.
- Sattari, M., Abedi, J., Zirrahi, M., and Mehrotra, A. K. (2016). Modeling the onset of asphaltene precipitation in solvent-diluted bitumens using cubic-plus-association equation of state. *SPE Canada Heavy Oil Technical Conference, June, Calgary, Alberta, Canada*.
- Schuler, B., Meyer, G., Peña, D., Mullins, O. C., and Gross, L. (2015). Unraveling the molecular structures of asphaltenes by atomic force microscopy. *Journal of the American Chemical Society*, 137(31), 9870–9876.
- Schulze, M., Lechner, M. P., Stryker, J. M., and Tykwinski, R. R. (2015). Aggregation of asphaltene model compounds using a porphyrin tethered to a carboxylic acid. *Organic and Biomolecular Chemistry*, 13(25), 6984–6991.
- Scott, R. L., and Magat, M. (1945). The thermodynamics of high-polymer solutions: I. The free energy of mixing of solvents and polymers of heterogeneous distribution. *The Journal of Chemical Physics*, 13(5), 172–177.
- Shaw, J. M., Satyro, M. A., and Yarranton, H. W. (2017). Phase Behavior and Properties of Heavy Oils. In Chang Samuel Hsu and P. R. Robinson (Eds.), *Springer Handbook of Petroleum Technology*. Springer International Publishing.
- Sheremata, J. M., Gray, M. R., Dettman, H. D., and McCaffrey, W. C. (2004). Quantitative molecular representation and sequential optimization of Athabasca asphaltenes. *Energy & Fuels*, 18(5), 1377–1384.
- Shirani, B., Nikazar, M., and Mousavi-Dehghani, S. A. (2012). Prediction of asphaltene phase behavior in live oil with CPA equation of state. *Fuel*, 97, 89–96.
- Sirota, E. B. (2005). Physical structure of asphaltenes. *Energy & Fuels*, 19(4), 1290–1296.

- Sisco, C., Abutaqiya, M. I. L., Wang, F., Zhang, J., Tavakkoli, M., and Vargas, F. M. (2018). Asphaltene Precipitation Modeling. In F. M. Vargas and M. Tavakkoli (Eds.), *Asphaltene Deposition: Fundamentals, Prediction, Prevention, and Remediation*. CRC Press.
- Sjöblom, J., Hemmingsen, P. V., and Kallevik, H. (2007). The Role of Asphaltenes in Stabilizing Water-in-Crude Oil Emulsions. In O. C. Mullins, E. Y. Sheu, A. Hammami, and A. G. Marshall (Eds.), *Asphaltenes, Heavy Oils, and Petroleomics* (pp. 549–587). Springer.
- Sjöblom, J., Øye, G., Glomm, W. R., Hannisdal, A., Knag, M., Brandal, Ø., Ese, M.-H., Hemmingsen, P. V., Havre, T. E., Oschmann, H.-J., and Kallevik, H. (2005). Modern Characterization Techniques for Crude Oils, Their Emulsions, and Functionalized Surfaces. In J. Sjöblom (Ed.), *Emulsions and Emulsion Stability (2nd ed.)*. CRC Press.
- Soave, G. (1972). Equilibrium constants from a modified Redlich-Kwong equation of state. *Chemical Engineering Science*, 27(6), 1197–1203.
- Speight, J. G. (1999). *The chemistry and technology of petroleum (3rd ed.)*. Marcel Dekker.
- Speight, J. G. (2004). Petroleum asphaltenes - Part 1: Asphaltenes, resins and the structure of petroleum. *Oil & Gas Science and Technology - Rev. IFP*, 59(5), 467–477.
- Speight, J. G. (2010). Chapter 7 - Deasphalting and dewaxing processes. In *The Refinery of the Future* (pp. 209–236). Elsevier Science & Technology Books.
- Speight, J. G. (2014). *The chemistry and technology of petroleum (5th ed.)*. CRC Press.
- Spencer, C. F., and Danner, R. P. (1972). Improved Equation for Prediction of Saturated Liquid Density. *Journal of Chemical and Engineering Data*, 17(2), 236–241.
- Spiecker, P. M., Gawrys, K. L., and Kilpatrick, P. K. (2003). Aggregation and solubility behavior of asphaltenes and their subfractions. *Journal of Colloid and Interface Science*, 267(1), 178–193.
- Stark, J. L., and Asomaning, S. (2003). Crude oil blending effects on asphaltene stability in refinery fouling. *Petroleum Science and Technology*, 21(3–4), 569–579.
- Tanaka, R., Sato, E., Hunt, J. E., Winans, R. E., Sato, S., and Takanohashi, T. (2004). Characterization of asphaltene aggregates using X-ray diffraction and Small-Angle X-ray scattering. *Energy & Fuels*, 18(4), 1118–1125.

- Tavakkoli, M., Kharrat, R., Masihi, M., and Ghazanfari, M. H. (2010). Prediction of asphaltene precipitation during pressure depletion and CO₂ injection for heavy crude. *Petroleum Science and Technology*, 28(9), 892–902.
- Tharanivasan, A. K., Svrcek, W. Y., Yarranton, H. W., Taylor, S. D., Merino-García, D., and Rahimi, P. M. (2009). Measurement and modeling of asphaltene precipitation from crude oil blends. *Energy & Fuels*, 23(8), 3971–3980.
- Tharanivasan, A. K., Yarranton, H. W., and Taylor, S. D. (2011). Application of a regular solution-based model to asphaltene precipitation from live oils. *Energy & Fuels*, 25(2), 528–538.
- Thomson, G. H., Brobst, K. R., and Hankinson, R. W. (1982). An improved correlation for densities of compressed liquids and liquid mixtures. *AIChE Journal*, 28(4), 671–676.
- Ting, P. D., Hirasaki, G. J., and Chapman, W. G. (2003). Modeling of asphaltene phase behavior with the SAFT equation of state. *Petroleum Science and Technology*, 21(3–4), 647–661.
- Usui, K., Kidena, K., Murata, S., Nomura, M., and Trisunaryanti, W. (2004). Catalytic hydrocracking of petroleum-derived asphaltenes by transition metal-loaded zeolite catalysts. *Fuel*, 83(14–15), 1899–1906.
- van der Waals, J. D. (1873). *Continuity of the Gaseous and Liquid State of Matter*. Leiden University.
- Von Solms, N., Kouskoumvekaki, I. A., Michelsen, M. L., and Kontogeorgis, G. M. (2006). Capabilities, limitations and challenges of a simplified PC-SAFT equation of state. *Fluid Phase Equilibria*, 241(1–2), 344–353.
- Wang, Z., Liu, H., Sun, X., Ji, S., Guo, A., and Chen, K. (2015). Compatibility of heavy blends evaluated by fouling and its relationship with colloidal stability. *Petroleum Science and Technology*, 33(6), 686–693.
- Watkinson, A. P. (2007). Deposition from crude oils in heat exchangers. *Heat Transfer Engineering*, 28(3), 177–184.
- Whitson, C. H., and Brulé, M. R. (2000). *Phase Behavior*. Henry L. Doherty Memorial Fund of AIME, Society of Petroleum Engineers.
- Wiehe, I. A., Yarranton, H. W., Akbarzadeh, K., Rahimi, P. M., and Teclemariam, A. (2005). The paradox of asphaltene precipitation with normal paraffins. *Energy & Fuels*, 19(4), 1261–1267.

- Wu, J., and Xu, Y. (2019). Effect of asphaltene content in bitumen on thermodynamic properties of light hydrocarbons dissolving in bitumen. *Fluid Phase Equilibria*, 490, 22–32.
- Wu, Q., Pomerantz, A. E., Mullins, O. C., and Zare, R. N. (2014). Laser-based mass spectrometric determination of aggregation numbers for petroleum- and coal-derived asphaltenes. *Energy & Fuels*, 28(1), 475–482.
- Xu, Y. (2018). Asphaltene precipitation in paraffinic froth treatment: Effects of solvent and temperature. *Energy & Fuels*, 32(3), 2801–2810.
- Yang, X., Hamza, H., and Czarnecki, J. (2004). Investigation of subfractions of Athabasca asphaltenes and their role in emulsion stability. *Energy & Fuels*, 18(3), 770–777.
- Yarranton, H. W. (2005). Asphaltene self-association. *Journal of Dispersion Science and Technology*, 26(1), 5–8.
- Yarranton, H. W., Alboudwarej, H., and Jakher, R. (2000). Investigation of asphaltene association with vapor pressure osmometry and interfacial tension measurements. *Industrial and Engineering Chemistry Research*, 39(8), 2916–2924.
- Yarranton, H. W., and Masliyah, J. H. (1996). Molar Mass Distribution and Solubility Modeling of Asphaltenes. *AIChE Journal*, 42(12), 3533–3543.
- Yarranton, H. W., Ortiz, D. P., Barrera, D. M., Baydak, E. N., Barré, L., Frot, D., Eyssautier, J., Zeng, H., Xu, Z., Dechaine, G., Becerra, M., Shaw, J. M., McKenna, A. M., Mapolelo, M. M., Bohne, C., Yang, Z., and Oake, J. (2013). On the size distribution of self-associated asphaltenes. *Energy & Fuels*, 27(9), 5083–5106.
- Yarranton, H. W., Powers, D., Okafor, J., and van den Berg, F. G. A. (2018). Regular solution based approach to modeling asphaltene precipitation from native and reacted oils: Part 2, molecular weight, density, and solubility parameter of saturates, aromatics, and resins. *Fuel*, 215, 766–777.
- Yarranton, H. W., Schoeggl, F. F., George, S., and Taylor, S. D. (2011). Asphaltene-rich phase compositions and sediment volumes from drying experiments. *Energy & Fuels*, 25(8), 3624–3633.
- Yazdani, A., and Maini, B. B. (2010). Measurements and modelling of phase behaviour and viscosity of a heavy oil/butane system. *Journal of Canadian Petroleum Technology*, 49(2), 9–14.

- Yen, T. F., Erdman, J. G., and Pollack, S. S. (1961). Investigation of the structure of petroleum asphaltenes by X-Ray diffraction. *Analytical Chemistry*, 33(11), 1587–1594.
- Zawala, J., Dabros, T., and Hamza, H. A. (2012). Settling properties of aggregates in paraffinic froth treatment. *Energy & Fuels*, 26(9), 5775–5781.
- Zhang, Y., Takanohashi, T., Sato, S., Saito, I., and Tanaka, R. (2004). Observation of glass transition in asphaltenes. *Energy & Fuels*, 18(1), 283–284.
- Zhang, Y., Arya, A., Kontogeorgis, G., and Yarranton, H. (2019). Modeling the phase behaviour of bitumen/*n*-alkane systems with the cubic plus association (CPA) equation of state. *Fluid Phase Equilibria*, 486, 119–138.
- Zou, X., Zhang, X., and Shaw, J. M. (2007). Phase behavior of Athabasca vacuum bottoms + *n*-alkane mixtures. *SPE Production & Operations*, 22(02), 265–272.
- Zúñiga-Hinojosa, M. A., Justo-García, D. N., Aquino-Olivos, M. A., Román-Ramírez, L. A., and García-Sánchez, F. (2014). Modeling of asphaltene precipitation from *n*-alkane diluted heavy oils and bitumens using the PC-SAFT equation of state. *Fluid Phase Equilibria*, 376, 210–224.

Appendix A: SARA and GC Assays

This appendix shows the conversion of SARA assays with distillates (DSARA) to conventional SARA assay. Modeled asphaltene yields from WC-B-B5 bitumen using the SARA assay with distillates (DSARA) are compared with modeled asphaltene yields using a conventional SARA assay. The measured GC assays of the petroleum solvents used in this thesis are provided.

To convert a SARA assay with distillates (DSARA) to a conventional SARA assay with no distillates (SARA), it is necessary to estimate the proportion of the SARA fractions in the distillates. Since the distillates consist of the lightest, most volatile components of the oil, it is safe to assume that they contain no resins or asphaltenes. Therefore, it is only necessary to determine the ratio of saturates to aromatics within the distillates. Tables A.1 and A.2 compare SARA assays with and without distillates for two Western Canadian bitumen reservoir formations (WC-B-A and WC-B-B). The assays were obtained from different samples from these reservoirs collected at different dates. Therefore, the comparison is qualitative. The assays with distillates were converted to a conventional basis assuming that the distillates contained 50 wt% saturates and 50 wt% aromatics. The tables show that the converted assays are an approximate match to the measured conventional assays, particularly for the WC-B-A oil. The WC-B-B oil assays were collected several years apart, have a significantly different asphaltene content, and may be a less reliable comparison. Nonetheless, the ratio of saturates to saturates+aromatics ($S/(S+A)$) in the converted assay is close the ratio in the measured SARA assay.

Table A.1 Comparison of converted DSARA with conventional SARA for WC-B-A oil. DSARA (WC-B-A3) from Rodriguez *et al.* (2019); SARA (WC-B-A2) from an in-house measurement.

Component	DSARA wt%	DSARA Converted wt%	SARA Measured wt%
Distillates	21.7	-	-
Saturates	7.1	18.0	16.5
Aromatics	31.6	42.4	41.2
Resins	17.4	17.4	20.9
Asphaltenes+TI	22.2	22.2	21.4
$S/(S+A)$	-	0.30	0.29

Table A.2 Comparison of converted DSARA with conventional SARA for WC-B-B oil. DSARA (WC-B-B5) from Perez Claro *et al.* (2019) ; SARA (WC-B-B2) from Agrawal *et al.* (2012).

Component	DSARA wt%	DSARA Converted wt%	SARA Measured wt%
Distillates	19.5	-	-
Saturates	7.7	17.4	17
Aromatics	29.8	39.6	46.9
Resins	18.9	18.9	16.7
Asphaltenes+TI	24.1	24.1	19.4
S/(S+A)	-	0.31	0.27

Figures A.1a and A.1b show the modeled asphaltene yields from WC-B-B5 bitumen using the SARA assay with distillates (DSARA) and the conventional SARA assay with no distillates (SARA). The model predicted the asphaltene yields with negligible difference. Therefore, the conventional SARA characterization is used in this thesis to model asphaltene yields from WC-B-B5 bitumen.

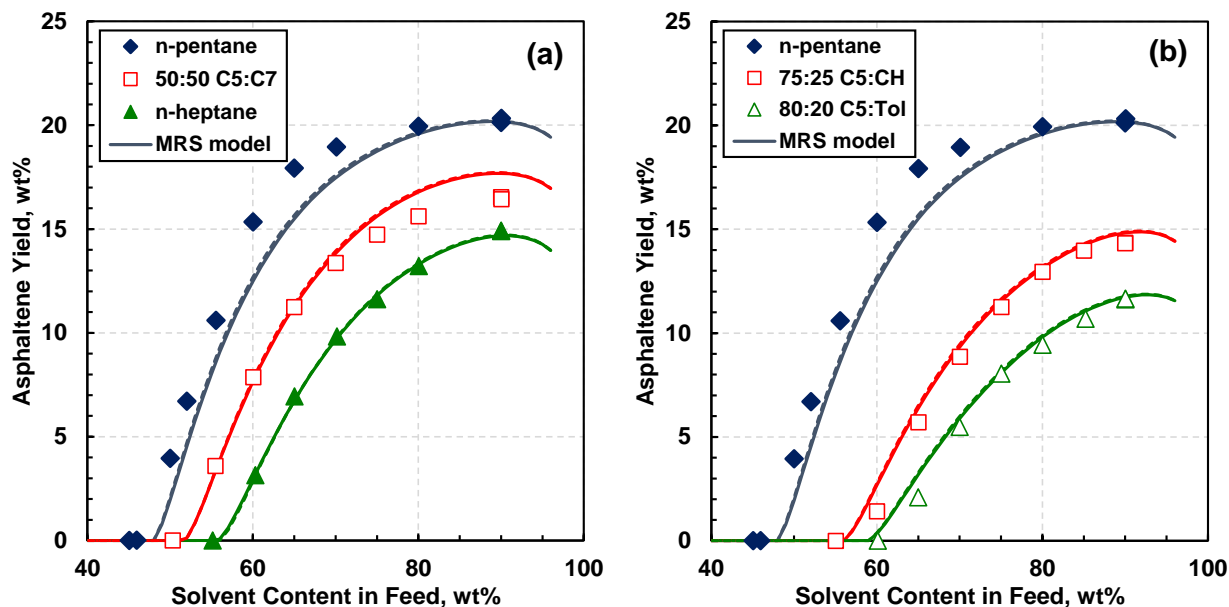


Figure A.1 Measured and modeled asphaltene yields from WC-B-B5 bitumen diluted with: a) *n*-pentane, *n*-heptane, and a binary blend of *n*-pentane and *n*-heptane at 21°C and 0.1 MPa; b) a binary blend of *n*-pentane and toluene and a binary blend of *n*-pentane and cyclohexane at 21°C and 0.1 MPa. The solid lines are the predicted asphaltene yields using SARA characterization and the dashed lines are the predicted asphaltene yields using the original DSARA characterization.

Table A.3 Measured GC assays of petroleum solvents.

Component	Condensate 1 wt%	Condensate 2 wt%	Kerosene 1 wt%	Diesel 1 wt%	Diesel 3 wt%	Naphtha 1 wt%
Methane	0.00	0.00	0.00	0.00	0.00	0.00
Ethane	0.00	0.00	0.00	0.00	0.00	0.00
Propane	0.00	0.00	0.01	0.00	0.00	0.00
Iso Butane	0.05	0.01	0.00	0.00	0.00	0.04
Normal Butane	3.75	13.18	0.03	0.00	0.00	0.05
Iso Pentane	18.36	75.92	0.02	0.00	0.00	0.12
Normal Pentane	17.29	10.06	0.04	0.00	0.00	0.00
Hexanes	16.83	0.33	0.07	0.03	0.01	23.05
Heptanes	9.20	0.14	0.12	0.25	0.12	22.16
Octanes	6.48	0.09	0.25	0.98	0.73	17.74
Nonanes	3.96	0.04	0.49	1.72	1.60	12.38
Decanes	2.68	0.04	0.96	3.71	3.85	5.25
Undecanes	1.68	0.03	1.71	6.90	6.62	2.01
Dodecanes	0.80	0.02	3.03	11.58	6.62	1.14
Tridecanes	0.63	0.00	4.97	13.93	12.97	0.52
Tetradecanes	0.51	0.00	8.12	13.41	14.22	0.20
Pentadecanes	0.40	0.00	10.77	11.09	12.60	0.05
Hexadecanes	0.33	0.00	13.21	9.74	10.41	0.00
Heptadecanes	0.21	0.00	10.10	8.11	8.56	0.00
Octadecanes	0.26	0.00	11.02	6.62	6.95	0.00
Nonadecanes	0.30	0.00	10.24	5.07	4.90	0.00
Eicosanes	0.20	0.00	8.21	2.25	3.29	0.00
Heneicosanes	0.18	0.00	5.81	1.55	1.97	0.00
Docosanes	0.18	0.00	3.68	0.78	1.05	0.00
Tricosanes	0.16	0.00	2.24	0.45	0.55	0.00
Tetracosanes	0.14	0.00	1.71	0.27	0.32	0.00
Pentacosanes	0.13	0.00	1.09	0.12	0.19	0.00
Hexacosanes	0.12	0.00	0.55	0.11	0.11	0.00
Heptacosanes	0.10	0.00	0.45	0.07	0.05	0.00
Octacosanes	0.10	0.00	0.38	0.04	0.00	0.00
Nonacosanes	0.06	0.00	0.18	0.03	0.00	0.00
Triacontanes Plus	0.21	0.00	0.29	0.04	0.00	0.00
Benzene	0.93	0.00	0.01	0.00	0.00	0.25
Toluene	1.69	0.01	0.01	0.04	1.20	1.85
Ethylbenzene, p+m-Xylene	1.32	0.02	0.09	0.41	0.48	5.09
o-Xylene	0.34	0.01	0.05	0.24	0.14	0.96
1,2,4 Trimethylbenzene	0.20	0.01	0.05	0.23	0.35	0.67
Cyclopentane	0.00	0.00	0.00	0.00	0.00	0.46
Methylcyclopentane	3.42	0.04	0.01	0.03	0.01	2.21
Cyclohexane	2.85	0.02	0.01	0.03	0.01	0.71
Methylcyclohexane	3.95	0.02	0.02	0.17	0.11	3.09

Appendix B: Pump Displacement Method for Saturation Pressure Measurements

The saturation pressures were measured for mixtures of WC-B-A3 bitumen diluted with binary solvent blends at 180°C. The solvent blends considered were a binary blend of 75 wt% *n*-pentane and 25 wt% cyclohexane (75:25 C5:CH), and a binary blend of 85 wt% *n*-pentane and 15 wt% toluene (85:15 C5:Tol). The saturation pressure for bitumen with 53.0 ±1.5 wt% of the 75:25 C5:CH blend was measured in the HPM apparatus. The saturation pressure for bitumen with 60.2 ±0.1 wt% of the 85:15 C5:Tol blend was measured in the blind cell apparatus. The procedures with each apparatus are similar and therefore only the blind cell procedure is described here.

To prepare the mixtures, known masses of the bitumen and the solvent blend were injected into the blind cells at ambient conditions. The blind cells were then pressurized to a pressure well above the expected saturation pressure and brought to the experimental temperature of 180°C. The samples were mixed by inverting the blind cells at 180°C twice daily for 5 days.

Once the samples were thoroughly mixed, the saturation pressure was determined following a stepwise isothermal expansion. The saturation pressure was detected based on the behavior of the pump. Using the pump in pressure mode, the pressure setpoint was decreased in a stepwise fashion. After each setpoint change, the pressure of the system was left to stabilize. When the mixture was in the liquid phase, the hydraulic oil flow rate from the pump stopped within approximately 15 minutes indicating that the pressure had equilibrated. In contrast, at pressures below the saturation pressure gas constantly evolved from the mixture, the pressure of the system did not reach the setpoint within 15 minutes, and the pump continuously withdrew hydraulic oil. The saturation pressure was taken to be the intermediate pressure between the lowest pressure at which the hydraulic oil flow rate stabilized and the highest pressure at which the hydraulic oil flow rate did not stabilize. The measured saturation pressures are provided in Table B.1. The uncertainty of the measured saturation pressure is taken as half the pressure step before the saturation pressure is detected (±5 psig) plus the accuracy of the pressure transducer of the pump (±5 psig) for a total of ±10 psig.

Table B.1 Measured saturation pressure for WC-B-A3 bitumen diluted with binary solvent blends at 180°C.

Solvent	Temperature °C	Solvent Content wt%	Pressure psig
85:15 C5:Tol	180	60.2	315±10
75:25 C5:CH	180	53.0	265±10

The methodology described above was validated by calculating the saturation pressure of the toluene blend with a different approach. Once the saturation pressure was detected, the pump was changed to volume mode and then controlled volumes of hydraulic oil were removed. After each volume step, the system was considered to have reached equilibrium when the temperature and pressure were constant for at least one hour. The equilibrium pressures were plotted against the cumulative hydraulic oil volume and the saturation pressure determined from the change in the slope of the pressure-volume isotherm, as shown in Figure B.1. The calculated saturation pressure was 296 psig. The volume expansion method has been tested previously and the uncertainty of the saturation pressure based on a 90% confidence interval is ± 25 psig (Perez Claro *et al.*, 2019). The pressure from the pump displacement method (315 psig) was within 20 psig of the volume expansion method value. Therefore, the pump displacement method is consistent with the volume expansion method.

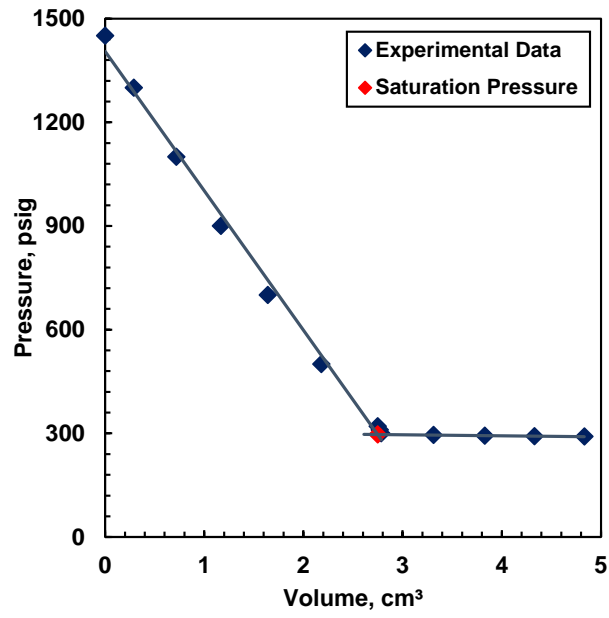


Figure B.1 Pressure-volume isotherm of 60.2 wt% 85:15 C5:Tol in WC-B-A3 bitumen at 180°C.

Appendix C: Solvent Properties

This appendix summarizes the required properties for asphaltene precipitation modeling of selected solvents used in this thesis. The fluid-specific parameters for the effective density correlation and the tuned compressibility factors for the modified Rackett correlation are provided. The measured densities of the petroleum solvents are provided.

Table C.1 Molecular weights and solubility parameters at 25°C and 0.1 MPa for selected solvents. Solubility parameters taken from Barton (1991).

Solvent	MW g/mol	δ° MPa ^{0.5}
Methane	16.04	9.60
Ethane	30.07	11.60
Propane	44.09	12.70
Isobutane	58.12	12.80
<i>n</i> -Butane	58.12	13.50
Isopentane	72.15	13.90
<i>n</i> -Pentane	72.15	14.40

The effective densities of the *n*-alkane solvents were calculated from the following correlation (Saryazdi *et al.*, 2013):

$$\rho = (a_1 + a_2T) + [(b_1 + b_2T)P] \quad (\text{C.1})$$

where a_1 , a_2 , b_1 and b_2 are fluid-specific parameters, T is the absolute temperature in K, and P is the pressure in MPa. The fluid-specific parameters for the solvents used in this thesis are provided in Table C.2.

Table C.2 Fluid-specific parameters for the effective liquid density correlation for *n*-alkanes.

Component	a_1 kg/m ³	a_2 kg/(m ³ K)	b_1 kg/(m ³ MPa)	b_2 kg/(m ³ MPa K)
Methane	532.157	-0.69737	0.42606	0.001143
Ethane	704.900	-0.82749	0.21442	0.002012
Propane	793.847	-0.85489	0.05309	0.002440
<i>n</i> -Butane	846.443	-0.85024	-0.05448	0.002648
<i>n</i> -Pentane	878.006	-0.82817	-0.09229	0.002648
<i>n</i> -Hexane	901.512	-0.80985	-0.14176	0.002685
<i>n</i> -Heptane	918.603	-0.79155	-0.17738	0.002692

The densities of toluene and cyclohexane were calculated from the Tait-COSTALD correlation (Thomson *et al.*, 1982) given by,

$$\rho_{T,P} = \rho_{T,P_0} \left[1 - c \ln \left(\frac{B+P}{B+P_0} \right) \right]^{-1} \quad (\text{C.2})$$

where $\rho_{T,P}$ is the density of the solvent at a given temperature and pressure, ρ_{T,P_0} is the density of the solvent at atmospheric pressure, and B and c are equation parameters given by:

$$c = 0.0861488 + 0.0344483\omega \quad (\text{C.3})$$

$$e = \exp(4.79594 + 0.250047\omega + 1.14188\omega^2) \quad (\text{C.4})$$

$$\frac{B}{P_c} = -1 - 9.0702A^{1/3} + 62.45326A^{2/3} - 135.1102A + eA^{4/3} \quad (\text{C.5})$$

$$A = 1 - T_r \quad (\text{C.6})$$

where T_r is the reduced temperature, ω is the acentric factor, and P_c is the critical pressure. The densities at atmospheric pressure ρ_{T,P_0} were calculated as the ratio of molecular weight to molar volume, and the molar volumes were determined from the modified Rackett correlation (Spencer and Danner, 1972):

$$v = \frac{RT_c}{P_c} Z_{RA}^{[1+(1-T_r)^{2/7}]} \quad (\text{C.7})$$

where v is the molar volume, R is the universal gas constant, T_c is the critical temperature, P_c is the critical pressure, Z_{RA} is the Rackett compressibility factor, and T_r is the reduced temperature. The Rackett compressibility factor was tuned to experimental saturated liquid densities (*NIST*

Standard Reference Database, n.d.). The tuned Z_{RA} for selected solvents are provided in Table C.3.

Table C.3 Tuned Rackett compressibility factors for selected solvents.

Solvent	Z_{RA}
Toluene	0.2642
Cyclohexane	0.2726
Isobutane	0.2753
Isopentane	0.2717

The densities of the petroleum solvents measured at temperatures of 21 and 25°C and pressure of 0.1 MPa are provided in Table C.4. Note that density at 25°C of Condensate 2 could not be measured due to its high volatility, therefore, its density was linearly extrapolated from measured densities at 5, 10, and 21°C.

Table C.4 Measured densities of petroleum solvents at temperatures of 21 and 25°C and pressure of 0.1 MPa.

Solvent	$\rho_{21^\circ C}$ kg/m ³	$\rho_{25^\circ C}$ kg/m ³
Condensate 1	681.84	678.79
Condensate 2	615.95	612.30
Diesel 1	838.32	836.17
Diesel 3	842.26	839.45
Kerosene 1	903.10	901.87
Naphtha 1	747.96	744.69

Appendix D: Yield Data

This appendix presents the yield data from ternary solvent blends not included in body of the thesis. The measured asphaltene yields from WC-B-A3 bitumen diluted with ternary solvent blends containing 75 wt% *n*-pentane and 75 wt% *n*-heptane are provided in Tables D.1 and D.2.

Table D.1 Measured asphaltene yields from WC-B-A3 bitumen diluted with ternary blends containing 75 wt% *n*-pentane at 21°C and 0.1 MPa.

Blend	Solvent Content	Asphaltene Yield
	wt%	wt%
75:5:20 C5:Tol:CH	55.1	0.4
	60.0	1.6
	65.1	4.4
	70.0	6.8
	75.0	9.0
	80.0	10.5
	85.0	11.5
	90.0	12.4
	90.0	12.3
75:20:5 C5:Tol:CH	60.0	0.1
	65.0	1.3
	70.2	3.5
	75.0	5.5
	80.0	7.1
	85.0	8.5
	90.0	9.6
	90.0	9.7

Table D.2 Measured asphaltene yields from WC-B-A3 bitumen diluted with ternary blends containing 75 wt% *n*-heptane at 21°C and 0.1 MPa.

Blend	Solvent Content	Asphaltene Yield
	wt%	wt%
75:5:20 C7:Tol:CH	65.1	0.0
	70.1	1.4
	75.0	3.5
	80.0	5.3
	85.0	7.1
	90.0	8.3
	90.0	8.4
75:20:5 C7:Tol:CH	70.0	0.0
	75.1	0.8
	80.0	2.5
	85.0	4.1
	90.0	5.6
	90.0	5.7